Modulating Cell Biology with Carbohydrates and their Derivatives

By

Lianyan L. Xu

Dissertation

Submitted to the Faculty of the

Graduate School of Vanderbilt University

in partial fulfillment of the requirements

for the degree of

DOCTOR OF PHILOSOPHY

in

Chemistry

May 31st, 2022

Nashville, Tennessee

Approved:

Steven D. Townsend, Ph.D.

Nathan D. Schley, Ph.D.

Timothy P. Hanusa, Ph.D.

Jennifer A. Gaddy, Ph.D.

Dedication

To my mother, father and brother.

ACKNOWLEDGMENTS

During my time at Vanderbilt, I have learned and grown so much over the years from so many people. I am thankful for the opportunities to work and interact with such talented and passionate researchers over the years.

First and foremost, I need to thank Dr. Steven D. Townsend for his mentorship, support and guidance as my advisor during my time at Vanderbilt. Not only was he my graduate career advisor, but he was also the one who introduced me to the marvel of the organic chemistry world when I was an undergraduate. His passion for chemistry and helping his students become the best version they can be is something I hope to emulate. Especially his unwavering faith, even when I was close to losing faith in myself and my abilities.

I would also like to thank my remaining committee members, Dr. Nathan D. Schley, Dr. Timothy P. Hanusa, and Dr. Jennifer A. Gaddy for all of the support and advice they have given. They have all been open to discussing ways to improve my research and career prospects. Their willingness to show their support and care have helped me improve as a scientist, and for that I am grateful. For the advice, support and guidance while searching for my next steps, which is now a postdoctoral fellow, I would like to thank Dr. Alissa Hare and Dr. Lars Plate for the continued discussions and for sharing their experiences with me.

It has been a pleasure working in the Townsend group from its inception till now. I have learned so much from everyone, especially synthetic technique and thought from the previous members. During my time as an undergraduate I had the opportunity to work with Dr. Dorothy Butler, John Hayes, Dr. Kelly M. Craft, Dr. D. Jamin Keith, Caroline Braun and Dr. Eric D. Huseman. With my fellow undergraduates, we learned together and grew as scientists. I am

grateful to have met Dr. Hunter Imlay, Dr. Isaiah Speight and Dr. Clark Stalling, and to have had the opportunity to mentor Linda Cui. I am glad that working with Linda was my first opportunity to give back and mentor someone as Dr. Townsend had done for me.

My first two years of graduate school at UIC with Dr. Leslie Aldrich had enriched my world, exposing me to how medicinal chemistry and biological inquires can be conducted in a single research group. I am thankful for the opportunity to work with my lab mates: Dr. Ivan Pavlinov, Dr. M. Alara Korkmaz-Vaisys, Dr. Erica Gerlach, Dr. Travis Helgren, Dr. Maryna Salkovski, and Dr. Qiwen Gao. I also had the opportunity to mentor the following undergraduates: Michelle Mavlyanova, Yash Mehta, Vincent Parise, and Daniel Sotelo. Besides my lab mates, I have so many close friends during my time in Chicago, most of whom I still regularly keep in contact with: Dr. Hyunjin (Jinnie) Lee, Mi Nguyen, Audra Lemley, Banafshe Samani, Stephanie Werner, Noel Leon, Semini Gaubagya Gunawardana and many others.

When I came back to Vanderbilt as a graduate student, I had the pleasure of continually being surrounded by wonderful people while working in the Townsend research group. I was familiar with Dr. Kelly Craft, Dr. D. Jamin Keith and Dr. Eric D. Huseman from my undergraduate days, while Dr. Schuyler Chambers and Dr. Johny Nguyen were new faces. They showed through example how to conduct rigorous research, how to persevere through challenges with hard work, how to think deeply about transformations, and how to be proactive and a force within the lab. I would also like to thank those in my cohort- Dr. Rebecca E. Moore and Cleo Evans. In particular, I would like to thank them for all the conversations where we shared our knowledge of organic synthesis and also microbiology that resulted in collaborations and publications.

I would also like to thank the remaining Townsend lab members for the discussions, help and support throughout the years: C. Elizabeth Adams, Alex J. Hughes, Sabrina K. Spicer, Xavier

Streety, Julie Talbert, and Nainoa Norman Ing. I also had the pleasure of mentoring Jair Powell during his undergraduate years at Vanderbilt. I look forward to seeing what you all do next. In addition to the research group, I would like to thank Dr. Don Stec and Dr. Markus Voehler for their help with NMR spectroscopy.

While I have known them but for a short while, I'd like to thank Dr. Daria Kim and Dr. Alex Schuppe for their enthusiasm and support during my last months of graduate school. It was invigorating and motivating to hear about the research they have conducted, thoughts on how to develop their research platforms and mostly just how inquisitive they still are about chemical transformations and the impact novel scaffolds can have.

As I have progressed from place to place during my journey, I have been blessed to have built a strong support system of friends, classmates, and fellow scientists where we can celebrate the wins, struggle through and overcome the challenges. There are too many to mention, but you come from my childhood and high school days to my early Vanderbilt undergraduate experience. Even during my UIC career I had those of you in my Majiang/Hotpot group in addition to graduate friends. While everyone is dear to me, my Vanderbilt graduate crowd has been crucial for helping me through and maintaining my sanity as well.

Finally, and most importantly, the pillars of my support system have been my family. My mother, father, and brother have been there to celebrate my wins with me, listen as I explain my failures, and voice support even as I rattle off plans of what reactions to set up next. They have been so accommodating throughout the years, even as I alter holiday plans to be centered at the city I'm located in, rather than my hometown.

I am eternally grateful to everyone for the support, mentorship, love and guidance.

Table of Contents

List of Schemes

List of Figures

List of Tables

Abbreviations

$(NH_4)_2CO_3$	Ammonium carbonate
$(NH_4)HCO_3$	Ammonium bicarbonate
°C	degrees Celsius
µL	microliter
2'-FL	2'-fucosyllactose
3-FL	3-fucosyllactose
6'-SL	6'-sialyllactose
Å	ångström
AA	*A. aurantia* lectin
AcOH	acetic acid
AMA	Arimetamycin A
aq.	aqueous
Asp	aspartate
$BF_3 \cdot Et_2O$	Boron trifluoride etherate
Bn	benzyl
calcd	calculated
CDC	Centers for Disease Control
$CDCl_3$	deuterated chloroform
CH_2Cl_2	dichloromethane
CMFRP	cyanoxyl-mediated free radical polymerization
ConA	Concanavalin A
COSY	correlation spectroscopy

d	doublet
dd	doublet of doublets
DFL	difucosyllactose
DGT	Desgalactotigonin
DIBAL-H	Diisobutylaluminium hydride
DMA-MB231	breast cancer
DMSO	dimethylsulfoxide
DNA	Deoxyribonucleic acid
DNR	Daunorubicin
DNR-AMA	daunorubicin-arimetamycin A
DOX	Doxorubicin
DOX-AMA	doxorubicin-arimetamycin A
EC	*E. crystagalli* lectin
EPO	Erythropoietin
equiv	equivalence
FDA	Food and Drug Administration
FEG-SEM	field emission gun scanning electron microscope
FITC	Fluorescein 5-isothiocyanate
Fuc	fucose
g	gram
Gal	galactose
GalNAc	N-acetyl galactosamine
Gal-NMe2-Tig	*N,N* dimethyl galactosamine-tigogenin

Gal-Tig	galactose-tigogenin
GBS	*Streptococcus agalactiae*
Glc	glucose
GlcNAc	N-acetyl glucosamine
Glc-Tig	glucose-tigogenin
h	hour
H_2	hydrogen gas
H69AR	lung cancer
HCl	hydrochloric acid
HCT116	colon cancer
$Hg(OAc)_2$	Mercury(II) acetate
HMO	human milk oligosaccharide
HRMS	High-resolution mass spectra
HSQC	heteronuclear single quantum coherence spectroscopy
HTS	high throughput screen
Hz	hertz
J	coupling constant
L	liter
Lac	lactose
Lemonose-NMe2-Tig	*N,N* dimethyl lemonose-tigogenin
LiHMDS	Lithium bis(trimethylsilyl)amide
LiMe	Methyllithium
LNT	lacto-*N*-tetraose

LNT-II	lacto-*N*-triose II
LSTa	lactosialyl tetrasaccharide a
LSTc	lactosialyl tetrasaccharide c
m	multiplet
M	molar
Mal	maltose
Man	Mannose
MDR	multidrug resistant
MeOD	deuterated methanol
MeOH	methanol
MFD	metal-free desulfurization
min	minutes
mmol	millimole
MOI	multiplicity of infection
mol	mole
MRSA	methicillin-resistant *Staphylococcus aureus*
MS	molecular sieves
N	normal
N_3	azide
$NaBH_3CN$	Sodium cyanoborohydride
NaOMe	sodium methoxide
NCL	native chemical ligation
NH_3	ammonia

NH_4Cl	ammonium chloride
NH_4CO_2H	ammonium formate
NIS	N-Iodosuccinimide
NMR	nuclear magnetic resonance
OMER	o-mercaptoaryl ester rearrangement
p	pentet
PBS	phosphate buffered saline
Pd/C	Palladium on carbon
Ph	phenyl
PMP	p-methoxyphenol
PMS	Phenazine methosulfate
PNA	peanut agglutinin
pyr	pyridine
q	quartet
RAE	reverse anomeric effect
ROS	reactive oxygen species
s	singlet
SDS-PAGE	sodium dodecyl sulfate–polyacrylamide gel electrophoresis
SEM	scanning electron microscopy
Ser	serine
SPPS	solid-phase peptide synthesis
t	triplet
TBAF	Tetra-n-butylammonium fluoride

TBS	tert-Butyldimethylsilyl
TFA	Trifluoroacetic
TfOH	triflic acid
THB	Todd-Hewitt broth
THF	tetrahydrofuran
Thr	threonine
Tig	Tigogenin
TLC	thin-layer chromatography
TV	*T. vulgaris* lectin
WHO	World Health Organization
XTT	(2,3-bis(2-methoxy-4-nitro-5-sulfophenyl)-5-[(phenylamino)carbonyl] -2H-tetrazolium hydroxide)
Xyl	xylose
βA-2'-FL	β-amino-2'-fucosyllactose
βA-HMO	β-amino-human milk oligosaccharide

1. Power of the Kochetkov Reaction: β-amino Human Milk Oligosaccharides Exhibit Antibacterial and Antibiofilm Properties

1.1. Introduction

Antimicrobial resistance threatens public health, with the Centers for Disease Control (CDC) reporting that antibiotic-resistant pathogens cause over 2.8 million infections every year in the United States. [1-2] Developing therapeutics capable of weakening microbial activity harmful to the host is a frontier approach to combating bacterial infection.[3] One method uses small molecules to regulate biofilms that can be employed alongside or instead of antibiotics.[4-7] Biofilm modulators that operate through a non-bactericidal mechanism are desirable as they do not exert evolutionary pressure on the bacterium to acclimate and develop resistance.

In particular, the Townsend research group was interested in Group B *Streptococcus* (GBS), an important neonate pathogen.[8-9] While the colonization of this bacterium in healthy adults, GBS is a major cause of preterm birth, septicemia, pneumonia, chorioamnionitis, and andmeningitis.[10-12] With antibiotic resistance on the rise and our interest in biofilm modulators as a method to avoid evolutionary pressure on the bacterium, the Townsend lab looked towards human milk oligosaccharides (HMOs). HMOs have been known to act as prebiotics by promoting the growth of commensal bacteria, immunomodulators against viruses as decoys and as antiadhesives against both pathogenic bacteria and viruses (Figure 1).[13-16]

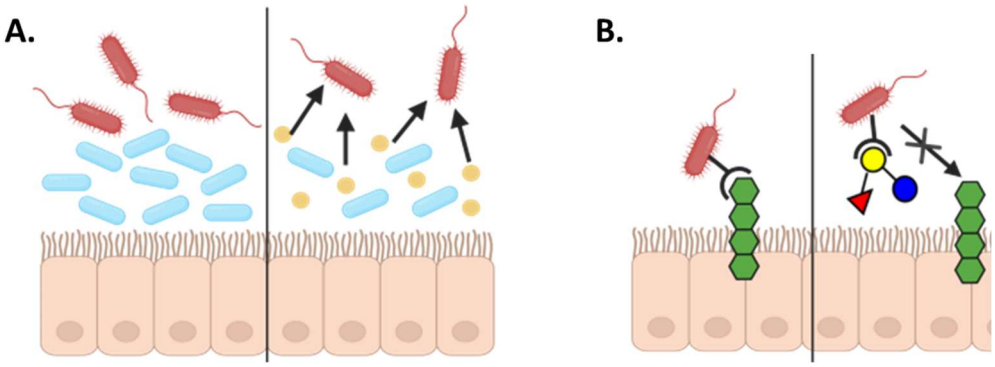

Figure 1 Effects HMOs provide. A. HMOs can act as prebiotics to help the commensals outgrow the pathogenic bacteria. B. HMOs can act as decoys to prevent pathogens from adhering to epithelial cells. Image adapted one Rebecca Moore created.

Since HMOs have been shown to inhibit viral and pathogenic bacterial growth, the Townsend lab began screening pooled heterogeneous mixtures of isolated HMOs for antimicrobial activity and observed that HMOs also had antibiofilm properties. The ability to inhibit biofilm formation led Townsend to identify HMOs as novel scaffolds to tackle the antibiotic resistance crisis.[16-18] The Townsend and Gaddy research groups discovered that HMO extracts possess bacteriostatic and antibiofilm activity against several gram-positive pathogens, including *Streptococcus agalactiae* (GBS). Initial studies revealed that HMOs govern both bacterial growth and biofilm assembly.[19]

In our second-generation work, we observed that HMOs potentiate the function of several intracellular-targeting antibiotics by, among other likely mechanisms, increasing cellular permeability.[20-21] Recently, we observed that while heterogeneous HMOs from isolated breast milk cocktails possess potent antibiofilm activity against GBS, single-entity HMOs (prepared by chemical or chemoenzymatic synthesis) are largely devoid of antibiofilm activity against this pathogen.[22-23]

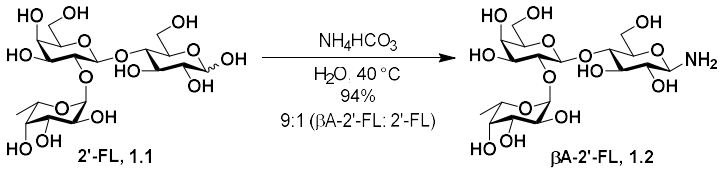

Scheme 1. Kochetkov Amination of 2'-FL **1.1** to access βA-2'-FL **1.2**.

However, in a later study, we observed that conversion of the prebiotic 2'-fucosyllactose (2'-FL, **1.1**) to its β-amino-variant (βA-2'-FL, **1.2**) via the Kochetkov amination generates a compound with impressive antibiofilm activity against GBS (Scheme 1). We initially hypothesized that positively charged β-amino HMO species employ an antibiofilm effect by acting as a surfactant, preventing the microbe from adhering to surfaces. The extracellular matrix of biofilm is stabilized through anionic substances, including polymeric sugars and negatively charged extracellular DNA, which is known to be destabilized by cationic molecules.[24-25] However, since a positive charge at the anomeric amine in acidic conditions would be transient, leading to the hydrolysis of the βA-HMO, an alternative hypothesis should be explored since at physiological pH the βA-HMOs should be stable against hydrolysis. While the mechanism behind this activity is unknown, we note that a related study by Aiassa and co-workers has shown that D-glucosamine reduces both adhesion and biofilm formation in a *Staphylococcus epidermidis* model.[26] In contrast, D-glucose promotes adhesion, biofilm production, and growth.

Once the significant antibiofilm activity of βA-2'-FL **1.2** was identified, we hypothesized that the antibiofilm activity was ubiquitous and that other βA-HMOs could serve as antibiofilm agents. In addition, while each bacteria uses differing mechanisms to form biofilms based on

environmental conditions and specific strain attributes, it is known that *Streptococcal* and *Staphylococcal* species share mechanistic pathways for producing biofilms.[27] Thus, we hypothesized that the antibiofilm activity of βA-HMOs would be observed in an additional gram-positive organism, *Staphylococcus aureu*s. Accordingly, we synthesized various βA-HMOs and assayed their abilities to inhibit biofilm production in GBS and methicillin-resistant *Staphylococcus aureus* (MRSA).

Before I describe the synthesis of these molecules and the results of the biological inquiry, I digress first to explore the anomeric effect and why a β-amine is the only product observed during the Kochetkov amination. The knowledge of this phenomenon is derived primarily from Lemieux's contribution to the area of carbohydrate-based stereoelectronic effects. Secondly, a brief account of the total synthesis of glycoprotein Erythropoietin (EPO) shows the utility of synthesizing glycosylamines to access glycopeptides.[28-31] Next, I will showcase how the community applies the Kochetkov amination to access glycosylamines for efficient access to biorthogonal probes, *N*-linked glycan polymers, and carbohydrate microassays.[32-34] Finally, I will discuss the antibiofilm activity of the synthesized βA-HMOs against both GBS and MRSA.

1.2. Stereoelectronic Effects in Carbohydrates

The current section focuses on covering some physical organic background on the anomeric effect, which is necessary to understand the reverse anomeric effect, as observed in the Kochetkov amination. While our studies utilize the Kochetkov amination to access glycosylamines for evaluation of antibiofilm activity, we do not conduct additional experiments to probe the reverse anomeric effect and its contributing factors.

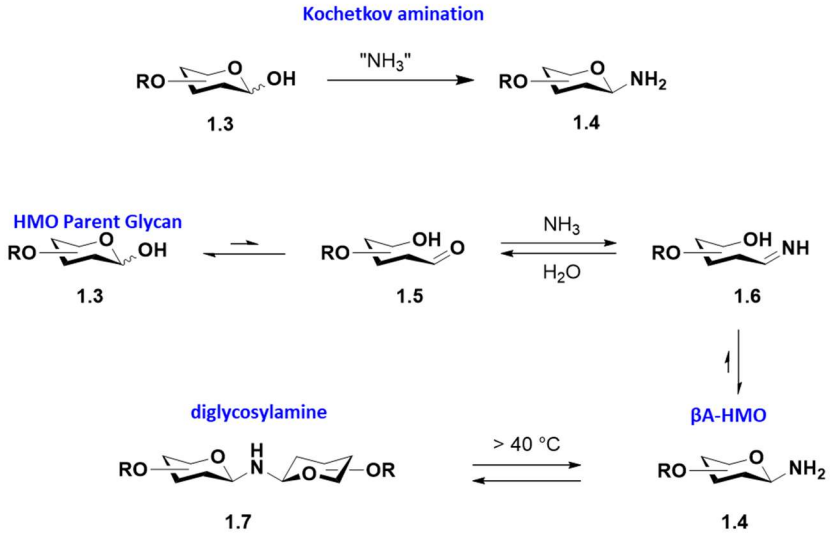

Scheme 2 Kochetkov amination mechanism

To synthesize a glycosylamine, a carbohydrate undergoes Kochetkov amination conditions by reacting with an excess of an ammonia source.[35] As seen in Scheme 1, the reaction begins with the HMO parent glycan **1.3** as the starting material. Since the carbohydrate used is the reducing sugar, it exists in equilibrium between the ring-closed state **1.3** and the open-chain state **1.5**. The addition of an ammonium source facilitates the condensation of ammonia onto the carbohydrate

aldehyde to provide the imine intermediate **1.6**. Upon ring closure, the βA-HMOs can be accessed. One thing to note is that since the βA-HMO product **1.4** contains just a primary amine at the anomeric center, a common by-product that can be observed are the formation of diglycosylamines **1.7**.

While seemingly simple on the surface, the Kochetkov reaction exclusively generates the β-anomer. Interestingly, the reaction rarely goes to completion and typically reaches an equilibrium that depends on the structure of the starting materials and products, as well as the reaction conditions, *vide infra*.

1.2.1. Origins of the Anomeric Effect

To appreciate why this reaction produces a single anomer, one must revisit a primary contribution from the Edward and Lemieux laboratories: proposing the anomeric effect and characterization of the phenomenon, respectively. In 1955, Edward observed a thermodynamic preference for polar substituents to be in an axial position in glycosyl halides (**1.9** and **1.11)** and intuitively thought that the lone pair on the in-ring oxygen contributes to the anomeric preference (Figure 2).[36-37] This observation is the basis for the electrostatic model of the anomeric effect.[36] It was later in 1958 that Lemieux characterized an axial preference for the orientation of electronegative substituents at the anomeric positions using nuclear magnetic resonance (NMR) spectroscopy.[38] [39]

1.8 1.9 1.10 1.11

Figure 2 The Anomeric Effect.

Historically, there has been much debate on what factors contribute to the anomeric effect. This debate can be distilled into two models: the electrostatic model **1.12** and hyperconjugation model **1.13**, both of which are supported through empirical data and computational models (Figure 3).[40] The electrostatic model is based on favorable local dipole-dipole interactions.[41-42]

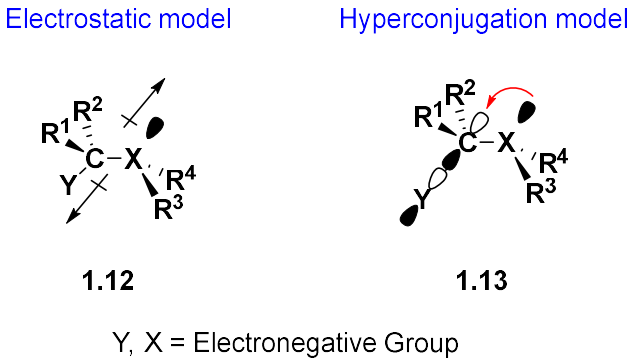

1.12 **1.13**

Figure 3 Two common models for the anomeric effect

Initially, negative hyperconjugation was the prevalent explanation for the anomeric effect. This model focuses on electron delocalization, where there is an increase in the double-bond character of O-C1 and a weakening of the C1-Y bond. Indeed, Romers reported the weakening of

the C-Cl bond with an increased bond length of the axial C-Cl bond (1.819 Å) compared to the equatorial C-Cl bond (1.7181 Å) on compound **1.14** in Figure 4.[43]

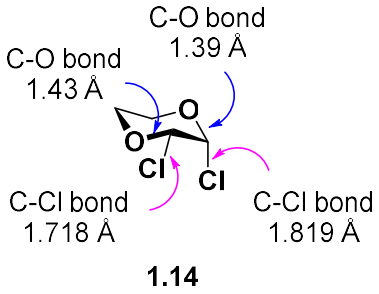

Figure 4 Bond length values for C-O and C-Cl

Initially, members of the community favored the hyperconjugation model, believing that the electrostatic model did not account for the varying bond lengths and bond angles seen in the empirically obtained data.[44-45] Later, however, the Box group showed that altering the electrostatic computational model for contributions from hydrogen bonding interactions leads to an improved model, as it accounts for both bond length and bond angle variations.[46]

1.2.2. Debated Existence of the Reverse Anomeric Effect

Early on, after detailing negative hyperconjugative effects, Lemieux described a more dubious aspect of hyperconjugation known as the reverse anomeric effect (RAE). The phenomenon was observed in 1965 when Lemieux and Morgan synthesized pyridinium α-glycopyranosides **1.16** (Figure 5).[47-48]

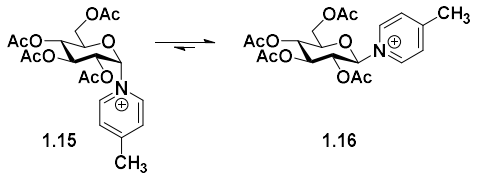

Figure 5 Lemieux's observation of the reverse anomeric effect (RAE)

The reverse anomeric effect attempts to explain the tendency of positively charged, electronegative groups at the anomeric center to adopt an equatorial orientation (Figure 6). *The reverse anomeric effect is often used to explain the stereochemical outcome of the Kochetkov amination.* The longstanding argument was that if electronegative substituents prefer an axial orientation due to an $n_{O5} \rightarrow \sigma^*_{C1\text{-}X}$ interaction, then a positively charged group would exist in an equatorial orientation to avoid the $n_{O5} \rightarrow \sigma^*_{C1\text{-}X}$ interaction. However, if one properly interprets a positively charged functional group as electronegative, then the concept of a reverse anomeric effect is unreasonable.

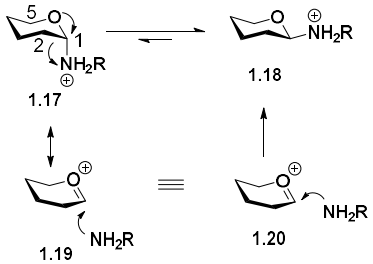

Figure 6 Generalized Reverse Anomeric Effect (RAE)

In contrast to Lemieux, Perrin and Pinto concluded there was no RAE for the specific compounds they studied in their paper.[48-50] Perrin evaluated several *N*-alkylglucosylamines in various solvents and used NMR titration to measure the shift of anomeric equilibrium. Perrin states that the reduced ratio of axial to equatorial anomers can be primarily accounted for by the steric bulk of the protonated species and only slightly by the normal anomeric effect. Therefore, the aforementioned study concluded that the reverse anomeric effect does not exist.[49] Similarly to Perrin's, the Pinto study was conducted to specifically address the general existence of RAE and concluded that there was no evidence of generalized RAE in either neutral or protonated species of *N*-arylglucopyranosylamines and *N*-aryl-5-thioglucopyranosylamines.[50] Pinto claimed that there is an enhanced endo-anomeric effect upon protonation. However, the anomeric effect was offset by steric effects from the associated counterion. Pinto claimed that the observed Keq values for each compound could be explained by the balance between the endo-anomeric and steric effects.[50] Therefore, based on the findings of Perrin and Pinto, there was no evidence of the reverse anomeric effect in neutral or protonated compounds. While the reverse anomeric effect was highly debated, the empirical evidence for the tendency of charged electronegative groups to be equatorial was observed. Therefore, it should be taken into consideration when evaluating computational models.

1.2.3. Advances in Computational Modeling

For several decades, the carbohydrate community accepted both the electrostatic and hyperconjugation models as contributors to the anomeric effect before the hyperconjugation model became more favored (Figure 3). When evaluating the two models, the analyses often failed to

account for the preference for amino substituents favoring the equatorial anomeric position. In 2010, the Mo group used computational modeling and found that the hyperconjugation theory was inconsistent with the empirical results for glycosides with equatorial anomeric amino substituents. Mo reported that steric effects dominated conformational preference without contributing effects from hyperconjugative electron delocalization.[51] In the model calculations, the steric effect is defined by the summation of both electrostatic interactions and Pauli repulsion.

After analyzing their model and concluding that electron delocalization does not mainly contribute to the anomeric effect, Mo decided in 2014 to next investigate improved hyperconjugation and electrostatic models.[42] They specifically interrogated how solvent influences the anomeric effect.[42] The results aligned with literature where conformational preference decreases as solvent polarity increases. Upon examination, it could be seen that solute-solvent interaction decreased intramolecular electron delocalization for β anomers over α anomers. The increase in solvent polarity destabilizes the β anomer, explaining how steric interactions impact solute-solvent interactions. Mo found a decrease in steric effect in β anomers where increased solvent polarity was more stabilizing for the β anomer. This means there is an overall reduction in the anomeric effect as the solvent polarity increases. Therefore, Mo concluded that while hyperconjugation can positively or negatively affect the configuration, it still contributes less than 50% of the α−β energy gap. Thus, the steric effect, specifically the electrostatic interactions, governs the anomeric effect.

1.2.4. General Information about the Anomeric Effect

In providing a historical overview of the anomeric effect, I have addressed its origins, the discussion between electrostatic and hyperconjugation models, the highly debated reverse anomeric effect, and the insight that advanced computation modeling imparts for the shifting understandings of the anomeric effect. Building from this, the present section serves to provide generally accepted information concerning the anomeric effect for carbohydrate chemists.

In pyranosides, the anomeric effect is operable in O5−C1−X systems. The anomeric effect, valued at ca. 1.0 kcal/mol, can be described as an *endo*- or *exo*-anomeric effect (Figure 7). The endo-anomeric effect refers to the preference of electronegative substituents, X, at the anomeric center to be oriented axially. This preference is dictated partly by a stabilizing $n_{O5} \rightarrow \sigma^*_{C1\text{-}X}$ interaction. If the electronegative substituent is oriented equatorially, the system lacks the bond "resonance" via back-bonding of an oxygen lone-pair to the antibonding (σ *) orbital of the C1-X bond. Moreover, dipole-dipole repulsion in the equatorial anomer favors axial orientation. The dipole repulsion argument is further supported by the reduction of the anomeric effect in polar solvents.[52] It should be noted, however, that computational studies suggest the anomeric effect is dominated by solely electrostatic interactions.[53]

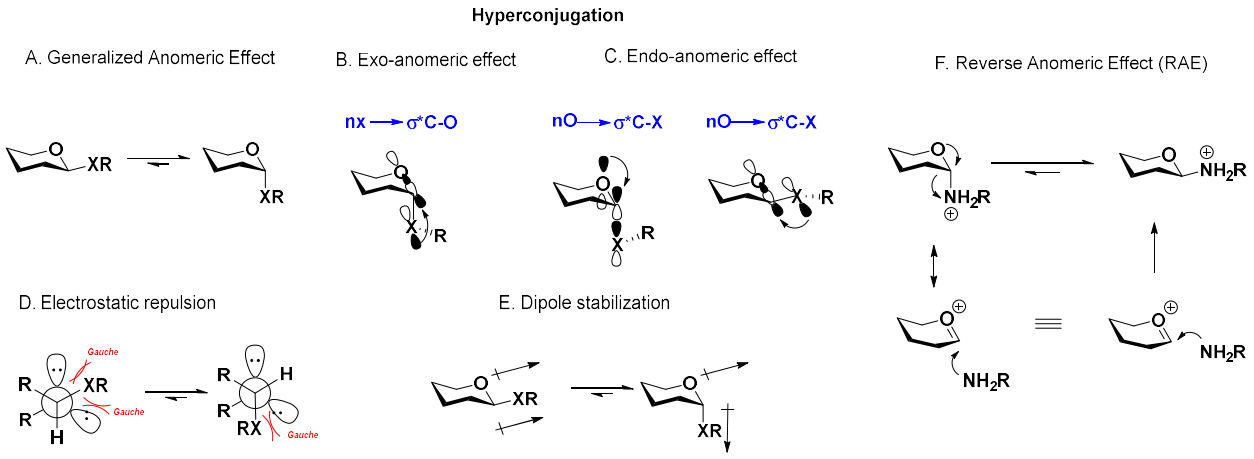

Figure 7 Stereoelectronic effects in carbohydrates. A. Anomeric effect generalized B. Endo anomeric effect. C. The exo-anomeric effect. D. Electrostatic repulsion E. Dipole stabilization F. Reverse anomeric effect (RAE).

Contrary to the endo-anomeric effect, the exo-anomeric effect is driven by a lone pair of electrons on the anomeric substituent (Figure 7). Empirically observed is the preference for this substituent to adopt a gauche conformation around the anomeric carbon, enabling an $n_X \rightarrow \sigma^*_{C1\text{-}O5}$ stabilizing effect. Because equatorial glycosides lack an endo-anomeric effect, the exo-anomeric effect predominates. The exo-anomeric effect has significant consequences for glycoside conformation in solution as it limits the number of possible conformations the molecule can adopt; conformational integrity is critical to biological function.[54]

Glycosides with varying ring sizes have been evaluated to see if the increase in ring flexibility changes whether the anomeric effect is observed. Furanosides have been rarely studied due to the considerable flexibility of the ring. A 2020 computational study indicated that while systemically higher, on an average of 2.7 kJ/mol, the endo-anomeric effect in furanoses is highly correlated with the energetic magnitude of pyranosides.[55] Computational studies on septosides in

2008 have shown that for the alpha anomer, the $n_{O5} \rightarrow \sigma^*_{C1\text{-}X}$ overlap is accessible within the expected conformation; therefore, it is likely that the anomeric effect is present.[56]

While the origin of selectivity for the configuration of glycosyl amines remains a contested topic, one could argue that in the "no-bond" resonance picture of the anomeric effect, positively charged groups should be oriented axially.[57] Thus, the greater equatorial preference observed in the Kochetkov amination is likely attributed to accentuated steric effects (in the case of alkyl amino groups) and generally to favorable electrostatic interactions (for any amine). Since I have synthesized βA-HMOs and observed the preference for the equatorial anomeric amine, it was important that computational studies considered the phenomenon. In conclusion, while hyperconjugation contributes to stabilizing the axial anomer, sterics and electrostatic repulsion govern the anomeric effect with empirical observations supported by computational studies that also consider assessing for evidence of reverse anomeric effects or results with anomeric amino substituents.

1.3. Biological applications of glycosylamines

After exploring the phenomenon that enables access to the anomeric β-amine during the Kochetkov amination, I wish to highlight the utility of synthesizing glycosylamines and what research groups have used this functional group to access. Danishefsky's total synthesis endeavor to access glycoprotein Erythropoietin (EPO) relies heavily on the Kochetkov amination to synthesize glycosylamines as precursors to *N*-linked glycosyl peptides.[28-31] The Townsend group has used the anomeric β-amine as a handle to append biorthogonal linkers to synthesize human milk oligosaccharide probes.[33] The Kochetkov amination has also enabled access to *N*-linked glycopolymer mimics from glycosylamines to photo-label specific proteins.[34] Seeberger envisioned using high throughput carbohydrate assays to screen chosen proteins' binding affinities by harnessing glycosylamine intermediates to attach a linker for facile immobilization of picomole scale micro assays.[32] Lastly, this dissertation uses the Kochetkov amination to access βA-HMOs for evaluating antibiofilm activities by potentially acting as a surfactant to inhibit bacterial adherence and disrupt biofilm formation.[58]

1.3.1. Accessing glycosylamines to synthesize glycoprotein Erythropoietin (EPO)

The following section showcases the utility of synthesizing glycosylamines via the Kochetkov amination to be coupled with aspartic acid residues and summarizes the Danishefsky group's journey toward the total synthesis of Erythropoietin (EPO). *N*-linked glycans on the glycoprotein EPO were synthesized from glycosylamines (Figure 8). Reducing end glycosylamines are precursors to glycoproteins as these amines accommodate selective derivatization with a variety of acylating reagents (e.g., the Lansbury reaction).[59-64]

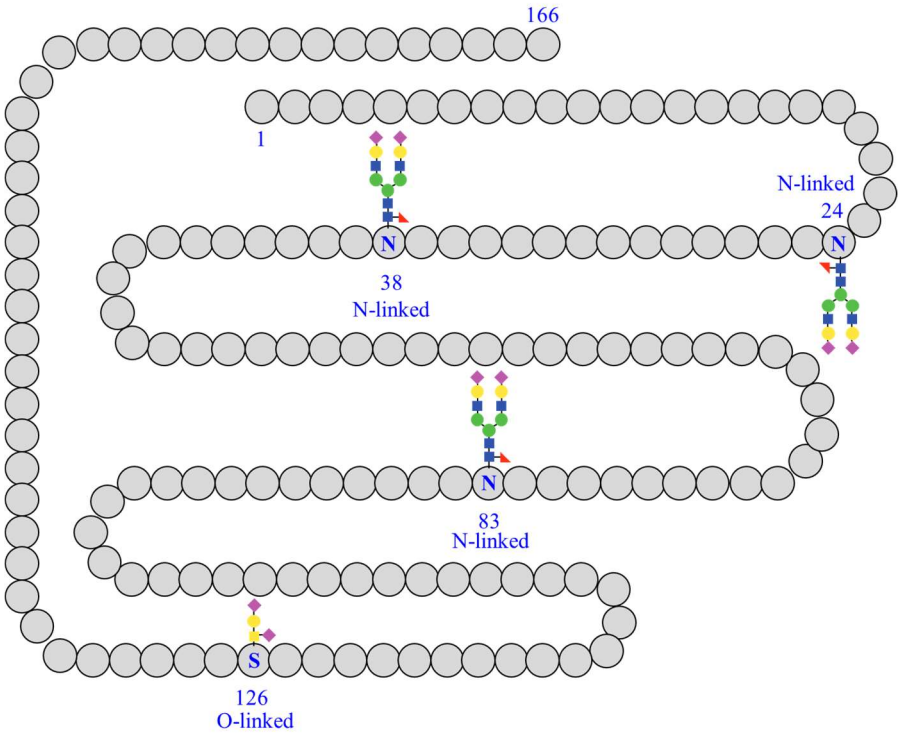

Figure 8 Schematic of Erythropoietin (EPO), a 166-mer glycoprotein with three *N*-linked glycans at 24. 38, and 83 and one *O*-linked glycan at 126.

EPO encompasses a large family of glycoproteins with a highly conserved primary protein structure and glycosylation sites. [29] For this 166-mer glycoprotein, while the glycan with an O-linkage is conserved at serine 126, the other sites with *N*-linked glycans had highly varied oligosaccharide domains.[29] The glycan variability leads to inseparable EPO glycoforms, sparking the interest of synthetic chemists to access pure, homogeneous EPO.[29]

Initially, the strategy to access EPO relied on stepwise glycopeptide synthesis by using solid-phase peptide synthesis (SPPS) to iteratively build out glycopeptides **1.25** from glycosylamino acid **1.21** (Scheme 3A). However, this linear strategy was limited by low-yielding

reactions, especially with complex carbohydrate fragments.[29] While the second strategy consisted of using SPPS first to synthesize the resin-bound peptide **1.22**, it often contained undesirable impurities that caused complications during coupling attempts with ornate glycosylamines **1.24** to access complex glycopeptide fragments **1.25** (Scheme 3B).[29] To tackle the synthesis of EPO, the Danishefsky group had been using the Lansbury reaction for coupling glycosylamines **1.24** with free aspartyl residues, as can be seen in Scheme 3 C.[29, 31]

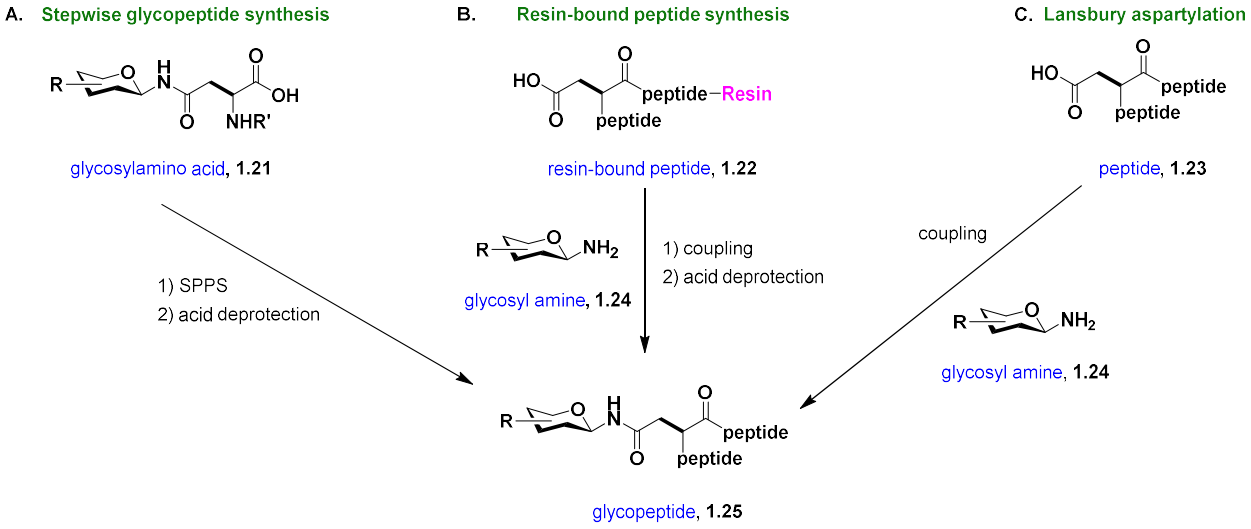

Scheme 3 Initial three strategies used to access complex glycopeptides. A. Stepwise glycopeptide synthesis. B. Resin-bound peptide synthesis C. Lansbury aspartylation.

For the synthetic route, the Danishefsky group began by using glycal assembly to build the complex glycans (Scheme 4). The reducing sugars **1.27** of these complex carbohydrates underwent a Kochetkov amination to provide the glycosylamine **1.28**. The small peptide fragments **1.29** were synthesized using SPPS from the corresponding amino acids **1.30**. The glycosylamine **1.28** and small peptide **1.29** undergo the Lansbury aspartylation conditions to

provide glycopeptide **1.31**. Using native chemical ligation (NCL), the glycopeptide **1.31** would be elongated to the more complex glycopeptide fragment **1.33** upon reacting with polypeptide thioester **1.32**.

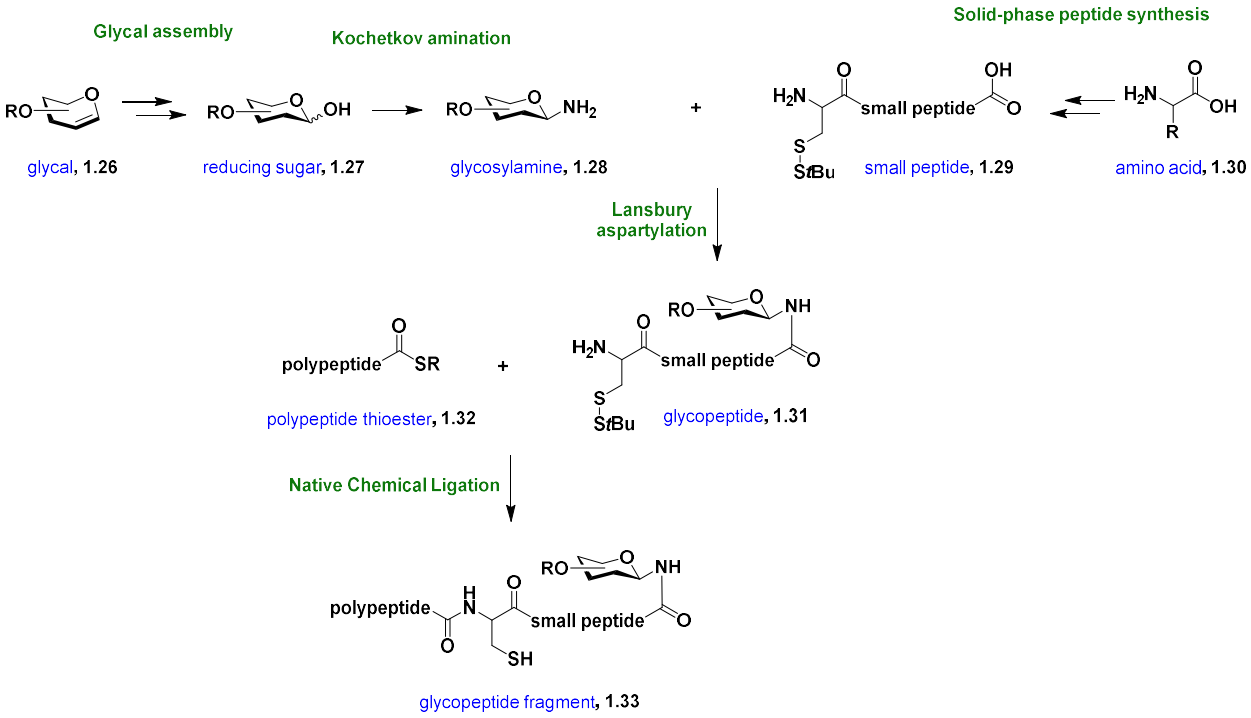

Scheme 4 Initial approach Danishefsky's research group undertook to access EPO.

While this approach helped access shorter peptide components, the formation of aspartimide by-product **1.37** increased when longer glycopeptides were attempted to be synthesized (Scheme 5).[29] Aspartimide formation was a significant problem during the Lansbury reaction if larger peptidyl fragments contained specifically the following sequence: aspartate-any amino acid- serine/threonine (Asp-**XXX**-Ser/Thr, **1.34**). The aspartimide issue occurs not only when installing the glycan **1.36** via Lansbury reactions, but also during SPPS synthesis of the

peptide fragment itself. It was hypothesized that installing a temporary protecting group at the problematic serine (Ser) or threonine (Thr) residue would change the peptide's electronic character or even induce a change in local structure enough to inhibit Lansbury side product formation.[31] Therefore, a pseudoproline protecting group was employed and installed on the residue (n+2) relative to the aspartate (Asp) reside to give pseudoproline peptide **1.38** (Scheme 5).

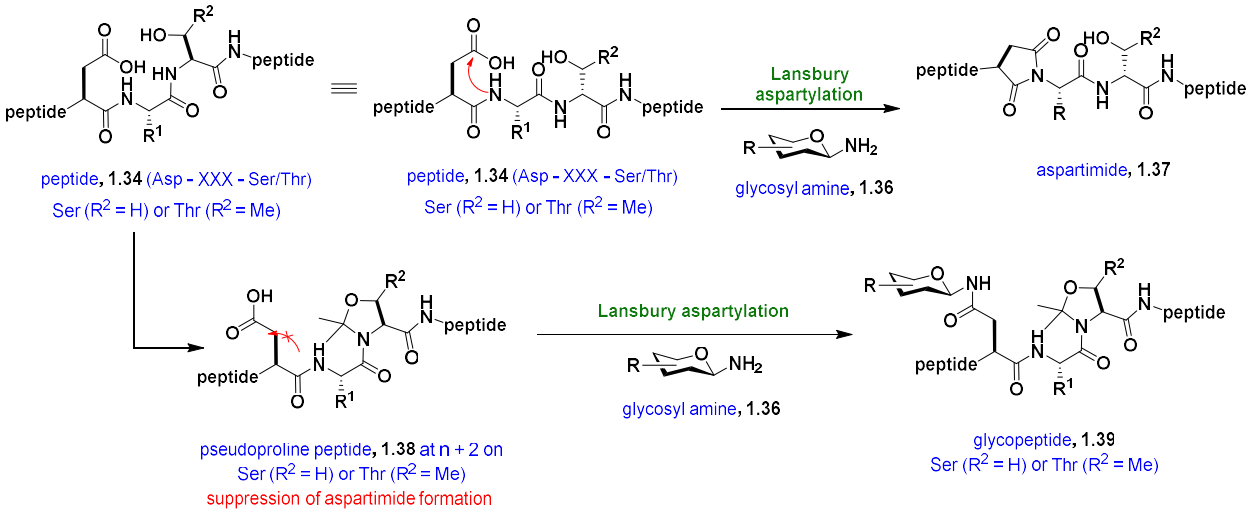

Scheme 5 The Lansbury aspartylation to couple glycosylamines to peptides with a specific pattern resulted in aspartimide by product. Formation of the pseudoproline before Lansbury aspartylation provided the desired glycopeptide.

The presence of the pseudoproline moiety served its intended purpose by inhibiting the formation of aspartimide **1.37** during the Lansbury reaction to couple the glycosyl amine **1.36** to the Asp residue of the peptide. With the mild trifluoroacetic (TFA) cleavage conditions to remove the pseudoproline moiety, the Danishefsky group could showcase the one-flask aspartylation then deprotection to access larger and more complex glycopeptides with greater control over sample purity.[28, 31]

Using the pseudoproline temporary protecting group, the Danishefsky group was finally able to access the first synthetically made EPO with ease and control over glycoprotein purity. The pseudoproline-based aspartylation concept was one of four critical methodologies used by Danishefsky during the EPO program for a convergent total synthesis of EPO. To undertake this program, four critical synthetic methodology entries were used: native chemical ligation (NCL), metal-free desulfurization (MFD), o-mercaptoaryl ester rearrangement (OMER)–mediated ligation, and one-flask aspartylation.[30] Having covered how the Kochetkov enables the facile synthesis of glycosylamines that are important intermediates to access EPO, the next section will discuss using glycosylamines to access bioorthogonal probes.

1.3.2. Synthesizing glycosylamines to access Bioorthogonal Human Milk Oligosaccharide probes

Dr. Schuyler Chambers, during her time in the Townsend lab, used the Kochetkov amination reaction to synthesize glycosylamines to access biorthogonal human milk oligosaccharide (HMOs) probes for antimicrobial target identification within *Streptococcus agalactiae*, a bacterial pathogen known to cause sepsis and other severe infections.[33, 65] Previous studies have shown that pooled heterogeneous HMO cocktails, composed of combined samples from different donors, exhibit antimicrobial activity against GBS.[16, 18] It has been hypothesized that the antimicrobial effects of HMOs are caused by their ability to increase cell permeability.[8, 66] However, studies have not been completed to discover HMO-protein interacting partners.

Dr. Chamber's work in the Townsend lab focused on probing the antibacterial activity of HMOs by building a library of biorthogonal probes. Ideally, these biorthogonal probes would be

synthesized by attaching the tag in a minimally invasive position on the HMO to avoid perturbing the parent glycan bioactivity.

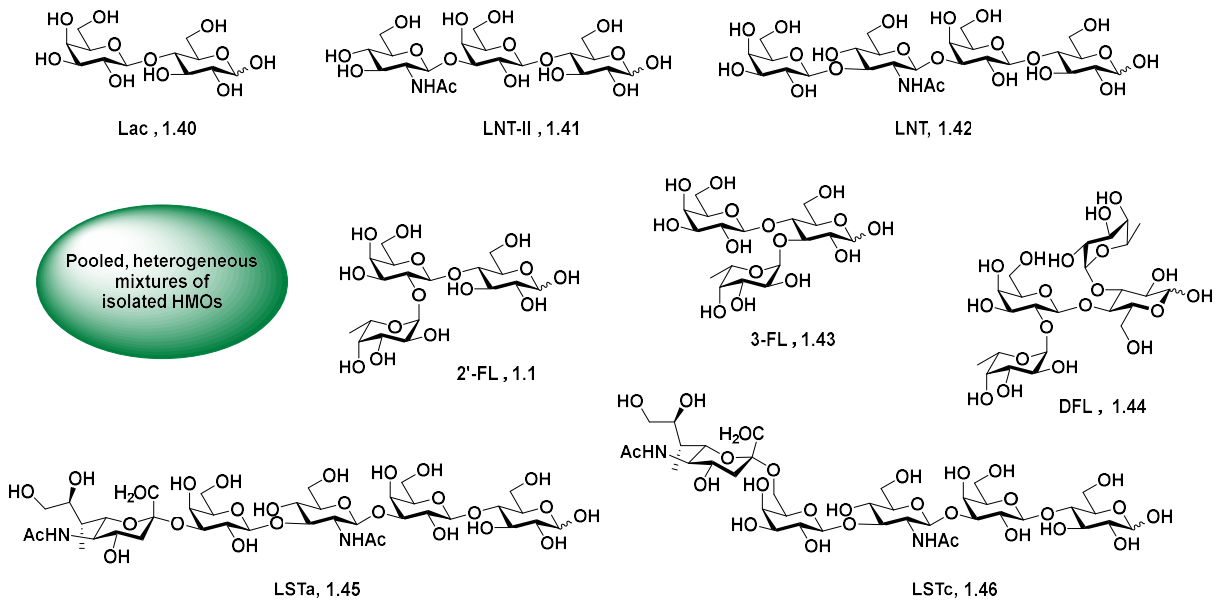

Figure 9 Carbohydrate samples assessed for antimicrobial activity against GBS: pooled HMO cocktails, lactose (Lac, **1.40)**, lacto-*N*-triose II (LNT-II, **1.41**), lacto-*N*-tetraose (LNT, **1.42**), 2'-fucosyllactose (2'FL, **1.1)**, 3-fucosyllactose (3-FL, **1.43**), difucosyllactose (DFL, **1.44**), lactosialyl tetrasaccharide a (LSTa, **1.45**), and lactosialyl tetrasaccharide c (LSTc, **1.46**).

Using pooled HMO cocktails as a positive control, the single entity HMOs were assessed for their antibacterial activity against GBS to choose which select HMOs would serve as the substrate scope for the probe library. The carbohydrates assessed were pooled HMO cocktails, lactose (Lac, **1.40)**, lacto-*N*-triose II (LNT-II, **1.41**), lacto-*N*-tetraose (LNT, **1.42**), 2'-fucosyllactose (2'FL, **1.1)**, 3-fucosyllactose (3-FL, **1.43**), difucosyllactose (DFL, **1.44**), lactosialyl tetrasaccharide a (LSTa, **1.45**), and lactosialyl tetrasaccharide c (LSTc, **1.46**) (Figure 9). Each carbohydrate sample was dosed at ~ 5 mg/mL, the lower end of physiological HMO concentrations

in human milk, against GB590 over 24 h of growth and assessed for the average growth reduction.[18, 67]

The results of the antimicrobial assay indicated that some single entity HMOs had weak activity while others exhibited significant antibacterial activity. 2'-FL **1.1** and LNT **1.42** had weak or no discernable antimicrobial activity. Many different HMOs showed significant antibacterial activity (35-60%). In order to represent the population of HMOs in mother's milk, both fucosylated and sialylated HMOs were chosen in addition to the neutral core backbone to give three compounds: LNT-II **1.41**, DFL **1.44**, and LSTa **1.45**.

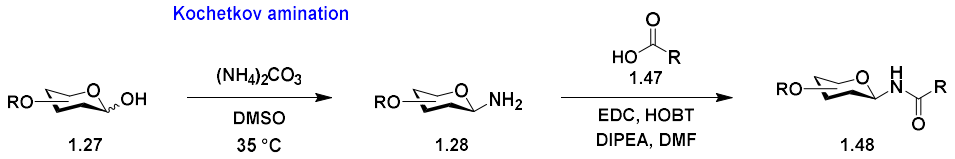

Scheme 6 Using the Kochetkov amination and amide coupling to access HMO bioorthogonal probes 1.48 from parent glycans 1.27.

After choosing which single-entity HMOs to transform into probes, the bioorthogonal handle was attached using the following synthetic steps (Scheme 6). To accomplish this goal, the parent HMOs **1.27** underwent a Kochetkov amination under traditional conditions to produce glycosyl amine **1.28**. Next, an amide coupling between the glycosyl amine **1.28** and the biorthogonal linker **1.47** would provide a 2-step approach to synthesizing the chemoproteomic probes **1.48**. The first set of probes was synthesized from each of the chosen single-entity HMOs (Figure 10).

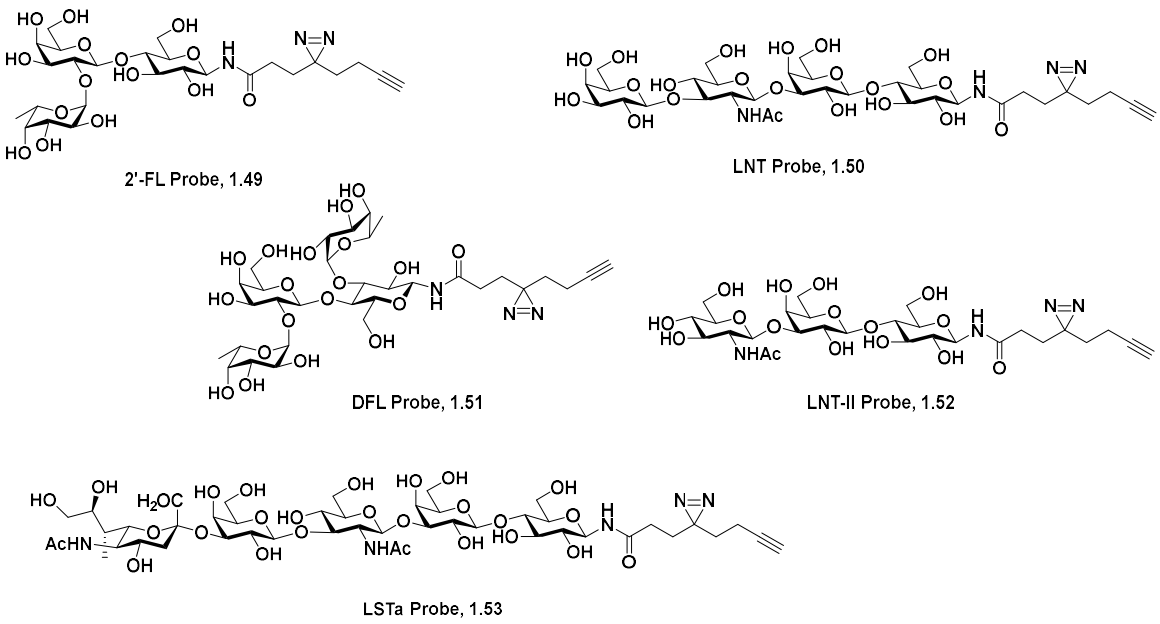

Figure 10 Glycan probe library

After synthesizing the glycan substrate scope, additional 2'-FL probes (**1.54- 1.56**) with various bioorthogonal handles were accessed (Scheme 7). The chosen crosslinking groups on the biorthogonal linker have been known to enable the elucidation of cellular target identities. Various diazirine-containing tags were accessed since it is minimal and useful for creating covalent linkages between the probe and target. Benzophenone-containing tags were also successfully synthesized and evaluated. Sulfonyl fluoride tags were unable to be incorporated, perhaps due to undesired reactivity with the deprotected oligosaccharide.

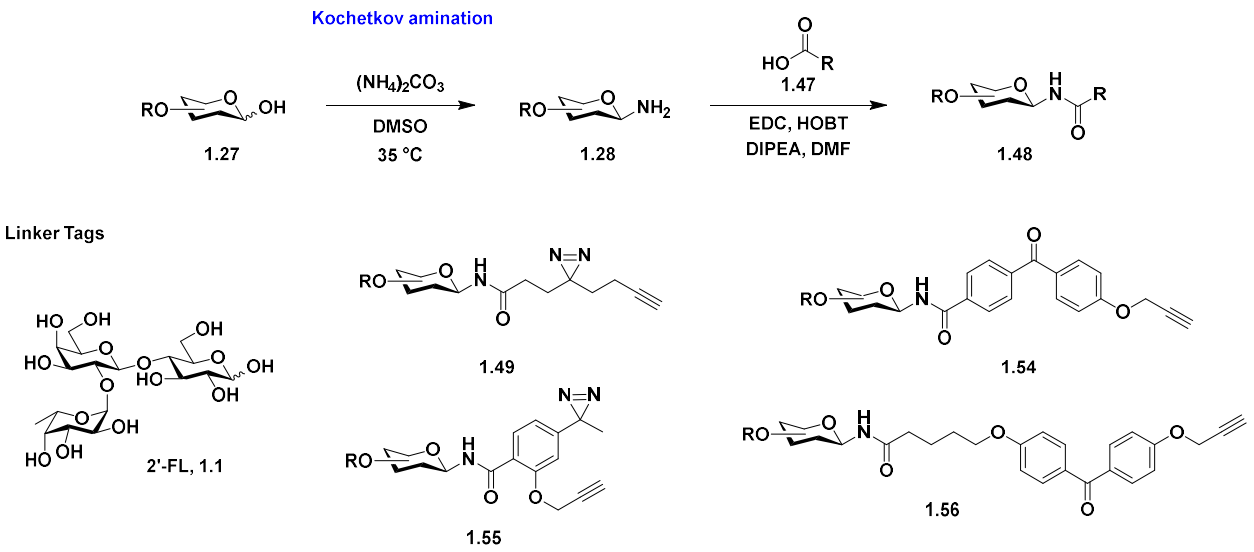

Scheme 7 Various different bioorthogonal handles were appended upon 2'-FL **1.1**.

The HMO probe library, encompassing different glycan substrates and bioorthogonal linkers, was then assessed for parent glycan biological activity retention. If the activity between the probe and parent glycan differs, the modification to install the bioorthogonal handle at the anomeric position would interrupt original macromolecule interactions, indicating that the synthesized probe would not be useful in future chemoproteomic studies. The results showed that the 2'FL and LNT probes (**1.49** and **1.50**) maintained inactivity. Of the other HMO probes assessed, the DFL and LNT-II probes (**1.51** and **1.52**) retained antibacterial activity, while the LSTa probe **1.53** lost the original parent antimicrobial activity. LSTa probe's **1.53** inactivity may indicate that sialylated HMOs undergo a different mode of action than the other HMOs assessed. These results suggest that the inactive 2'-FL and LNT probes (**1.49** and **1.50**) and antibacterial DFL and LNT-II probes (**1.51** and **1.52)** can be used in the future chemoproteomic studies to discover the cellular target identities.

With the ability to perform chemical derivatization at the reducing end of HMOs via the Kochetkov amination, a vast library of bioorthogonal probes can be synthesized to help elucidate targets within GBS during chemoproteomic studies.

1.3.3. *N*-glycan polymers capable of photolabeling specific proteins

The power of the Kochetkov amination can be seen again in creating *N*-linked glycan polymers for specific protein photo-labeling.[34] The advantage of using this method to synthesize the glycosyl amines is that it allows access to monomer units without any protecting group manipulations. In addition, the glycosyl amines can incorporate different end chains to access polymers with dual functionalities.

The Sun group recognized a global need to identify carbohydrate-binding proteins.[34] One of the biggest hindrances to synthesizing glyco-probes with multivalent sugars is ineffective crosslinking due to steric hindrance from polymer backbone and glycan components. These glyco-probes typically consist of glycopolymers with pendant glycan groups to mimic the native glycoprotein structure, and therefore function.

Since *O*-linked glycopolymers have been accessed before, the Sun group focused on identifying efficient ways to access the other most common type of glycoconjugate, those that are *N*-linked. Synthesizing *N*-linked mimics in addition to existing *O*-linked mimics is vital as the specific *N* or *O*- linkages in natural conjugates are associated with protein properties, such as stability, folding, molecular recognition, and interactions with the immune system. Therefore,

these *N*-linked glycan polymer mimics can elucidate specific protein-binding and function information.

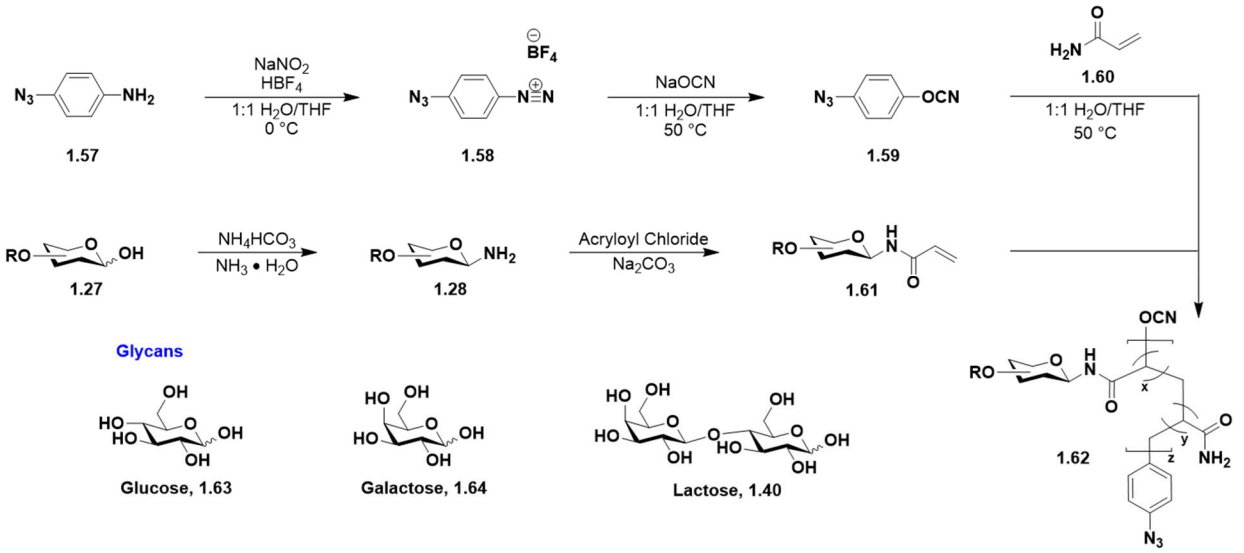

Scheme 8 Synthesis of N-linked glycopolymer mimic. Carbohydrates used are glucose, galactose and lactose.

To chemically synthesize the glycopolymers mimics, the free glycan **1.27** first undergoes a Kochetkov amination to access the glycosyl amine **1.28** (Scheme 8). After acylation, the glyco-monomer **1.61** would undergo cyanoxyl-mediated free radical polymerization (CMFRP) to synthesize the *N*-linked polymer **1.62**. CMFRP polymerization was chosen since it could be performed under aqueous conditions and, like the Kochetkov amination, does not require any protecting group manipulation.[68] With the broad tolerance of functional groups during CMFRP polymerization, this was the ideal method to synthesize the chosen glycopolymers, with the option of adding additional functionalities in future studies.

The carbohydrate units chosen for assessing the protein-specific interactions of the resulting glycopolymers are lactose (Lac, **1.40)** and its monosaccharide components, glucose (Glc, **1.63)** and galactose (Gal, **1.64)** (Scheme 8). Linkage-specific lectins and carbohydrate-specific lectins were selected for testing the protein-specific binding of the synthesized *N*-linked glycopolymers. The ability to photo-label a specific protein was assessed after UV irradiation of the *N*-glycan polymers with the protein and then confirmed with silver staining sodium dodecyl sulfate–polyacrylamide gel electrophoresis (SDS-PAGE).

For assessing the linkage-specific lectins, peanut agglutinin (PNA) from *Arachis hypogaea* was chosen for its preference for binding to β-galactose. Therefore, it performed as expected when screened against all the different polymers. Only in the presence of *N*-lactosyl polymer did PNA display any affinity, showing no binding affinity to any negative controls: acrylamide polymer, *N*-glucosyl polymer, or *N*-galactosyl polymer.

Concanavalin A, ConA from *Canavalia ensiformis*, was chosen to assess the carbohydrate-specific lectins, as ConA is a glucose-specific lectin. Indeed, when the binding affinity was assessed, only the *N*-glucosyl polymer displayed any affinity, while the other polymers showed no reactivity: acrylamide, *N*-lactosyl, and *N*-galactosyl.

In addition to evaluating the linkage and carbohydrate specificities of the lectins with multivalent polymers, the Sun group also performed competition and concentration-dependent studies with the *N*-lactosyl polymer and PNA. The competition experiment involved introducing the free lactose disaccharide before or alongside the *N*-lactosyl polymer to PNA, followed by UV irradiation. The results showed that the order of addition of the free glycan was irrelevant, each providing the same results; the lectins preferred the *N*-lactosyl polymer over the single-unit ligands. For the concentration studies, gradients of *N*-lactosyl polymer and PNA were assessed.

It was discovered that the amount of crosslinking between the glycomimics and the lectin was directly correlated to the molar ratio of the two substrates. The evidence of direct correlation points to the presence of specific interactions between the lectin and glycomimic.

Lastly, the specific reactivity of the arylazide functional group was also assessed against the chosen negative control, using arylchloride polymer mimics. Since only the arylazide showed evidence of photo-crosslinking, this further supported that the azide is highly reactive and will covalently modify only proteins close to the polymer.

With the streamlined method of transforming free glycans to the glycosyl amine via the Kochetkov amination, followed by acrylation before polymerization, these *N*-linked glycopolymers mimics can be used for specific protein labeling and functionality studies. Since the *N*-linked polymers can be further modified on the *O*-cyanate chain end group, it allows for dual functionality. One possibility is that the *N*-linked polymers can be further functionalized with biotin to enable a proteomics approach for target identification. An alternative approach would be to append a fluorophore onto the glycopolymer mimics to enable specific-protein imaging.

1.3.4. Miniaturized picomole immobilized carbohydrate assays to efficiently determine protein-binding profiles

Using the Kochetkov amination to synthesize glycosylamines is critical to Seeberger's streamlined method to synthesize immobilized glycans for miniaturized assays in high throughput screens (HTS) to determine protein-binding profiles to specific carbohydrates.[32]

In the world of glycomics, where scientists study the interactions and impact carbohydrates impart in biological pathways, one challenge that has always hindered progress was

access to pure carbohydrates. Microassays have been viewed as a reliable tool to study carbohydrate-biopolymer interactions as only picomole amounts of carbohydrates are required. While microassays have been designed before where substrates are robotically immobilized onto slides, the challenge lies in designing quicker synthetic routes to minimize loss of material.

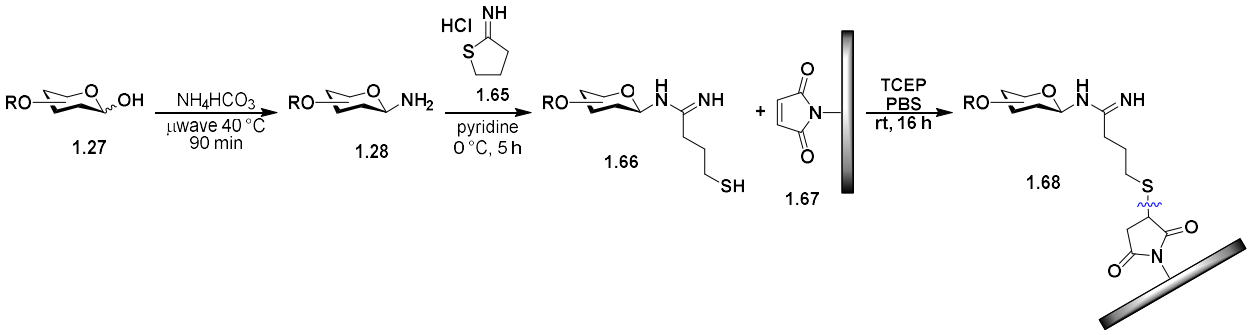

Scheme 9 Kochetkov amination is used to access glycosylamines from the parent glycans. Then after reacting with iminiothiolane to produce glycosylamidines, the glycans are immobilized onto slides.

Seeberger's method entails an introduction of the linker **1.65** to the reducing end of free glycans **1.27,** followed by immobilization of carbohydrates in three simple chemical derivatization steps, which is more efficient than previous microassays designs.[32] The method entails first subjecting the reducing sugar parent glycan **1.27** to microwave irradiation Kochetkov conditions to access glycosylamines **1.28**. Following a reaction with iminothiolane **1.65** to provide a handle at the reducing end of the carbohydrate, the tethered end is then used to immobilize samples onto maleimide-functionalized slides **1.67**. After quenching the slides with 2-mercaptoethanol, the microarrays would be incubated with fluorescently labeled lectins to develop a protein-binding profile.

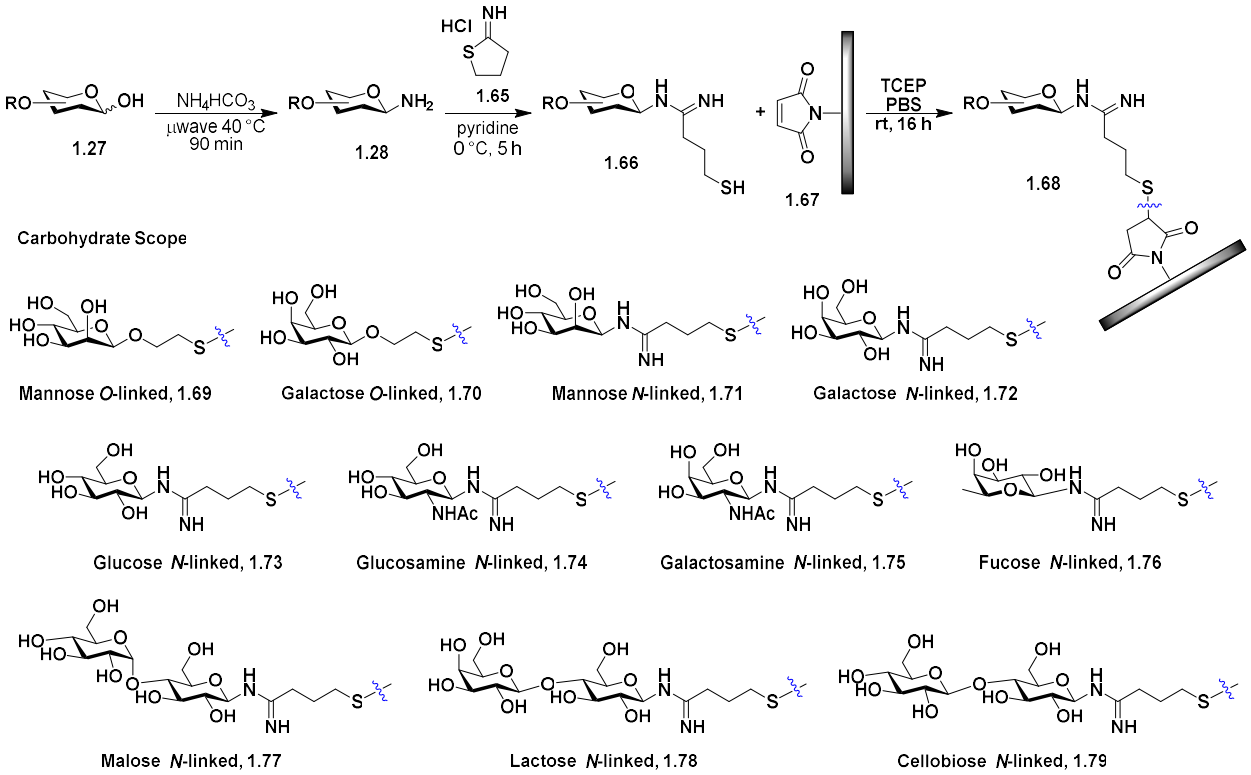

Scheme 10 Seeberger's microassay carbohydrate scope depicting glycans with *O*- and *N*-linkage.

The Seeberger lab chose to evaluate monosaccharides and disaccharides with *O* and *N*-linkers to evaluate the lectins based on linkage and carbohydrate specificities. The carbohydrates chosen were *O*-linked mannose **1.69**, *O*-linked galactose **1.70**, *N*-linked mannose **1.71**, *N*-linked glucose **1.72**, *N*-linked galactose **1.73**, *N*-linked GlcNAc **1.74**, *N*-linked GalNAc **1.75**, *N*-linked fucose **1.76**, *N*-linked maltose **1.77**, *N*-linked lactose **1.78** and *N*-linked cellobiose **1.79**.

The Seeberger method is only three steps and uses microwave conditions to synthesize glycosylamines **1.28** in just 90 minutes. When using microwave irradiation conditions, very little

diglycosylamine by-products were produced. The glycosylamines then reacted with iminiothiolane **1.65** to produce glycosylamidines **1.66** with no purification steps from the parent glycan **1.27**. With as little as 100 μg of carbohydrate sample, this approach not only streamlined the process of constructing arrays but also uses minimal amounts of material.

The lectins chosen for building a protein-binding profile were fluorescently labeled and had specific carbohydrates and linkages they were preferentially bound to. Fluorescein 5-isothiocyanate (FITC) labeled *T. vulgaris* lectin (TV) was expected to display a stronger binding affinity to GlcNAc than GalNAc, which was seen in the microarray. FITC labeled *E. crystagalli* lectin (EC) was expected to be more promiscuous, with a known ability to bind to both *O*- and *N*-linked galactose, GalNAc, and lactose. As expected, a protein-binding profile could be generated for *O*-linked galactose **1.70**, *N*-linked galactose **1.72**, *N*-linked GalNAc **1.75**, and *N*-linked lactose **1.78**. FITC labeled Concanavalin A (ConA) was assessed and expected to recognize terminal *O*-linked mannose and glucose residues. As expected, the microassay showed the fluorescently bound proteins only where the *O*-linked mannose **1.69** was located. ConA also showed a low binding affinity for *O*-linked maltose **1.77**. Interestingly, and unexpectedly, there was a slight signal for *N*-linked GlcNAc **1.74** and *N*-linked glucose **1.73.** The last lectin to be assessed was rhodamine-labeled *A. aurantia* lectin (AA), which has a known affinity to *N*-linked fucose. The microarray results did indeed show that a protein-binding profile could be generated to reflect the affinity of AA to *N*-linked fucose **1.76**.

The Seeberger research group has established a streamlined way to access carbohydrate microarrays requiring only picomoles of free glycan. Perhaps the next step would be to synthesize *S*-linked platforms to access protein-binding profiles. *S*-linked glycans are currently of interest to scientists because of their differing metabolic activity from *N*- or *O*-linked glycans. Overall, the

glycomics field can be advanced with developing this efficient assembly to study carbohydrate interactions with proteins, which can also be used with other biopolymers better to understand the roles of sugars in biological processes.

1.4. Kochetkov amination enabled synthesis of β-amino human milk oligosaccharides to interrogate antibiofilm activity

The biological applications shown above all used the Kochetkov amination to access glycosylamines as intermediates, which were then used to synthesize a more complex target (EPO), various probes, glycomimics, and microassays. The upcoming section dictates this dissertation's current work of optimizing and using the Kochetkov amination to access complex β-amino derivatives of prebiotic human milk oligosaccharides. After accessing these β-amino derivatives, this dissertation will evaluate the perturbations these new compounds have on the biofilm formation of S. *agalactiae* GB00590 and methicillin-resistant *Staphylococcus aureus* (MRSA).

1.4.1. Optimization of Kochetkov amination to access β-amino glycans

Even though the Kochetkov amination is considered the state-of-the-art method to synthesize β -amino glycans, the reaction is not without complications.[35] The mechanism for the Kochetkov amination was shown in **Error! Reference source not found.** and again below in Scheme 11 for ease of reference. For a brief overview, the Kochetkov amination involves HMO parent glycan, which exists in equilibrium between the ring-closed state **1.3** and the open-chain state **1.5**. After condensation of ammonia to provide the imine intermediate **1.6**, ring closure provides βA-HMO **1.4**.

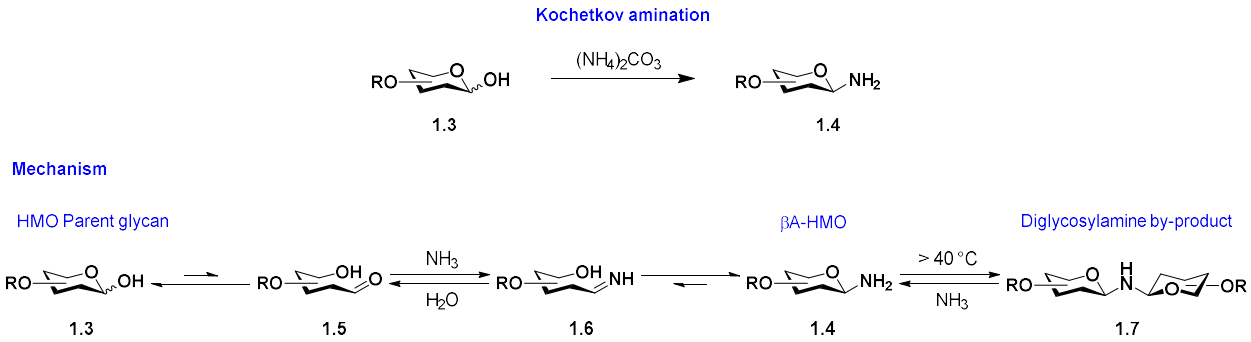

Scheme 11 Kochetkov amination mechanism

First, while the reaction does produce the β-glycosyl amine **1.4**, the product exists in equilibrium with both reducing sugar anomers of the parent glycan **1.3**. Second, the reaction traditionally requires excess ammonium salt of around 50 equivalents, complicating purification. Lastly, since the reaction generally requires long reaction times (e.g., 48 to 120 hours), elevated temperatures have been employed to increase the reaction rate. However, when monosaccharides are used, increasing temperatures also yield an increase in diglycosylamino by-products **1.7**. Microwave irradiation conditions has been employed for the Kochetkov amination in hopes to reduce byproduct formation.[69-70] Contrary to thermal conditions, microwave irradiation requires only 5-fold excess of an ammonium salt and generally proceeds to equilibrium within an hour at 50 ºC.[71-72] Additionally, microwave irradiation suppresses formation of dimerized byproducts, even with monosaccharide starting materials. While microwave irradiation has proven useful in Kochetkov amination reactions of monosaccharides, the reaction conditions were not amenable for carbohydrates that are disaccharides or larger. The Seeberger lab yielded only 17% of the β -amino cellobiose when the parent disaccharide underwent microwave mediated Kochetkov conditions.[29]

The present study commenced with determining the ideal conditions to achieve Kochetkov amination on complex oligosaccharides, specifically using 2'-FL **1.1**, as a model substrate, one of the most common HMOs found in human breast milk (Table 1).

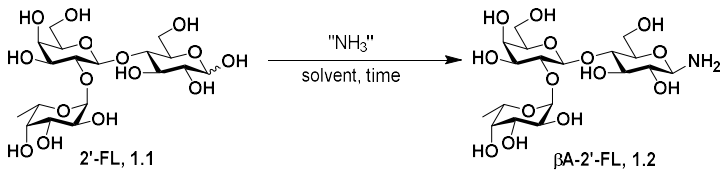

Table 1 Evaluation of the Kochetkov amination on 2'-FL, **1.1**.

	NH_3 Source	NH_3 Source Fold-Excess	Solvent	Time	Ratio[d] **1.1: 1.2**
1[a]	$(NH_4)_2CO_3$	5	CH_3OH	1 h	1 : 2
2[a]	$(NH_4)HCO_3$	5	CH_3OH	1 h	1 : 0.6
3[a]	NH_4Cl	5	CH_3OH	1 h	1 : 0
4[b]	NH_3/CH_3OH	3	CH_3OH	1 h	1 : 0
5[a]	$(NH_4)_2CO_3$	5	DMSO	1 h	1 : 2.7
6[c]	$(NH_4)_2CO_3$	5	DMSO	48 h	1 : 2.2
7[c]	$(NH_4)_2CO_3$	5	H_2O	48 h	1 to 0.6
8[c]	$(NH_4)_2CO_3$	5	CH_3OH	48 h	1 : 4.7

[a] Reaction conditions**:** HMO **1.1** (1.0 equiv., 0.2 mmol) and ammonia source (amount of fold-excess) were placed into a microwave vial and diluted with solvent (2.5 mL). The microwave vial was sealed and irradiated for 1 h at 200 W and 50°C. After cooling to ambient temperature, the reaction mixture was lyophilized to dryness, providing the βA-HMO **1.2**, which was used without further purification. [b] Reaction follows the same general procedure but 7N NH_3 in CH_3OH is used as the solvent. [c] Reaction follows the same general procedure but is heated thermally at 40 °C for 48 h. [d] Ratio was calculated according to Table 2, located in the SI.

Microwave and thermal mediated reaction conditions were compared in addition to ammonium salt sources. Beginning with microwave mediated reactions, we first employed ammonium carbonate ($(NH_4)_2CO_3$) as the ammonia source. In this reaction, we observed that conversion of 2'-FL **1.1** to its amino sugar **1.2**, occurred in 1:2 selectivity (Table 1, entry 1). Interestingly, both longer (3 h) and shorter (5 min) reaction times did not enhance the yield of the system. When the ammonia source was changed to ammonium bicarbonate $(NH_4)HCO_3$, ammonium chloride NH_4Cl, and a solution of ammonia in methanol (Table 1, entries 2-4), it was observed that none of the systems provided superior results. Our investigation of microwave mediated reaction conditions ended with focusing on entry 1 and exchanging solvents from methanol to dimethylsulfoxide (DMSO). Interestingly, the change in reaction conditions provided an increased conversion to 1:2.7 of starting material to product (Table 1, entry 5).

Since conversion of 2'-FL **1.1** to its β -amine **1.2** was generally low under all conditions examined, our next point of investigation was a thermal reaction. Contrary to standard conditions that employ 50 to 100 molar equivalents or even 40-fold mass equivalents of ammonium salt, we used only 5-fold excess in the reaction, which means that we used 5 times the HMO mass.[73] The ammonia source chosen was $(NH_4)_2CO_3$ as it provided the highest conversion under microwave irradiation conditions. The thermal reactions stirred for 48 h at 40 ^oC and three solvents were evaluated (DMSO, water, and methanol). A lower temperature was chosen for thermal conditions compared to microwave ones to mitigate diglycosylamine byproduct formation. DMSO provided a similar result thermally as it did under microwave irradiation (Table 1, entry 6, 1:2.2 ratio). Using water as the solvent decreased productivity of the reaction (Table 1, entry 7, 1:0.6 ratio). In an interesting development, using methanol as the solvent provided an increased conversion to 1:4.7 of starting material to product (Table 1, entry 8).

1.4.2. Synthesis of βA-HMO Substrate Scope

Next, we sought to evaluate the effectiveness and robustness of the optimized reaction conditions on additional HMOs that would be used in the biological assays. The additional HMOs were chosen to enable facile evaluation of βA-HMO antibiofilm activity.

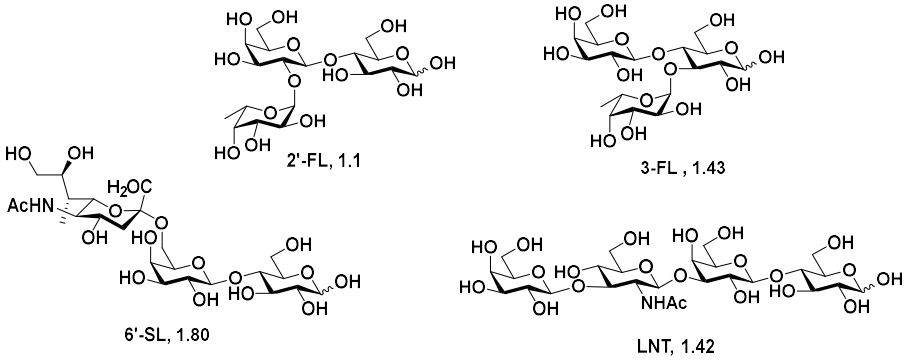

Figure 11 Scope of HMOs to undergo the Kochetkov amination.

First, we evaluated HMOs with structural features different from that of 2'-FL **1.1**, i.e., more steric bulk near the reducing end, acidic residues, or longer chains. Second, we evaluated HMOs that had shown no antimicrobial or antibiofilm activity in previous screens.[22-23] Based on these criteria, we selected the following HMOs as parent glycans: 2'-fucosyllactose (2'-FL, **1.1)**, 3-fucosyllactose (3-FL, **1.43**), 6'-sialyllactose (6'-SL, **1.80**), and lacto-*N*-tetraose (LNT, **1.42**) (Figure 11).

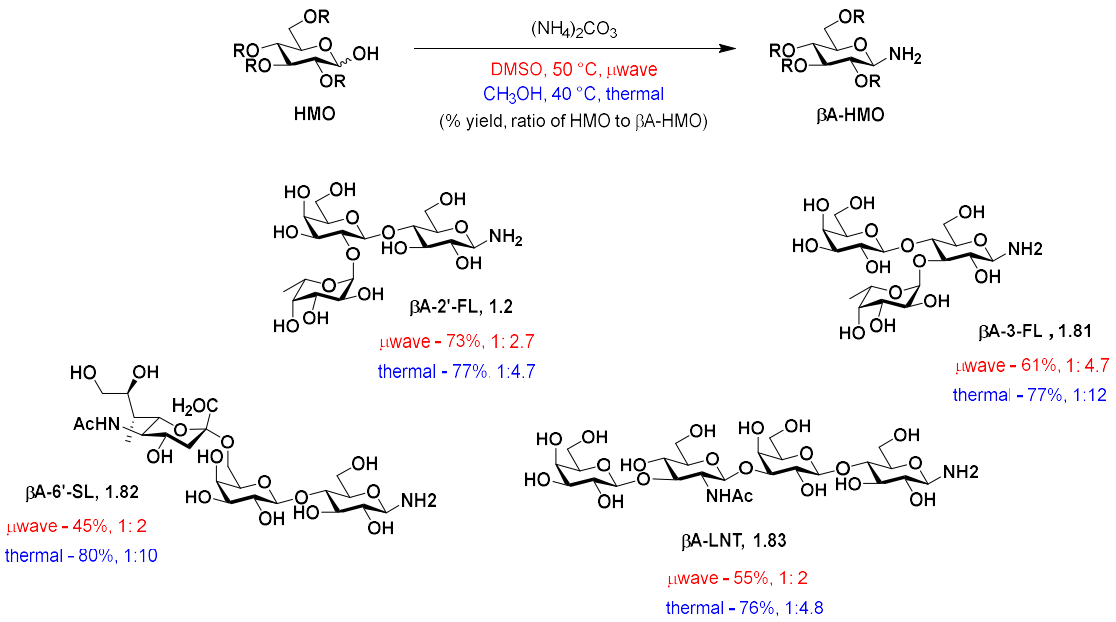

Scheme 12 Synthesis of βA-HMOs). Anomeric proton shifts used to calculate the ratio are reported in the SI (Table 2).

As seen in Scheme 12, each HMO was converted to its β-amine under both thermal (blue) and optimized microwave (red) conditions (Scheme 12). In general, complex oligosaccharides are converted to their amino sugars with superior yields under thermal conditions in methanol. While purification was not a necessary step in conversion to the βA-HMOs, the loss of product mass can be explained in three ways: transfer of product to conical tubes between sequential lyophilization, escaping the vial through permeabilization through Kimwipe barrier during lyophilization, or hydrated starting material HMOs elevating the initial mass.

1.4.3. βA-HMO Antibacterial Assay Results

With the βA-HMOs in hand, we moved to evaluate their antimicrobial and antibiofilm properties against GBS (strain GB00590) and *S. aureus* (MRSA, strain USA300). Antimicrobial

activity was assessed by monitoring bacterial growth in the presence of each carbohydrate over 24 h, while antibiofilm activity was assessed by evaluating biofilm production levels at 24 h. Importantly, biofilm levels were expressed as ratios of biofilm to biomass to account for any accompanying antimicrobial activity. Growth and biofilm trends for each βA-HMO were compared to those of their respective parent HMOs as well as those of bacteria grown in the absence of HMO additive. For all assays, HMO additives (βA-HMO and natural HMOs) were dosed at the lower end of physiological HMO concentrations, ca. 5 mg/mL.[18, 67] The βA-HMOs were added as a mixture of starting material HMO and βA-HMO product in the ratio as reported in (Scheme 12). Moreover, previous work from our lab has shown that this concentration of parent HMO is non-lethal for GBS and *S. aureus* thus ensuring our ability to evaluate compounds for antibiofilm activity.[19, 74]

As expected, based on our prior studies with parent HMOs and βA-2'-FL **1.2** that showed no evidence of antimicrobial activity against GBS, none of the βA-HMOs used in the present study significantly inhibited GBS growth at any time point (Figure 12 A). Moreover, similar results were observed in *S. aureus* as none of the HMO additives were found to significantly inhibit *S. aureus* growth at any point in 24 h (Figure 12 B).

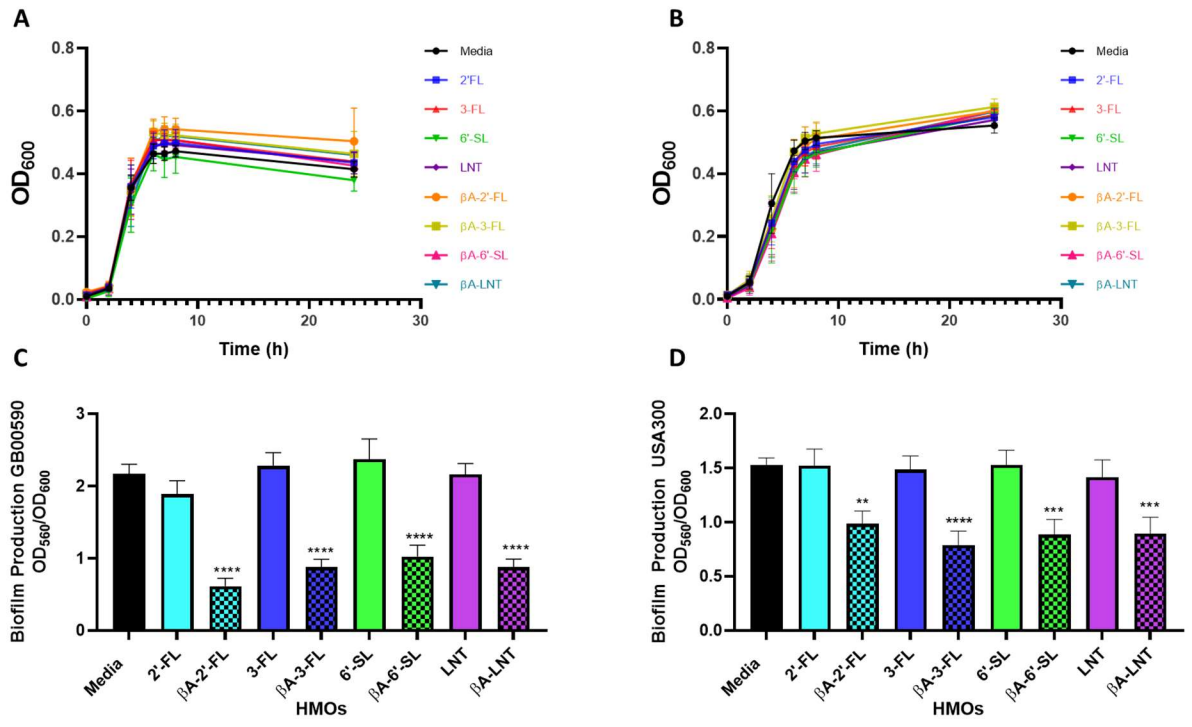

Figure 12 Evaluation of HMOs and (βA-HMO) dosed at ca. 5 mg/mL on S. agalactiae (GB00590) and S. aureus (USA300). Growth was quantified via OD600 readings at 0, 2, 4, 6, 7, 8, and 24 hours. Mean OD600 for each time point is indicated by the corresponding symbols. Biofilm was quantified via OD560 readings at 24 h. Biofilm production is expressed as a ratio of biofilm/biomass (OD560/OD600). Growth of GB00590 (A) and USA300 (B) in the presence of parent HMOs and βA-HMOs. Biofilm production of GB00590 (C) and USA300 (D) in the presence of parent HMOs and βA-HMOs. Data displayed represent the relative mean growth or biofilm/biomass ratios ± SEM of three independent experiments, each with three technical replicates. Statistical analysis was performed in (C) and (D) in which **** represents $p < 0.0001$, *** represents $p = 0.0010$, and ** represents $p = 0.0081$ by one-way ANOVA, with post hoc Dunnett's multiple comparison test comparing biofilm production of HMO supplemented conditions to biofilm production in either GB00590 or USA300 in HMO-free THB media.

However, in terms of antibiofilm activity, it was gratifyingly to observe that while no parent HMOs exhibited antibiofilm activity, all βA-HMOs significantly inhibited biofilm production in both GBS and *S. aureus* (Figure 12 C and D). Remarkably, βA-HMOs decreased biofilm production in GBS and *S. aureus* by an average of 62% and 42%, respectively. Also notable is the observation that all βA-HMOs reduced GBS and *S. aureus* biofilm production to

similar extents despite their structural differences. This finding supports our hypothesis that chemical derivatization of HMOs at the anomeric position can impart antibiofilm activity to otherwise inert compounds.

1.4.4. High resolution FEG-SEM imaging to analyze βA-HMO impact on biofilm formation

High resolution field emission gun scanning electron microscope (FEG-SEM) analyses were employed to investigate the effect prebiotic β-amino HMO derivatives have on perturbating bacterial biofilm formation. Since all βA-HMOs reduced GBS and *S. aureus* biofilm production by similar amounts, βA-2'-FL **1.2**, βA-3-FL **1.81**, and βA-6'-SL **1.82**, were chosen for the imaging experiments based on ease of access to the parent glycans. Our analyses revealed that *S. agalactiae* GB00590 adhered to the surface of the coverslip and formed colonies of bacterial cells (Figure 13). The observed colonies showed bacterial cells stacked in clumps with defined tertiary architecture, which we have defined in previous studies as a criterion for biofilm formation.[75-77]

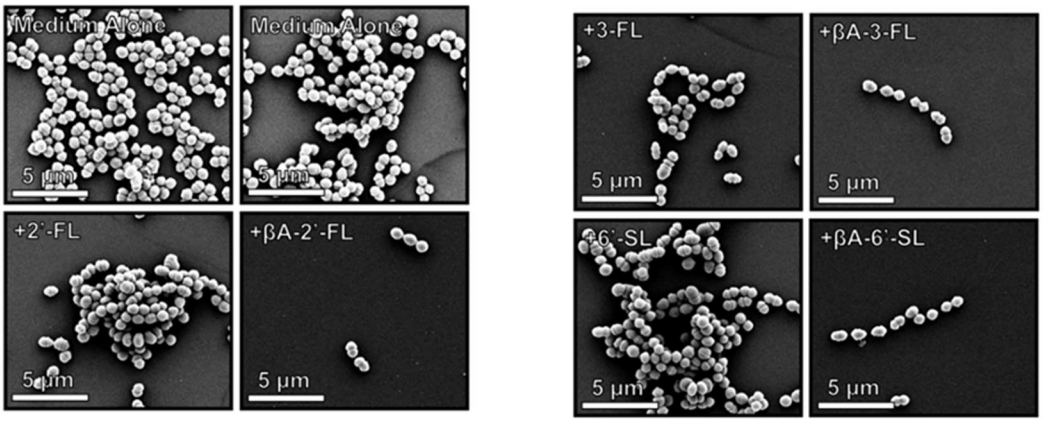

Figure 13 High resolution field-emission gun scanning electron microscopy analyses of S. agalactiae strain GB00590 bacterial biofilm formation. FEG-SEM imaging of bacterial biofilms were performed on GBS samples grown in medium alone (Medium Alone), or medium supplemented with 2'-FL **1.1** (+2'-FL), βA-2'-FL **1.2** (+βA-2'-FL), 3-FL **1.43** (+3-FL), βA-3-FL **1.81** (+βA-3-FL), 6'-SL **1.80** (+6'-SL), or βA-6'-SL **1.82** (+βA-6'-SL). The addition of β-amino variants significantly inhibits GBS biofilm formation. Micrographs were collected at 20,000x magnification and magnification bars indicate 5 µm.

The addition of the parent compounds 2'-FL **1.1** or 6'-SL **1.80** did not significantly alter bacterial cell adherence to the abiotic substrate, nor did it alter the ability of GBS bacterial cells to stack on top of each other to form biofilms. Interestingly, the addition of parent prebiotic 3-FL **1.43** did not impact bacterial adherence to the coverslip, but it was correlated with a slight decrease in biotic adherence between bacterial cells to form the tertiary architecture of the biofilm. But interestingly, the addition of all β-amino derivatives βA-2'-FL **1.2**, βA-3-FL **1.81** and βA-6'-SL **1.82** resulted in a significant inhibition of bacterial adherence to the coverslip and abolished the ability of GB00590 to form biofilms (Figure 13).

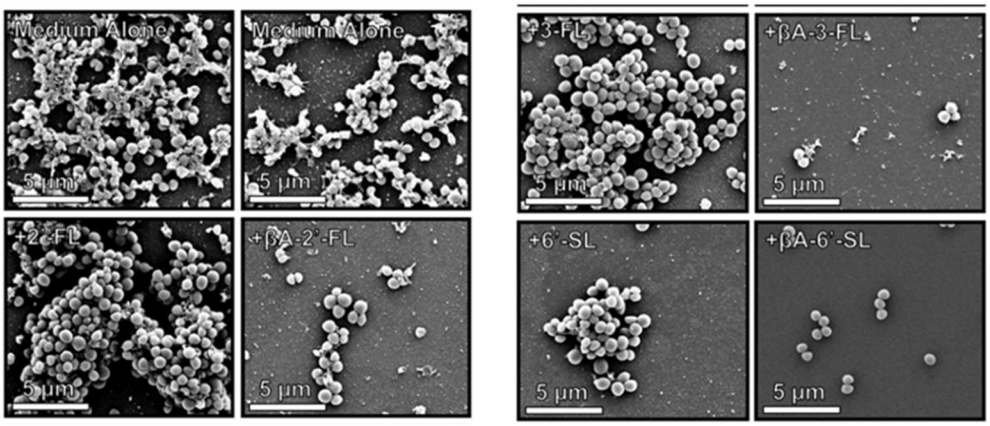

Figure 14 High resolution field-emission gun scanning electron microscopy analyses of S. aureus strain USA300 bacterial biofilm formation. FEG-SEM imaging of bacterial biofilms were performed on USA300 samples grown in medium alone (Medium Alone), or medium supplemented with 2'-FL **1.1** (+2'-FL), βA-2'-FL **1.2** (+βA-2'-FL), 3-FL **1.43** (+3-FL), βA-3-FL **1.81** (+βA-3-FL), 6'-SL **1.80** (+6'-SL), or βA-6'-SL **1.82** (+βA-6'-SL). . The addition of β-amino variants significantly inhibits USA300 biofilm formation. Micrographs were collected at 20,000x magnification and magnification bars indicate 5 µm.

Similar to our results in GB00590, our analyses revealed that *S. aureus* USA300 adhered to the coverslip and formed biofilms (Figure 14). The observed USA300 biofilms were characterized by the presence of a fibrous and globular extracellular matrix as has been previously seen (Figure 14). [75-77] The addition of parent glycans 2'-FL **1.1** or 3-FL **1.43** did not significantly alter bacterial cell adherence to the abiotic substrate, nor did it alter the ability of the bacterial cells to stack on top of each other to form biofilms. Interestingly, the addition of parent prebiotic 6'-SL **1.80** did not impact bacterial adherence to the coverslip, but the concentration of 6'-SL **1.80** added correlated with a slight decrease in bacterial aggregates, in terms of both the size and number. But, interestingly, the addition of the βA-HMOs (βA-2'-FL **1.2**, βA-3-FL **1.81** and βA-

6'-SL **1.82**) resulted in a significant inhibition of bacterial adherence to the coverslip and abolished the ability of USA300 to form biofilms.

The addition of the β-amino derivatives to both *S. aureus* and GBS resulted in significant abrogation of biofilm formation as determined by quantitative colorimetric assays and high-resolution SEM analyses. Previous work by our lab has demonstrated that other glycosides (such as synthetic ellagic acid) also have the capability to inhibit early stage adhesion during bacterial biofilm formation.[75]

1.5. Conclusion

To conclude, we have applied a thermal mediated and optimized microwave irradiation conditions on prebiotic HMOs to undergo the Kochetkov amination to enable access to βA-HMOs that show anti-biofilm activity across two gram-positive test strains. The addition of the βA-HMOs, as determined by FEG-SEM, revealed a significant inhibition of bacterial surface adherence and disrupts the ability of bacteria to form biofilms. An evaluation of genetic changes that occur when microbes engage βA-HMOs, and the spectrum of microbes that are susceptible to these interesting molecules will be reported in due course.

1.6. Materials and Methods

1.6.1. Materials

All reactions were performed in a microwave compatible vial. The reagents and solvents were purchased from commercial sources and were used as received unless mentioned otherwise. 2'-fucosyllactose, 3-fucosyllactose, and 6'-siallylactose were purchased from Carbosynth. Lacto-*N*-tetraose (LNT) was synthesized as previously described.[78]

1.6.2. Instrumentation

The MW experiments were conducted in a closed reaction vessel using an Anton Paar G10 Monowave 200 (8.0 mL microwave vial), capped with reusable snap caps and silicon-Teflon septa. All reactions were irradiated for 1 h at 200 W and 50 °C. ^{1}H NMR spectra were obtained on a Bruker 600 MHz spectrometer and are reported relative to deuterated solvent signals. Data for ^{1}H NMR spectra are presented as follows: chemical shift (δ ppm), multiplicity (s = singlet, d = doublet, t = triplet, q = quartet, p = pentet, m = multiplet, br = broad, app = apparent), coupling constants (Hz) and integration. Deuterated methanol was standardized to 3.31 ppm. ^{13}C NMR spectra were obtained on a Bruker 151 MHz spectrometer and are reported relative to deuterated solvent signals. Deuterated methanol was standardized to 49.0 ppm. Structural assignments were made with additional information from gHSQC experiments. High-resolution mass spectra (HRMS) were obtained from the Department of Chemistry, Vanderbilt University using a Synapt G2-S HDMS TOF (Milford, Ma, USA) mass spectrometer.

1.6.3. Microwave Activated Kochetkov Amination Procedure

HMO (0.1 mmol) was dissolved in reaction solvent (2 mL), ammonia source (5 x mass of HMO) was added, and the reaction was irradiated for 1 h at 200 W and 50°C. The reaction mixture was diluted to 45 mL with water in a 50 mL conical centrifuge tube, frozen with liquid nitrogen, and lyophilized repeatedly until a constant mass of white solid was obtained. Ratio of conversion was determined by integration of the C-1 anomeric protons of the starting material to that of the desired product (Table 2).

1.6.4. Thermally Activated Kochetkov Amination Procedure

HMO (0.1 mmol) was dissolved in reaction solvent (2 mL), ammonia source (5 x mass of HMO) was added, and the reaction warmed for 48 h at 40°C in an oil bath. The heating medium was silicone oil purchased from Sigma-Aldrich (St. Louis, MO, USA) and was carried out in a Pyrex® crystalizing dish. The reaction mixture was diluted to 45 mL with water in a 50 mL conical centrifuge tube, frozen with liquid nitrogen, and lyophilized repeatedly until a constant mass of white solid was obtained. Ratio of conversion was determined by integration of the C-1 anomeric protons of the starting material to that of the desired product (Table 2).

1.6.5. Compound characterization

(2*S*,3*S*,4*R*,5*S*,6*S*)-2-(((2*S*,3*R*,4*S*,5*R*,6*R*)-2-(((2*R*,3*S*,4*R*,5*R*)-6-amino-4,5-dihydroxy-2-(hydroxymethyl)tetrahydro-2*H*-pyran-3-yl)oxy)-4,5-dihydroxy-6-

(hydroxymethyl)tetrahydro-2*H*-pyran-3-yl)oxy)-6-methyltetrahydro-2*H*-pyran-3,4,5-triol (**1.2**, βA-2'-FL): White solid, 37 mg, 77%, 1:4.7 ratio of HMO:βA-HMO; Spectral data for **1.2** was consistent with known values.[15]

(2*S*,3*S*,4*R*,5*S*,6*S*)-2-(((3*R*,4*R*,5*R*,6*R*)-2-amino-3-hydroxy-6-(hydroxymethyl)-5-(((2*S*,3*R*,4*S*,5*R*,6*R*)-3,4,5-trihydroxy-6-(hydroxymethyl)tetrahydro-2*H*-pyran-2-yl)oxy)tetrahydro-2*H*-pyran-4-yl)oxy)-6-methyltetrahydro-2*H*-pyran-3,4,5-triol (**1.81**, βA-3-FL): White solid; 42 mg, 86%, 1:12 ratio of HMO:βA-HMO; R_f 0.15 (60 : 30 : 5 : 5 $CHCl_3$: CH_3OH : AcOH : H_2O); **^{1}H NMR** (600 MHz, MeOD): δ 5.42 (d, *J* = 3.9 Hz, 0.92H), 4.84 – 4.78 (m, 2.33H), 4.40 (d, *J* = 7.3 Hz, 1.02H), 3.97 (d, *J* = 8.7 Hz, 1.09H), 3.94 (dd, *J* = 10.2, 3.4 Hz, 1.38H), 3.92 – 3.65 (m, 13.23H), 3.53 – 3.42 (m, 4.29H), 3.38 (dt, *J* = 9.8, 3.1, 3.1 Hz, 1.05H), 3.28 (t, *J* = 8.8, 8.8 Hz, 1.01H), 1.20 – 1.18 (m, 3H);**^{13}C NMR** (150 MHz, MeOD): δ 102.4, 98.9, 85.5, 78.9, 77.2, 76.4, 75.3, 73.5, 73.1, 72.4, 71.5, 69.8, 69.5, 69.0, 68.6, 66.0, 61.5, 39.1, 15.2; **IR** (ATR) ν = 3344, 3099, 2978, 1617, 1490 cm^{-1}; **HR-ESI-MS** (m/z): calcd for $C_{18}H_{32}NO_{14}^-$ $(M-H)^-$ 486.1823, found 486.1816.

(2*R*,4*S*,5*R*,6*R*)-5-acetamido-2-(((2*R*,3*R*,4*S*,5*R*,6*S*)-6-(((2*R*,3*S*,4*R*,5*R*)-6-amino-4,5-dihydroxy-2-(hydroxymethyl)tetrahydro-2*H*-pyran-3-yl)oxy)-3,4,5-trihydroxytetrahydro-2*H*-pyran-2-yl)methoxy)-4-hydroxy-6-((1*R*,2*R*)-1,2,3-trihydroxypropyl)tetrahydro-2*H*-pyran-2-carboxylic acid (**1.82**, βA-6'-SL): White solid; 50 mg, 80%, 1:10 ratio of HMO:βA-HMO; R_f 0.10 (60 : 30 : 5 : 5 $CHCl_3$: CH_3OH : AcOH : H_2O); **^{1}H NMR** (600 MHz, MeOD): δ 5.13 (d, *J* = 3.7 Hz, 0.51H), 4.53 (d, *J* = 7.9 Hz, 0.62H), 4.37 – 4.32 (m, 2.21H), 4.05 (dq, *J* = 10.1, 7.6, 7.4, 7.4 Hz, 2.34H), 4.01 (d, *J* = 8.6 Hz, 1.00H), 3.94 – 3.76 (m, 14.65H), 3.76 – 3.71 (m, 2.36H), 3.72 –

3.61 (m, 9.14H), 3.59 – 3.49 (m, 8.46H), 3.50 – 3.42 (m, 4.23H), 3.28 – 3.22 (m, 0.60H), 3.17 – 3.12 (m, 0.86H), 2.81 (dtd, *J* = 12.4, 5.6, 5.1, 2.8 Hz, 2.24H), 2.04 – 2.00 (m, 6.72H), 1.71 – 1.63 (m, 2.18H); **^{13}C NMR** (150 MHz, MeOD): δ 173.6, 173.1, 103.8, 100.1, 96.5, 85.1, 80.4, 80.3, 76.2, 75.6, 75.1, 74.8, 74.7, 74.4, 73.2, 72.8, 71.8, 71.0, 69.9, 69.2, 68.8, 68.4, 63.3, 63.1, 60.9, 52.4, 41.1, 39.0, 21.4; **IR** (ATR) ν = 3489, 3002, 2978, 1725, 1627, 1490 cm^{-1}; **HR-ESI-MS** (m/z): calcd for $C_{23}H_{39}N_2O_{18}^-$ $(M-H)^-$ 632.2276, found 632.2270.

***N*-((2*S*,3*R*,4*R*,5*S*,6*R*)-2-(((2*S*,3*R*,4*S*,5*S*,6*R*)-2-(((2*R*,3*S*,4*R*,5*R*)-6-amino-4,5-dihydroxy-2-(hydroxymethyl)tetrahydro-2*H*-pyran-3-yl)oxy)-3,5-dihydroxy-6-(hydroxymethyl)tetrahydro-2*H*-pyran-4-yl)oxy)-5-hydroxy-6-(hydroxymethyl)-4-(((2*R*,3*R*,4*S*,5*R*,6*R*)-3,4,5-trihydroxy-6-(hydroxymethyl)tetrahydro-2*H*-pyran-2-yl)oxy)tetrahydro-2*H*-pyran-3-yl)acetamide** (**1.83**, βA-LNT): White solid; 54 mg, 76%, 1:4.8 ratio of HMO:βA-HMO; Spectral data for **1.83** was consistent with known values.[28]

1.6.6. Bacterial Strains and Culture Conditions

S. agalactiae strain GB00590 is a clinical isolate provided by Dr. Shannon Manning at Michigan State University. *S. aureus* strain USA300 is the laboratory-adapted strain USA300 JE2; USA300 JE2 is derived from the parental community-associated methicillin-resistant *S. aureus* isolate USA300. All strains were grown on tryptic soy agar plates supplemented with 5% sheep blood (blood agar plates) at 37 °C in ambient air overnight. Strains were subcultured from blood agar plates into 5 mL of Todd-Hewitt broth (THB) and incubated under shaking conditions at 180 rpm at 37 °C in ambient air overnight. Following overnight incubation, bacterial density was

quantified through absorbance readings at 600 nm (OD_{600}) using a Promega GloMax-Multi Detection System plate reader. Bacterial numbers were determined using the predetermined coefficient of 1 OD_{600} = 10^9 CFU/mL.

1.6.7. Bacterial Growth Assays

Bacterial strains were grown overnight as described above and used to inoculate fresh THB at a multiplicity of infection (MOI) of 10^6 colony forming units per 200 µL of growth medium in 96 well tissue culture treated, sterile polystyrene plates (Corning, Inc). HMOs and βA-HMOs were dissolved in deionized water to achieve a concentration of 80 mg/mL and filtered through a 0.2 µm syringe filter. HMOs or βA-HMOs were added to achieve a final carbohydrate concentration of ca. 5 mg/mL. Bacteria grown in THB in the absence of any HMOs served as the control. Cultures were grown under static conditions at 37 °C in ambient air for 24 h. Growth was quantified through spectrophotometric reading at OD_{600} with readings taken at 0, 2, 4, 6, 7, and 8 hours then a final reading at 24 hours.

1.6.8. Bacterial Biofilm Assays

Bacterial strains were grown overnight as described above and used to inoculate fresh THB at a multiplicity of infection (MOI) of 10^6 colony forming units per 200 µL of growth medium in 96 well tissue culture treated, sterile polystyrene plates (Corning, Inc.). HMOs and βA-HMOs were dissolved in deionized water to achieve a concentration of 80 mg/mL and filtered through a 0.2 µm syringe filter. HMOs or βA-HMOs were added to achieve a final carbohydrate

concentration of ca. 5 mg/mL. Bacteria grown in THB in the absence of any HMOs served as the control. Cultures were incubated under static conditions at 37 °C in ambient air for 24 h. Bacterial growth was quantified through absorbance readings at an optical density of 600 nm (OD_{600}). Following growth quantification, the culture medium was removed, and wells were washed gently with phosphate buffered saline (PBS, pH 7.4) to remove nonadherent cells. The remaining biofilms were stained with a 10% crystal violet solution for 10 min. Following staining, wells were washed with PBS and allowed to dry at room temperature for at least 30 min. The remaining crystal violet stain was solubilized with 200 μL of 80% ethanol/20% acetone solution. Biofilm formation was then quantified through absorbance readings at an optical density of 560 nm (OD_{560}). Results are expressed as biofilm/biomass ratios (OD_{560}/OD_{600}).

1.6.9. High resolution field-emission gun scanning electron microscopy (FEG-SEM) analyses

Bacterial biofilms were analyzed via FEG-SEM as previously described. [75-77] Briefly, bacterial cells were cultured in biofilms adhering to glass coverslips coated with poly-L-lysine overnight in the culture conditions described above. HMOs and βA-HMOs were dissolved in deionized water to achieve a concentration of 80 mg/mL and filtered through a 0.2 μm syringe filter. HMOs or βA-HMOs were added to achieve a final carbohydrate concentration of ca. 5 mg/mL. The following day, bacterial cells were fixed in a solution of 2.5% glutaraldehyde, 2.0% paraformaldehyde, and 0.05 M sodium cacodylate buffer pH 7.4. Samples were dehydrated with sequential washes of increasing concentrations of ethanol before being subjected to critical point drying, mounting on aluminum stubs, and sputter coating with 20 nm of gold-palladium. Samples were viewed using an FEI Quanta 250 field-emission gun scanning electron microscope at 5 kEV with a spot size of 2.5.

1.6.10. Statistical Analysis

All data shown signify three independent experiments each with three technical replicates. Data are expressed as the mean ± SEM. Statistical analyses were performed in GraphPad Prism Software v. 8.2.1. Statistical significance for growth was determined using two-way ANOVA with *post hoc* Dunnett's multiple comparison test comparing growth in the presence of HMOs or βA-HMOs to growth in media alone. Statistical significance for biofilm production was determined using one-way ANOVA with *post hoc* Dunnett's multiple comparison test comparing biofilm production in the presence of HMOs or βA-HMOs to biofilm production in media alone.

1.7. Relevant Spectra

^{1}H NMR (600 MHz, MeOD) spectra of **1.2**

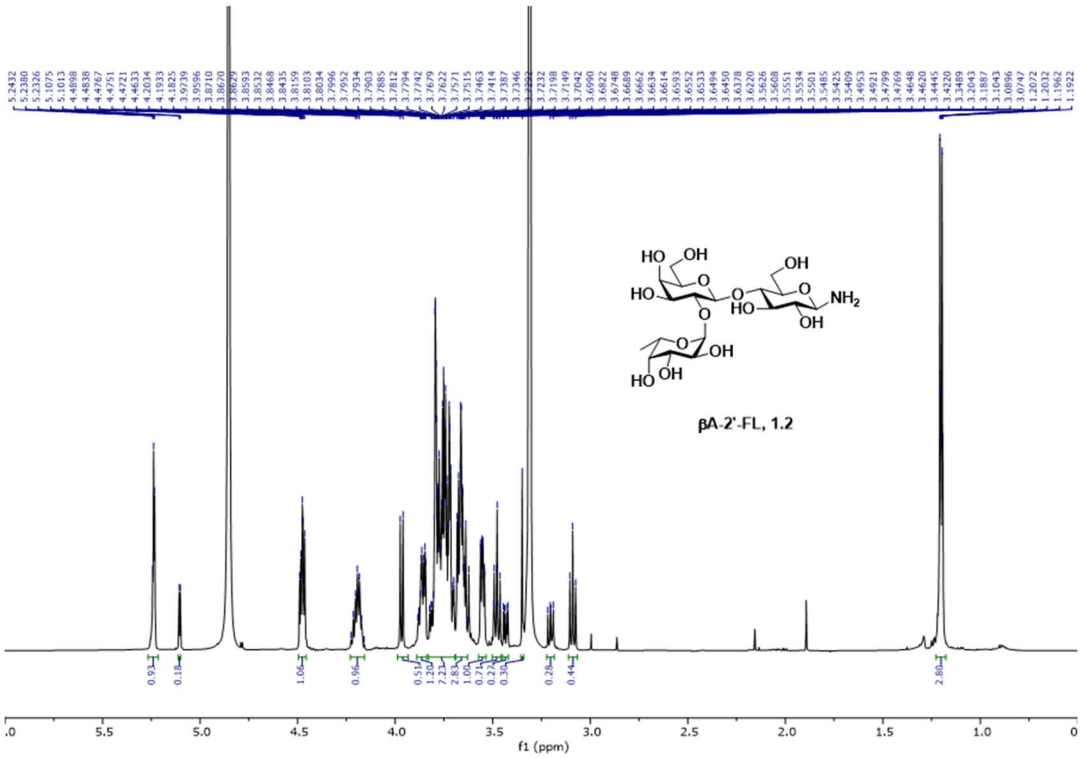

^{1}H ^{13}C HSQC NMR (600 MHz, MeOD) spectra of **1.2**

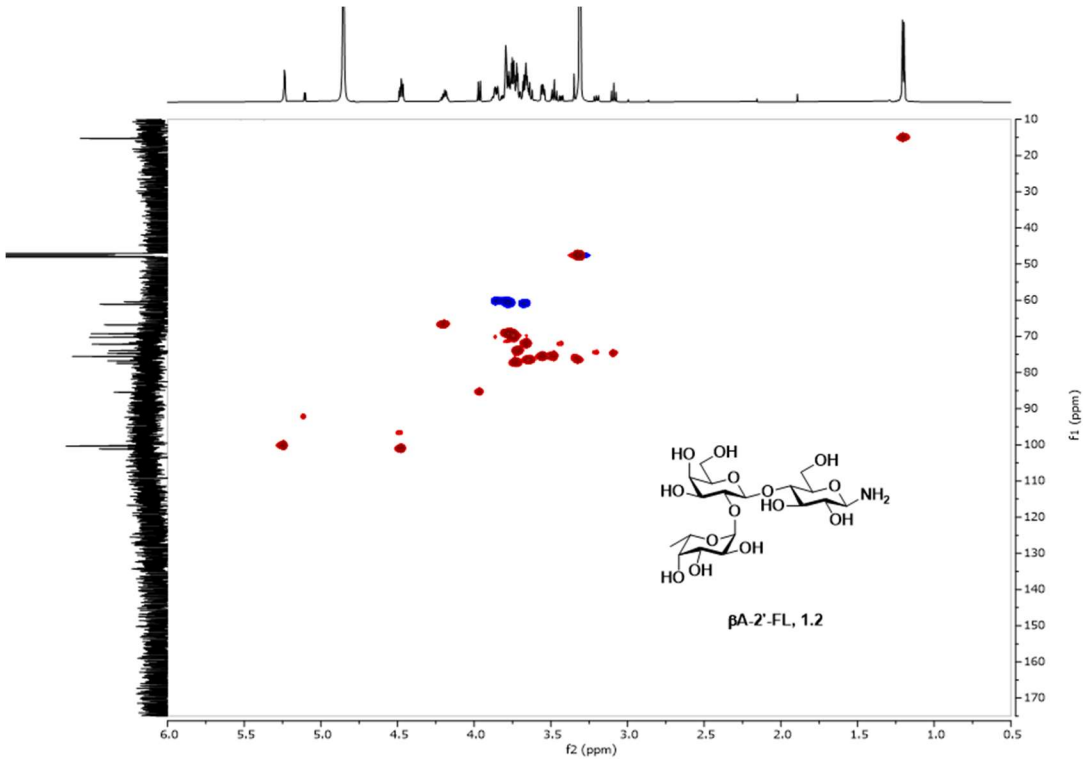

[1]H NMR (600 MHz, MeOD) spectra of **1.81**

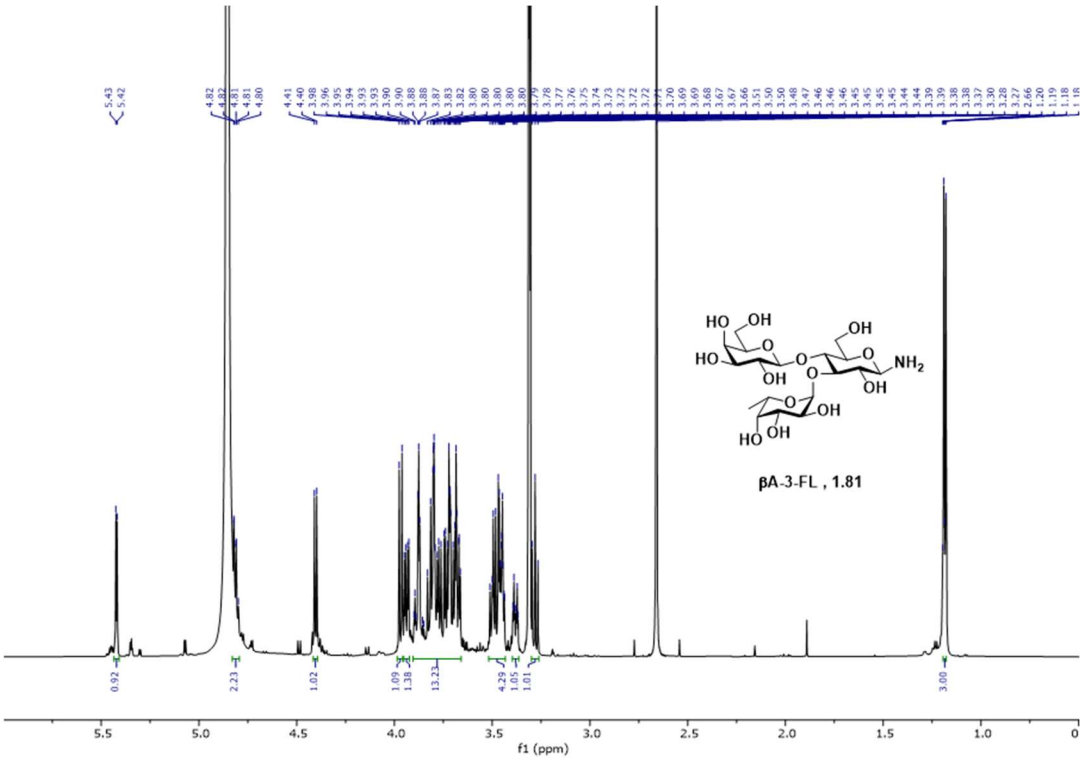

[13]C NMR (151 MHz, MeOD) spectra of **1.81**

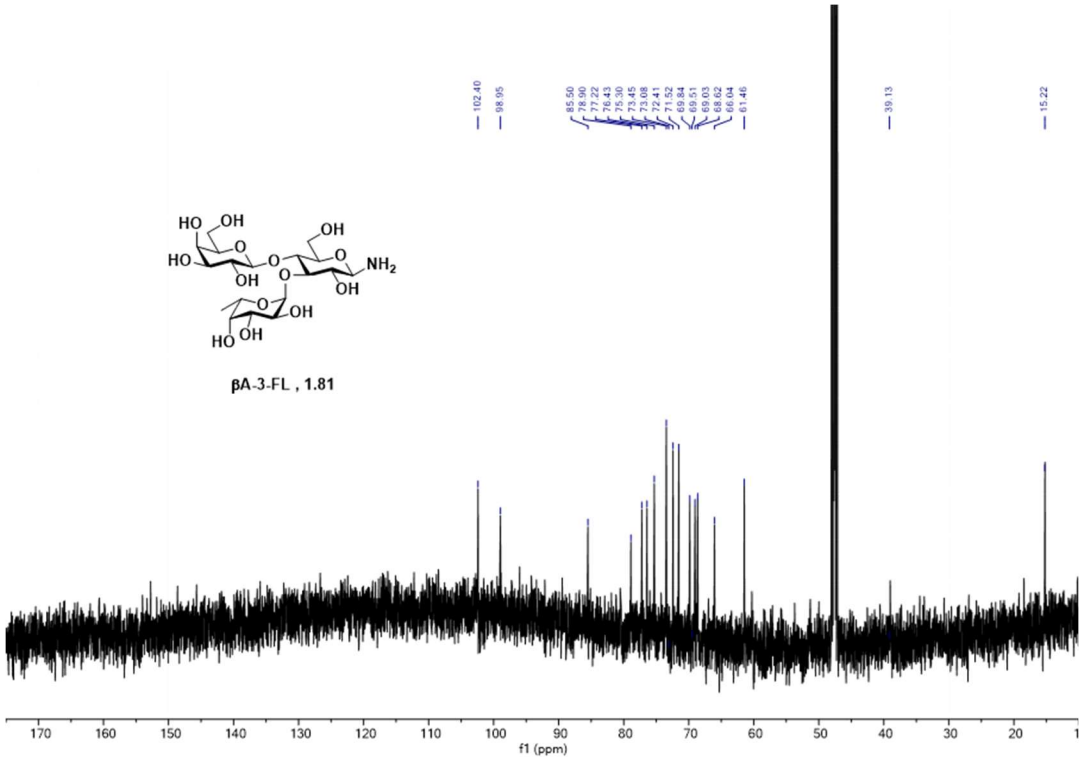

^{1}H ^{13}C HSQC NMR (600 MHz, MeOD) spectra of **1.81**

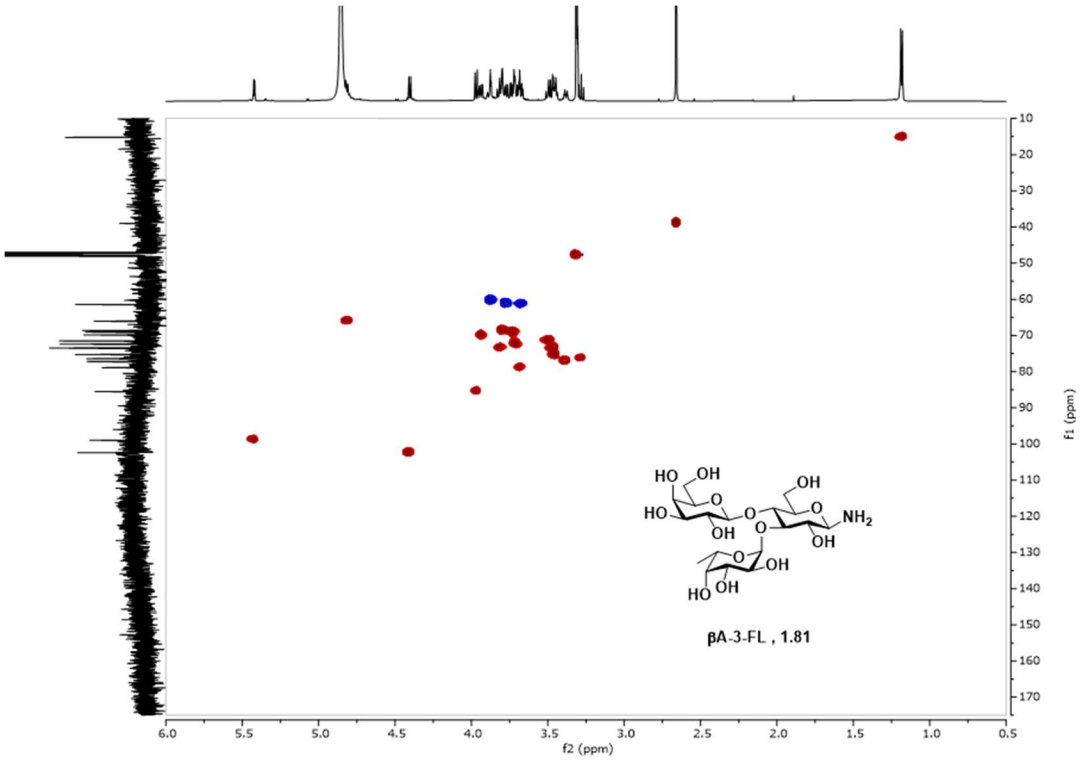

^{1}H NMR (600 MHz, MeOD) spectra of **1.82**

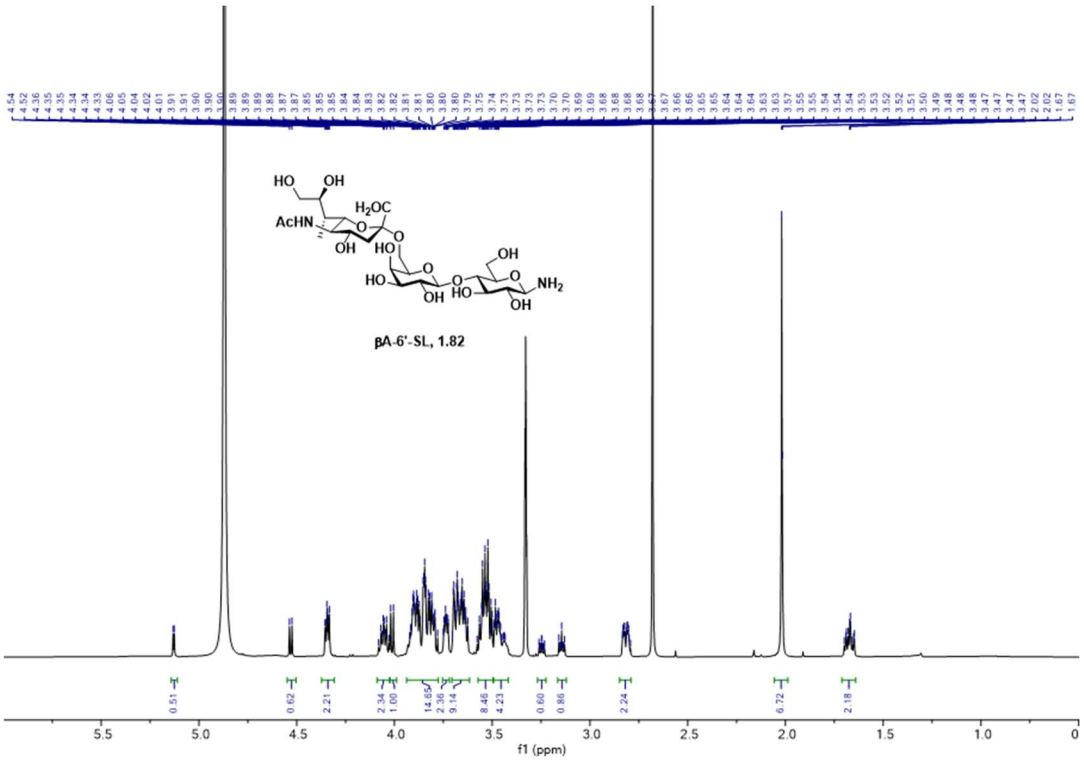

^{13}C NMR (150 MHz, MeOD) spectra of **1.82**

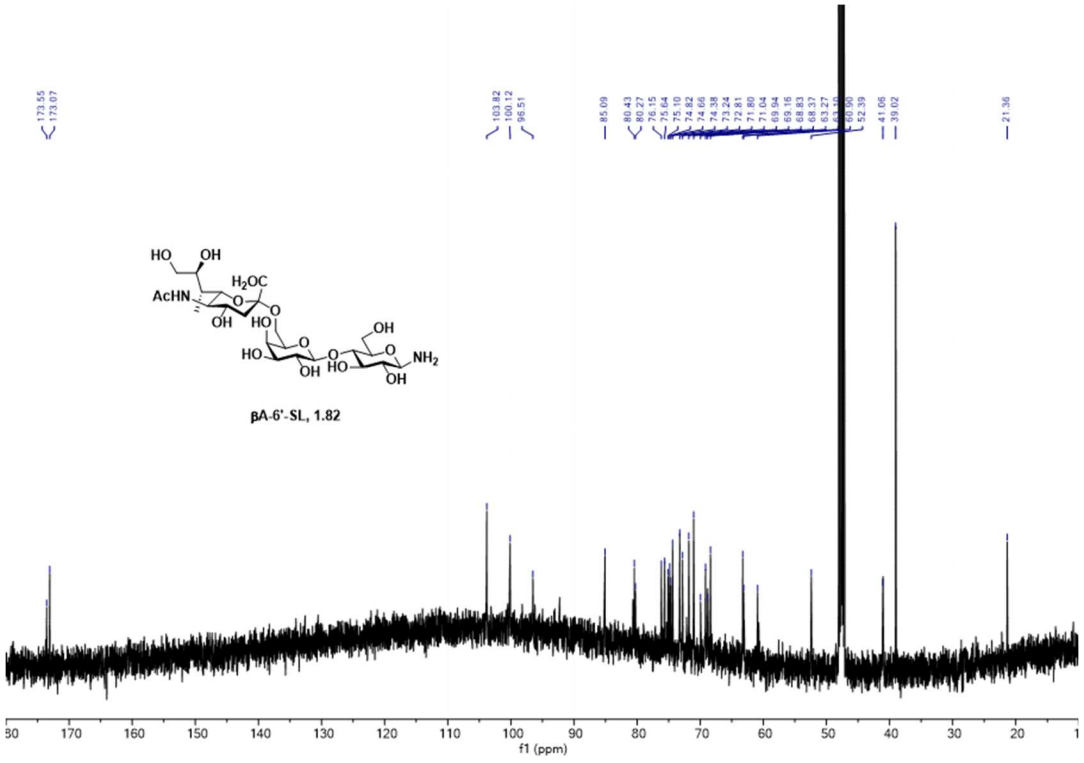

^{1}H ^{13}C HSQC NMR (600 MHz, MeOD) spectra of **1.82**

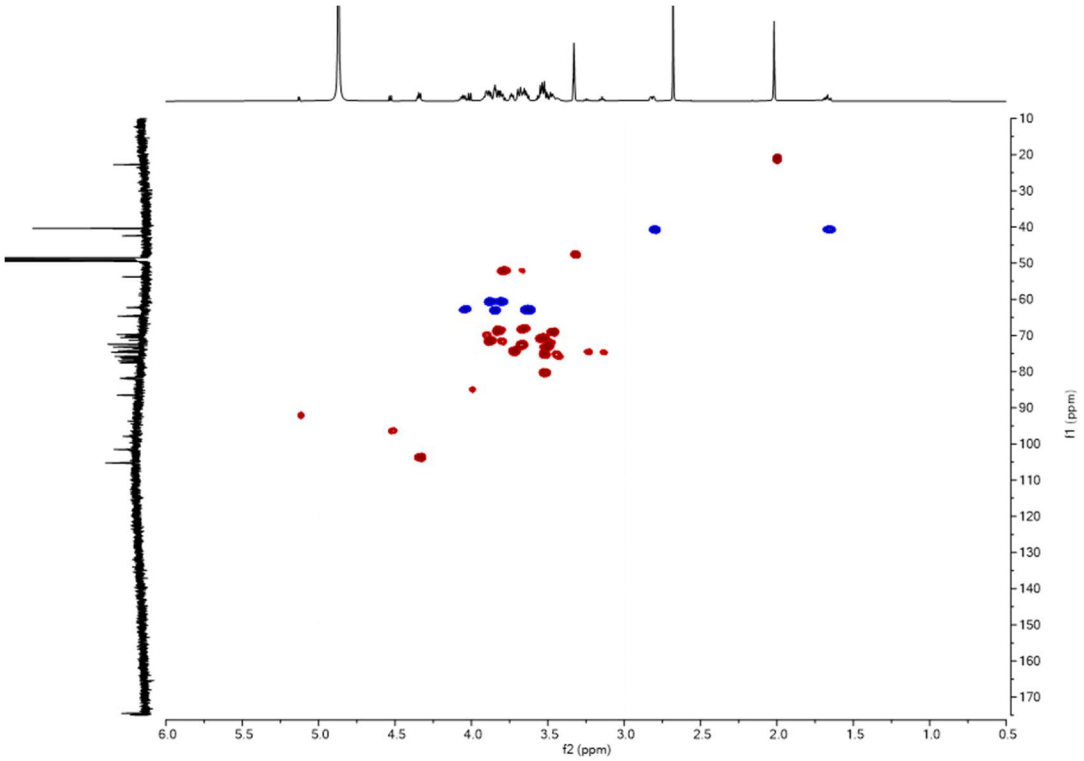

^{1}H NMR (600 MHz, MeOD) spectra of **1.83**

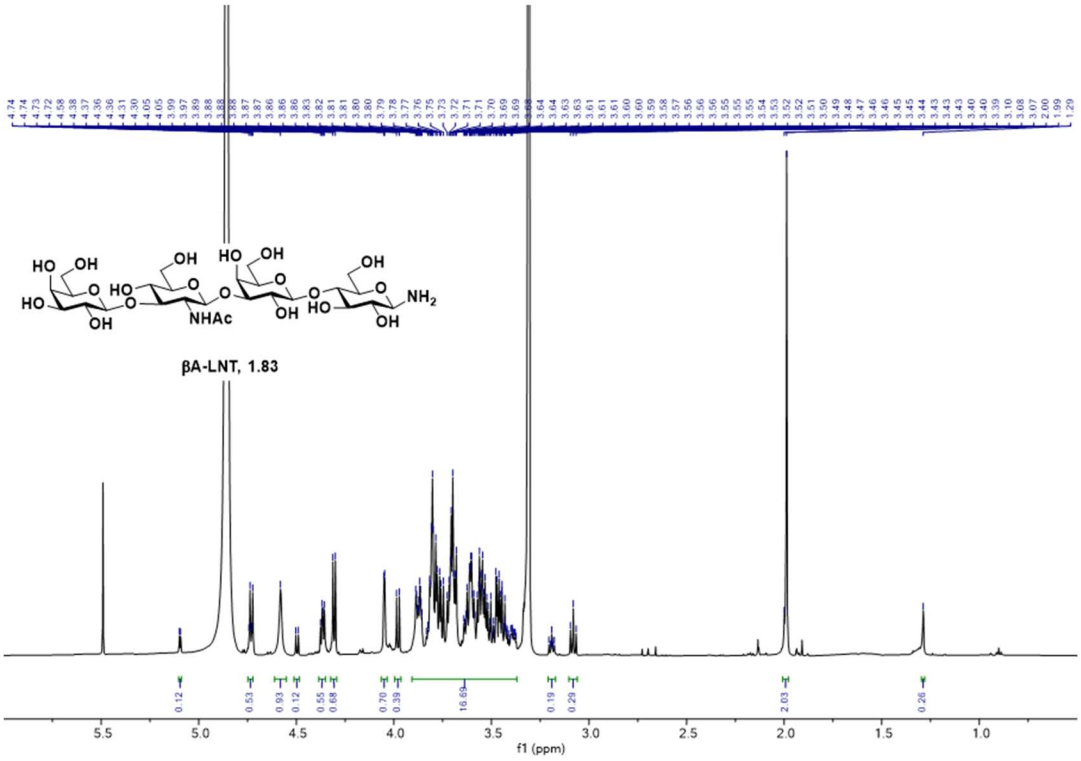

^{1}H ^{13}C HSQC NMR NMR (600 MHz, MeOD) spectra of **1.83**

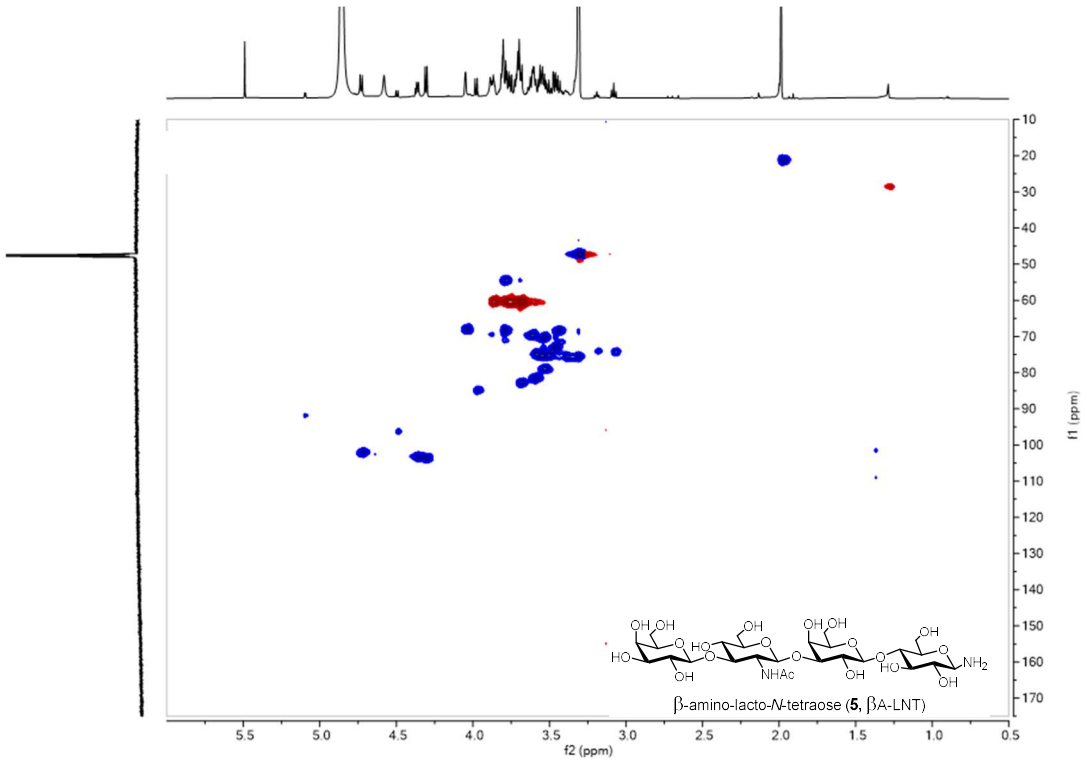

Table 2 Anomeric Proton Shifts to determine HMO: βA-HMO Ratio based on ^{1}H NMR*

HMO	HMO shift (ppm)*	βA - HMO	βA – HMO shift (ppm)*
2’ - FL **1.1**	5.10	βA - 2’ – FL **1.2**	3.97
3 - FL **1.43**	5.07	βA – 3 – FL **1.81**	3.97
6’ - SL **1.80**	5.13	βA - 6’ – SL **1.82**	4.01
LNT **1.42**	5.10	βA – LNT **1.83**	3.98

* ^{1}H NMR data obtained in MeOD

2. Truncated and Derivatized Tigogenyl Saponins Exhibit Anticancer Properties

2.1. Introduction

Cancer is an important research focus due to its prevalence, complexity, and high mortality rate. In 2020, the World Health Organization (WHO) estimated that 19.3 million new cancer cases were diagnosed.[79] Breast, lung and colorectal cancer were the three highest in estimated incidences in 2020. Cancer is usually treated by surgery, chemoradiation, or chemotherapy which combats cancer by targeting targets different cellular processes. With cancer as the second leading cause of death globally, there is an urgent need to develop anti-cancer agents, such as chemotherapeutics.[79]

Anthracyclines are a class of FDA-approved chemotherapeutics often administered to cancer patients (Figure 15). The two most common anthracyclines clinically used are Doxorubicin (DOX, **2.1**) and Daunorubicin (DNR, **2.2**).

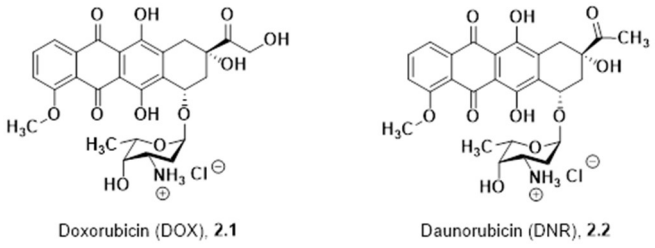

Figure 15 FDA Approved Anthracycline Chemotherapeutics

Anthracyclines target the DNA replication and mitosis process within cancer cells by inhibiting topoisomerase activity.[80] The role of topoisomerases is to relax the topology of DNA by cleaving the supercoiled DNA and then ligating the DNA strands back together to relieve tension.[81]

However, targeting topoisomerases within cardiomyocytes yields detrimental, cumulative cardiotoxic side effects leading to a maximum lifetime total dosage that cancer patients need to be aware of.[82] Often times, patients who are administered anthracycline chemotherapeutics also need to undergo cardioprotective treatments as well.[83]

In addition, since these FDA-approved drugs are often used, some patients have developed multidrug-resistant cancers.[84] Structurally, anthracyclines consist of sugar subunits and flat planar aromatic rings (Figure 15). It is thought that the aglycone contributes to the increase in reactive oxygen species (ROS) in cells treated with compounds from the anthracycline class. Over the years, it has become apparent that drug resistant cancers have developed, including ones that are resistant to anthracyclines.[85] Some common ways to combat resistance are via modification of a known drug scaffold or by finding a new scaffold that targets the same cellular pathway.[86-87] Ideally, the solution would be to find a new small molecule scaffold with known anticancer activity, yet less toxic toward human cells.

2.2. Novel approaches to access chemotherapeutics

Anthracyclines are a class of anticancer drugs that have been employed to combat and treat cancer by inhibiting the topoisomerase activity, essentially rendering the cancer cells unable to grow and proliferate. However, studies have exposed limitations of this FDA-approved chemotherapeutic with the cumulative cardiotoxic side effects and development of multi-drug resistant cancer cell lines.[83] This section will cover three different approaches to making novel small molecule scaffolds and platforms by focusing on anthracycline derivatives, hybrid compounds, and novel saponin scaffold. While the synthesized compounds were different, the Codée research group and Dr. Eric Huseman in the Townsend lab used anthracyclines as parent scaffold and varied the glycan substituent.[88] The Codée lab focused on derivatizing anthracyclines by *N,N* dimethylating amines or incorporating deoxyglycans to probe the structure-activity relationship between the anthracycline's ability to kill cancer cells through inhibition of topoisomerases or histone ejection.[89] Dr. Eric Huseman's work focused on synthesizing anthracycline hybrids by combining the glycan portion from potent anthracycline Arimetamycin A with the aglycones of FDA-approved anthracycline drugs to provide potent compounds that were effective against multi-drug resistant cancer cell lines. Finally, I will cover how saponins

are being explored as a novel scaffold to access chemotherapeutics by focusing on cytotoxic glycosteroid, Desgalactotigonin (DGT, **2.6**).

2.2.1. Characterization of *N,N* dimethyl amino sugar anthracyclines cytotoxic and toxicity properties

The Codée group synthesized various anthracycline analogs to probe the derivatives' cytotoxicity and cardiotoxicity properties (Figure 16).[89] Codée's examination focused on avoiding cardiotoxicity by evaluating the compound's ability to induce double-strand damage vs. histone eviction. Double-stranded DNA damage is known to cause cardiotoxicity side effects.

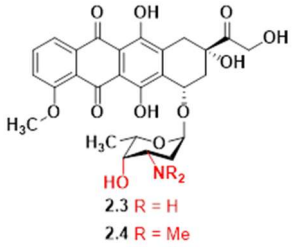

Figure 16 Codée research group synthesized *N,N* dimethyl amino sugar anthracyclines

The Codée group synthesized *N,N* dimethyl, or deoxy derivatives, establishing a preliminary structure-activity relationship for what caused the anthracycline toxicity. One trait was to cause topoisomerase poisoning that induced double-stranded DNA damage, and therefore cardiotoxicity. The other pathway was that the anthracycline derivatives caused histone ejection, bypassing harm to the cardiomyocytes. The *N,N* dimethyl amino sugar derivatives tended to cause

histone ejection and less toxicity. In terms of cytotoxicity, the *N,N* dimethyl amino sugar derivatives had similar, if not superior, potency compared to the non-methylated parent compound. However, since these are anthracycline derivatives, they are inherently toxic to non-transformed cells and may be accompanied by cardiotoxicity side effects.

2.2.2. Glycan swapped anthracycline hybrids have increased effectiveness against multi-drug resistant cancers

Dr. Eric Huseman in the Townsend research group synthesized anthracycline hybrids as a new platform to synthesize more potent chemotherapeutics and invent ones that had efficacy against multi-drug resistant cell lines. Huseman's approach was to create hybrid anthracyclines, mixing and matching the aglycone and glycans of clinically used anthracyclines and other promising potent anthracyclines.

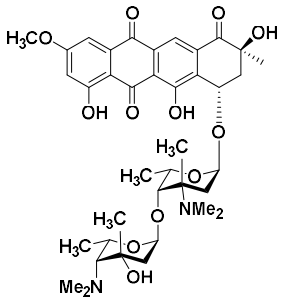

Arimetamycin A (AMA), **2.5**

Figure 17 Structure of potent anti-cancer anthracycline, Arimetamycin A

It was discovered that the disaccharide glycan of promising anthracycline Arimetamycin A (AMA, **2.5**), as seen in Figure 18, was responsible for the increased potency against not only

colon and breast cancer but also against multi-drug resistant lung cancer. The FDA-approved anthracyclines were the parent compounds. Therefore, the aglycone portion was conserved when glycan swapping for the anthracycline hybrids.

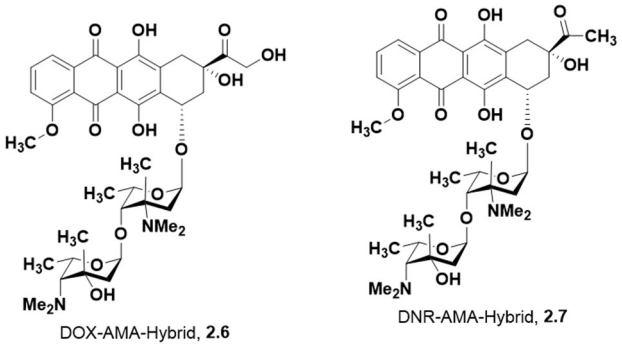

Figure 18 Anthracycline hybrids using DOX and DNR aglycones and the disaccharide glycan from AMA

Dr. Huseman synthesized DOX-AMA-Hybrid **2.6** and DNR-AMA-Hybrid **2.7**, designed by combining the Arimetamycin A glycan and aglycones of Doxorubicin and Daunorubicin (Figure 18). Interestingly enough, the hybrids were the first glycoconjugates that contained two *N,N*-dimethyl amine moieties on the glycosyl donor. [88]

After evaluating the biological activity of the hybrid compounds, it was found that the hybrids were extremely potent against all three cell lines. DNR-AMA-Hybrid **2.7** with TC50 values of 90 nM, 90 nM, and 200 nM against cancer cell lines HCT116 (colon), DMA-MB231 (breast), and H69AR (lung/MDR), respectively. DOX-AMA-Hybrid **2.6** exhibited even more potency with TC50 values of 40nM, <30 nM and 30 nM against cancer cell lines HCT116 (colon), DMA-MB231 (breast) and H69AR (lung/MDR), respectively. The assessed hybrids even showed

evidence of reversing anthracycline resistance against the multi-drug resistant lung cancer cell line H69AR[88]. The next step for this hybrid anthracycline platform is the assessment of the cardiotoxicity properties.

2.2.3. Novel Saponin Scaffold based on the anti-cancer properties of glycosteroid Desgalactotigonin

Our logic is that the inherent cytotoxic nature of the anthracyclines that leads to the severe cardiotoxicity side effects stems from the aglycone portion of the molecule. The approach this work will display is exploring a new saponin scaffold to combat drug-resistant cancer cell lines and bypass anthracycline-induced cardiotoxic side effects. Anthracyclines and other known topoisomerase inhibitors contain planar, aromatic aglycone moieties. Therefore, our solution to this problem is to find a different aglycone that is cytotoxic against cancer cells is non-planar to avoid inducing ROS production within normal cardiomyocytes (heart cells). The small molecule class chosen was the saponins, specifically glycosteroids. One aspect to be aware of is that saponins are known to exhibit hemolytic properties, rendering intravenous treatments unusable.[90] On the other hand, other saponins are effective against some drug-resistant cancer cell lines.[91] Evaluating not only the cytotoxicity for any saponin derivatives against various drug-resistant cancers and hemolytic properties would be useful pieces of information.

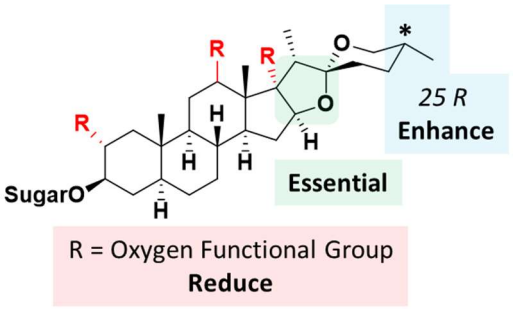

Figure 19 Established steroidal saponin structure-activity relationship with regards to cytotoxicity

The steroidal saponin scaffold was chosen because of the known structure activity relationship information for the steroid aglycones.[92] Studies have shown that if there is an oxygen atom at any R position in red, it would significantly reduce the cytotoxicity of the compound (Figure 19). In addition, the tetrahydrofuran ring is essential to retain, as removal would cause a severe decrease in cytotoxicity. Finally, studies have shown that having the 25 R methyl group, where the methyl group is equatorial rather than axial, can enhance the potency of the compound. This data implies that using tigogenin as the aglycone would be ideal for maximum cytotoxicity of the spirostane saponins.

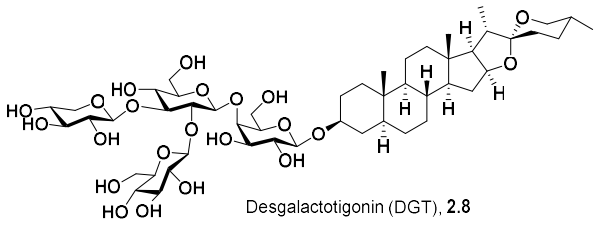

Figure 20 Structure of Desgalactotigonin, **2.8**

Desgalactotigonin (DGT, 2.7) (Figure 20), is spirostane saponin that contains tigogenin as the aglycone. [93-94] Isolated from various plants such as *Chenopodium album*, desgalactotigonin belongs to a class of molecules called saponins, composed of carbohydrate subunits and a terpene aglycone[94-95]. DGT **2.7** is composed of Tigogenin (Tig. **2.8**) and lycotetraose. [96] Lycotetraose consists of galactose, glucose, and xylose, and desgalactotigonin contains a steroidal aglycone with sp^3 centers, meaning that the aglycone alone takes up different three-dimensional space compared to the planar aromatic aglycones of known topoisomerase inhibitors. Mondal and coworkers first characterized its cytotoxicity against breast and colorectal cancer cell lines *in vitro* at an IC_{50} of 8.27 μM and 15.44 μM respectively.[94] Other research groups observed that DGT can inhibit the growth and metathesis of osteosarcomas as well as displays ccytotoxic activity against pancreatic and lung cancer cells lines.[97-98] With its known cytotoxicity and optimal steroidal aglycone component, DGT is a great parent scaffold for developing novel saponin derivatives as chemotherapeutics.

2.3. Designing saponin scope consisting of natural products, derivatives and hybrids and the expectations

With Desgalactotigonin as the parent compound, we want to evaluate the role carbohydrates have on anti-cancer activity by attempting to find what functional groups or sugars are necessary for the minimum pharmacophore. Our approach was to develop a platform with different anti-cancer scaffolds. We would explore how various saponins could increase cytotoxicity for cancer yet decrease the toxicity for normal cells. We hypothesized that since DGT lacks the anthracycline quinoline aglycone, it would not produce reactive oxygen species (ROS) which would harm cardiomyocytes to induce cardiotoxic side effects. This parent scaffold could be truncated or derivatized to evaluate the structure-activity relationship between saponin glycans and anti-cancer activity.

In designing the saponin scope for anti-cancer evaluation, we attempted to maximize our findings with the minimum number of compounds, ending up with six saponins. First, we begin by assessing DGT and its truncated congeners before moving onto the *N,N* dimethyl amino saponin derivative and then finally the simplified anthracycline-saponin hybrid. The *N,N* dimethyl amino saponin was designed for retaining the potency of the compound, while mimicking the Codée lab's findings that the derivative would induce histone ejection, to avoid commonly seen anthracycline-induced cardiotoxic side effects.[89] Inspired by Huseman's work, the anthracycline-saponin hybrid was designed to assess if we could retain potency and perhaps be effective against multi-drug resistant cancer cell lines.[88] The dissertation work will focus on developing chemotherapeutics with differing scaffolds than anthracyclines and then proceed to assess the anti-cancer properties on the two deadliest cancers leading in mortality rates, specifically multi-drug resistant lung cancer H69AR and colorectal cancer HCT116.

2.3.1. Desgalactotigonin and truncated congeners

Beginning with Desgalactotigonin and truncated congeners, DGT **2.8** was chosen as the positive control. Desgalactotigonin is a branched tetrasaccharide saponin with known anticancer activity against various cancer cell lines as stated above.

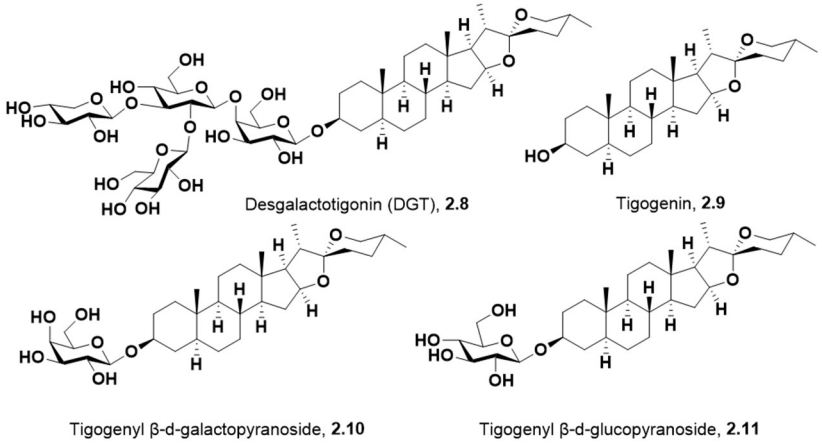

Figure 21 Desgalactotigonin and truncated congeners

Tigogenin **2.9** was chosen for evaluation (Figure 21). Since Tigogenin contains the steroidal backbone, it would be likely that it does not exhibit anti-cancer activity since it could incorporate into the cell membrane yet not disrupt the membrane enough to induce cell death. The tetrasaccharide was not tested due to the 2006 study that the glycan portion of the molecule alone

did not elicit any cytotoxicity against non small-cell lung cancer (NCI-H450) or breast cancer (MDA-MB-231).[93]

Truncated versions of DGT were evaluated and anticancer activity would help indicate what the minimum pharmacophore would be (Figure 21). Gal-Tig **2.10** was chosen since galactose is the monomer directly linked to the aglycone. Glc-Tig **2.11** was chosen since glucose was not only the most abundant monosaccharide in the saponin glycan, but also protrudes as part of the branched glycan.

2.3.2. *N,N* dimethylated amino sugar saponin to combat cardiotoxicity while retaining anti-cancer activity

Since we are looking for the minimum pharmacophore to efficiently explore the new scaffold chemical space, we chose Gal- NMe_2-Tig **2.12** as the representative compound with hopes that it exhibits potent anti-cancer activity (Figure 22). However, we would first want to evaluate for cytotoxicity before performing biological assays for toxicity against cardiomyocytes. In addition, the amine was *N,N* dimethylated since the Codée study found that dimethylation of the amine would change the anthracycline class of compounds from going through topoisomerase inhibition to incite cytotoxicity and instead undergo the histone ejection mechanism, which lessens cardiotoxic side effects. In addition, Gal-NMe_2-Tig **2.12** was synthesized to compare with the anthracycline-saponin hybrid Lemonose-NMe_2-Tig **2.13** to determine if cytotoxicity could be induced with a simpler *N,N*-dimethyl amino sugar rather than one based on rarer sugar lemonose.

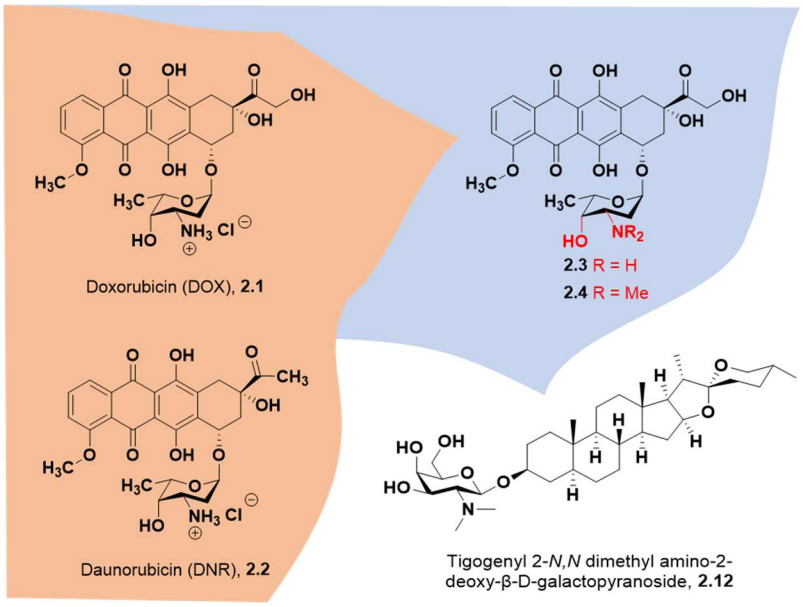

Figure 22 Structures of DOX **2.1**, DNR **2.2**, Codée's *N,N* dimethylated work, then the Gal- NMe_2-Tig saponin **2.12**

2.3.3. Anthracycline saponin hybrid that retains anti-cancer activity and is effective against resistant cell lines

The anthracycline-Saponin **2.13** with an *N,N* dimethyl amine was synthesized to determine if combining the glycan fragment of a known potent anthracycline on the different aglycone scaffold would increase the potency of the compound with regards to the parent compound (Figure 23). The amine was dimethylated to incorporate the Codée lab's findings that *N,N* dimethyl amino sugar anthracycline induced the histone eviction pathway, avoiding the topoisomerase poisoning that would cause the double stranded DNA damage known to cause cardiotoxicity. In choosing what anthracycline-derived glycan should be incorporated, we must refer to a recent Townsend publication synthesizing novel anthracycline hybrids (**2.6** and **2.7**) via glycan swapping. An anthracycline-saponin hybrid was designed, inspired by Huseman's work in using glycan

switching to synthesize a hybrid drug to access more potent molecules, effective even against multidrug-resistant cell lines. Our approach was to install a monosaccharide from the potent DOX-AMA-Hybrid **2.6**, specifically lemonose, onto the saponin aglycone.

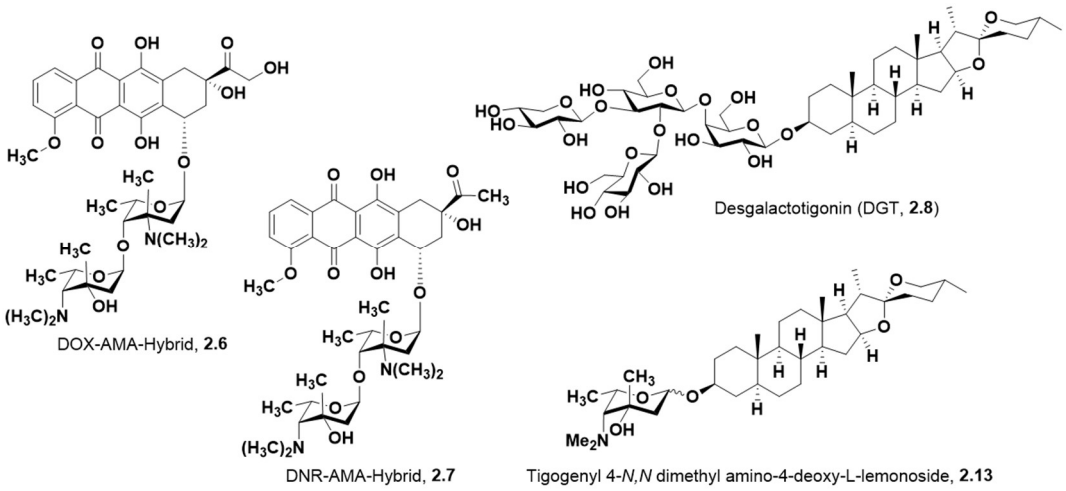

Figure 23 Anthracycline hybrids and saponin DGT inspire the design of anthracycline-saponin hybrid **2.13**

2.4. Chemical Synthetic Routes

The synthesis of the following compounds are depicted below: Gal-Tig **2.10**, Glc-Tig **2.11**, Gal-NMe_2-Tig **2.12**, and Lemonose-NMe_2-Tig **2.13**.

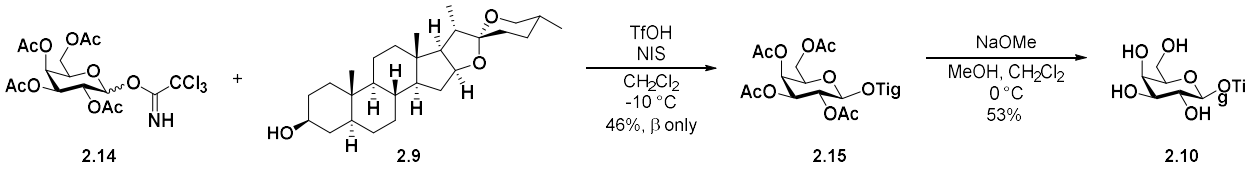

2.14 2.9 2.15 2.10

Scheme 13 Synthesis of Gal-Tig **2.10**

Gal-Tig **2.10** and Glc-Tig **2.11** were synthesized similarly, starting from the corresponding peracetylated donors **2.14** and **2.16** to undergo a triflic acid (TfOH) mediated glycosylation with Tigogenin to yield the monosaccharide saponin **2.15** and **2.17**. Due to solubility reasons, the glycoconjugates were dissolved in a mixture of dichloromethane and methanol during a sodium methoxide saponification to yield test compounds Gal-Tig **2.10** and Glc-Tig **2.11**.

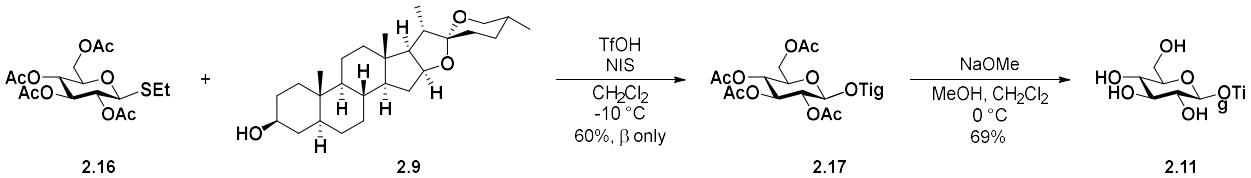

2.16 2.9 2.17 2.11

Scheme 14 Synthesis of Glc-Tig **2.11**

To synthesize Gal-NMe_2-Tig **2.12**, advanced intermediate thioglycoside **2.18** was used as a donor in a triflic acid/*N*-Iodosuccinimide (TfOH/NIS) mediated glycosylation with aglycone Tigogenin **2.9** to provide saponin **2.19**. After a global deprotection under Palladium on carbon (Pd/C) hydrogenation conditions to yield amino sugar saponin **2.20**, a final reductive amination with formaldehyde and sodium cyanoborohydride ($NaBH_3CN$) yielded the Gal-NMe_2-Tig **2.12** in 21% yield.

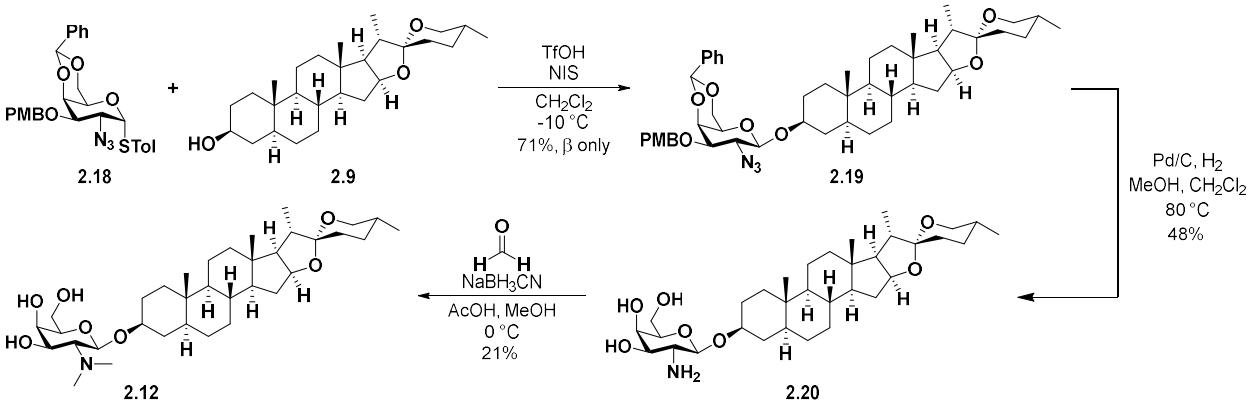

Scheme 15 Synthesis of Gal-NMe_2-Tig

To synthesize the anthracycline-saponin hybrid, advanced intermediate **2.27** was used in synthesizing anthracycline hybrid **2.6** during the study of how swapping glycans affect the anthracycline derivatives' anti-cancer activity. Dr. Huseman had previously synthesized the advanced intermediate **2.27** from D-threonine, **2.21** in 8 steps. D-threonine **2.21** undergoes an acid-catalyzed esterification, followed by a double benzyl protection of the amine. Then after an acetylation, affords **2.22**. After treatment with Lithium bis(trimethylsilyl)amide (LiHMDS) to enable the Dieckmann condensation, quenching with dimethyl sulfate and ammonia in methanol to provide the vinylogous ester **2.23**. Next, a Diisobutylaluminium hydride (DIBAL-H) reduction

of lactone **2.23** followed by the addition of acid facilitated a Stork-Danheiser like transposition to provide the vinylogous ester **2.24**. Treatment of methyllithium (LiMe) with **2.24** afforded glycal **2.25**, which then proceeded to undergo hydration with mercury(II) acetate ($Hg(OAc)_2$) to provide **2.26**. Reducing sugar **2.26** was then doubly tert-Butyldimethylsilyl (TBS) protected to afford the advanced intermediate **2.27**.

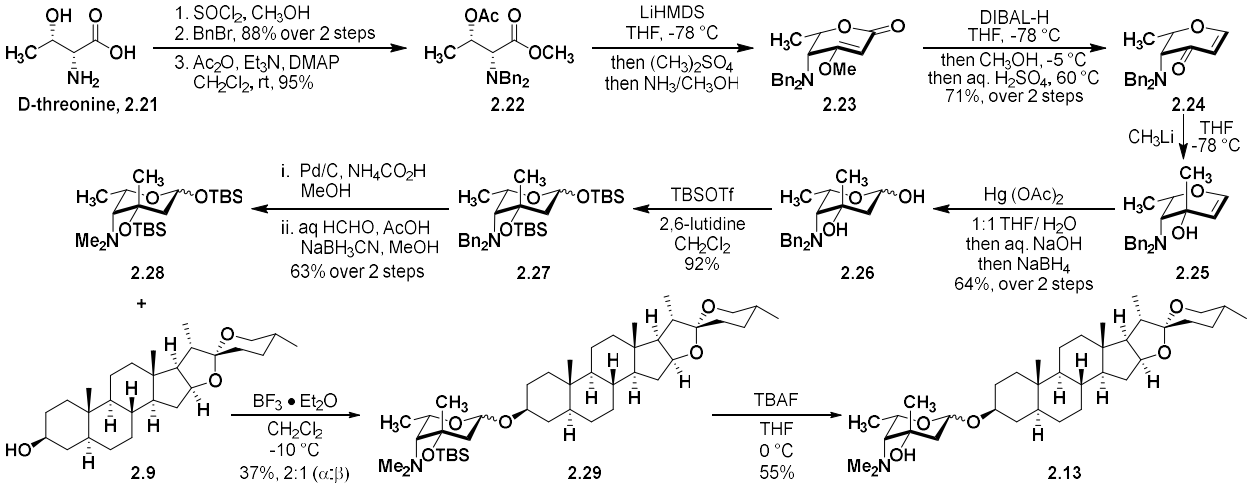

Scheme 16 Synthesis of Lemonose-NMe_2-Tig

Then, the TBS protected monosaccharide **2.27** was subjected to Pd/C and ammonium formate conditions to debenzylate the amine, followed by reductive amination with formaldehyde and $NaBH_3CN$ to yield the *N,N* dimethylated amine donor **2.28**. Then donor **2.28** undergoes a boron trifluoride etherate ($BF_3 \cdot Et_2O$) mediated glycosylation with Tigogenin **2.9** to yield saponin **2.29**. A tetra-n-butylammonium fluoride (TBAF) desilylation of the TBS protecting group yielded the Lemonose- NMe_2-Tig **2.13** compound in 55% yield.

2.5. Biological Evaluation of Tigogenyl Saponins

After successful synthesis of saponins Gal-Tig **2.10**, Glc-Tig **2.11**, Gal-NMe_2-Tig **2.12**, and Lemonose-NMe_2-Tig **2.13**, I wanted to test their anti-cancer activity against different cancer cell lines. The natural product DGT **2.8** was used as a positive control, as well as aglycone Tig **2.9** as a negative control. Staurosporine was used as a non-saponin positive control. We hypothesized that the four monosaccharide saponins would exhibit anti-cancer activity as seen with DGT **2.8** in other cancer cell lines.[94, 97-98] We tested DGT **2.8**, Tig **2.9**, Gal-Tig **2.10**, Glc-Tig **2.11**, Gal-NMe_2-Tig **2.12**, and Lemonose-NMe_2-Tig **2.13** in two cancer cell lines, human lung carcinoma (H69AR) and human colorectal carcinoma (HCT116).

Table 3 TC_{50} of compounds in H69AR and HCT116 cancer cell lines

Compound	H69AR (Human Lung Carcinoma) TC_{50} (μM)	HCT116 (Human Colorectal Carcinoma) TC_{50} (μM)
Staurosporine	0.2	0.1
	0.1	0.1
Tig (**2.9**)	> 40.0	> 40.0
DGT (**2.8**)	15.2	12.0
Gal-Tig (**2.10**)	29.9	26.0
Glc Tig (**2.11**)	> 40.0	> 40.0
Gal-NMe_2-Tig (**2.12**)	19.0	7.7
Lemonose-NMe_2-Tig (**2.13**)	> 40.0	> 40.0

These initial anti-cancer assays indicate that some of the saponins had no anti-cancer activity, while others exhibited anti-cancer activity even more potent than the natural product. Staurosporine exhibited potent anti-cancer activity across both cell lines, as expected. Natural product DGT **2.8** exhibited anti-cancer activity with 15.2 μM TC_{50} in H69AR

and comparable 12.0 μM TC_{50} in HCT116. Aglycone Tigogenin **2.9** had no anti-cancer activity as expected against either cancer cell line. While Gal-Tig **2.10** exhibited anti-cancer activity, slightly less than that of DGT **2.8**, with 29.9 μM TC_{50} in H69AR and 26.0 μM TC_{50} in HCT116, Glc-Tig **2.11** showed no anti-cancer activity against either cancer cell lines. Unexpectedly, the Lemonose-NMe_2-Tig **2.13** did not have any cytotoxicity against either cancer cell line as well. Gal-NMe_2-Tig **2.12** was the most interesting with 19.0 μM TC_{50} in H69AR and a 7.7 μM TC_{50} in HCT116.

2.6. Conclusion

Our initial hypothesis that truncated and derivatized tigogenyl saponins would have potent anti-cancer activity lead us to synthesize compounds Gal-Tig **2.10**, Glc-Tig **2.11**, Gal-NMe_2-Tig **2.12**, and Lemonose-NMe_2-Tig **2.13**. While our initial hypothesis that anthracycline-saponin hybrids with *N,N*-dimethylated amines were potent anticancer agents was unfounded as Lemonose-NMe_2-Tig **2.13** showed no cytotoxicity against either lung cancer H69AR or colorectal cancer HCT116 cell lines. An interesting finding that Gal-Tig **2.10** and the amino sugar variant Gal-NMe_2-Tig **2.12** were potent was exciting. The next aspect to explore is if the Gal-NMe_2-Tig **2.12** and Gal-Tig **2.10** analogs can mitigate the cardiotoxicity exhibited by FDA-approved anthracyclines.

One other question to address is what mechanism of action these two promising compounds go through to exhibit anti-cancer activity. Is it as simple as increasing cell permeability with galactose-saponin scaffolds, or rather is it important that glycosteroids have axial substituents on the glycan portion? Further synthesis of other tigogenyl saponins could help answer more

structure-activity-relationship questions by synthesizing mannose and mannosamine saponin analogs to see if potent activity is unique to the galactose species, or any glycan with an axial substituent, as either the alcohol or the amine.

2.7. Materials and Methods

2.7.1. Materials and General Procedures

Solvents were obtained from Sigma Aldrich sure-seal bottles or obtained from a MBraun MB-SPS solvent system and used immediately. Commercial reagents were used as received.

All non-aqueous reactions were performed in flame-dried or oven-dried round-bottomed flasks under an atmosphere of nitrogen or argon, unless otherwise noted. Disposable needles, oven-dried stainless-steel syringes or cannula were used to transfer moisture- and air-sensitive liquids. Reaction temperatures were controlled and monitored using a hot plate stirrer with a thermocouple thermometer. Reactions were conducted at ambient temperature (rt, approximately 23 °C) unless otherwise noted. Analytical thin-layer chromatography (TLC) was performed on Sorbtech Silica XHL UV254, glass-backed, 250 μm plated, and visualized using UV, iodine stain, cerium ammonium molybdate stain, anisaldehyde stain, vanillin stain, dinitrophenylhydrazine stain or potassium permanganate stain. Flash column chromatography was performed as described by Still et al. using silica gel 230-400 mesh (particle size 40 – 63 μm) silica gel purchased from SiliCycle.[1]

2.7.2. Instrumentation

^{1}H NMR spectra were recorded on Bruker 300, 400, 500, or 600 MHz spectrometers and are reported relative to deuterated solvent signals. Data for ^{1}H NMR spectra are reported as follows: chemical shift (δ ppm), multiplicity (s = singlet, d = doublet, t = triplet, q = quartet, p = pentet, m = multiplet, br = broad, app = apparent), coupling constants (Hz), and integration. Deuterated chloroform was standardized to 7.26 ppm. Deuterated methanol was standardized to

3.31 ppm. Deuterated methanol was standardized to 49.0 ppm. ^{13}C NMR spectra were recorded on Bruker 75, 100, 125, or 150 MHz spectrometers and are reported relative to deuterated solvent signals. Deuterated chloroform was standardized to 77.0 ppm. High-resolution mass spectra were obtained from the Mass Spectrometry Core Lab, Vanderbilt University using a JEOL AX505HA or JEOL LMS-GC mate mass spectrometer.

2.7.3. Compound Characterization

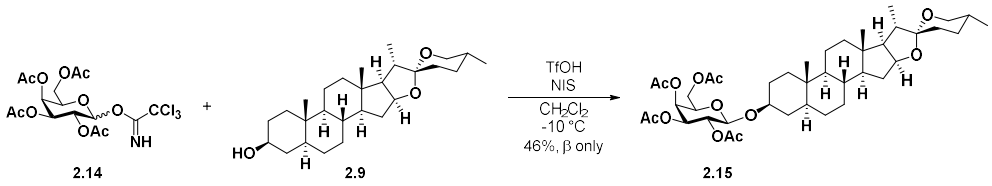

(2*R*,3*S*,4*S*,5*R*,6*R*)-2-(acetoxymethyl)-6-(((2a*S*,4*S*,5'*R*,6a*S*,6b*S*,8a*S*,8b*R*,9*S*,10*R*,11a*S*,12a*S*,12b*R*)-5',6a,8a,9-tetramethyldocosahydrospiro[naphtho[2',1':4,5]indeno[2,1-*b*]furan-10,2'-pyran]-4-yl)oxy)tetrahydro-2*H*-pyran-3,4,5-triyl triacetate, 2.15. Acceptor **2.9** (1.0 eq., 100 mg, 0.24 mmol) and donor **2.14** (1.1 eq., 130.1 mg, 0.26 mmol) were coevaporated with dichloromethane (CH_2Cl_2, 3 x 5 mL) followed by coevaporation with hexanes (3 x 5 mL) and placed on the high vacuum overnight. To the donor/acceptor mixture was added 4Å powdered molecular sieves and then purged with argon. The reaction flask was then rinsed with anhydrous dichloromethane ([0.15 M], 1.6 mL). The reaction mixture was stirred for an hour at ambient temperature before cooling to -10 °C with an ice and brine bath. Then 0.1 mL of a solution of triflic acid in anhydrous dichloromethane (1 drop of triflic acid in 0.3 mL of anhydrous dichloromethane) was added

dropwise to the reaction. After stirring for 45 min, the reaction was quenched with triethylamine, diluted with dichloromethane, filtered through celite, dried (sodium sulfate), and then concentrated *in vacuo.* The crude residue was purified via flash column chromatography to yield saponin **2.15** as a white foam (83.3 mg, 46 %). **^{1}H NMR** (600 MHz, $CDCl_3$) δ = 5.37 (d, *J* = 3.5 Hz, 1H), 5.17 (dd, *J* = 10.4, 7.9 Hz, 1H), 5.01 (dd, *J* = 10.4, 3.5 Hz, 1H), 4.54 (d, *J* = 7.9 Hz, 1H), 4.38 (q, *J* = 7.5 Hz, 1H), 4.19 (dd, *J* = 11.2, 6.4 Hz, 1H), 4.10 (dd, *J* = 11.3, 7.1 Hz, 1H), 3.88 (t, *J* = 6.8 Hz, 1H), 3.54 (tt, *J* = 10.8, 4.8 Hz, 1H), 3.46 (dt, *J* = 10.6, 3.8 Hz, 1H), 3.37 (t, *J* = 11.0 Hz, 1H), 2.14 (s, 3H), 2.05 (s, 3H), 2.04 (s, 3H), 1.98 (s, 3H), 1.95 (d, *J* = 7.5 Hz, 1H), 1.85 (p, *J* = 6.9 Hz, 2H), 1.75 (dd, *J* = 8.7, 6.8 Hz, 1H), 1.69 (td, *J* = 13.1, 3.8 Hz, 2H), 1.66 – 1.54 (m, 2H), 1.49 (dtd, *J* = 39.5, 13.2, 12.1, 3.9 Hz, 3H), 1.24 (q, *J* = 11.9, 10.7 Hz, 10H), 1.16 – 1.01 (m, 2H), 0.95 (d, *J* = 7.0 Hz, 3H), 0.94 – 0.81 (m, 2H), 0.81 – 0.76 (m, 6H), 0.75 (s, 3H), 0.63 (ddd, *J* = 14.3, 11.1, 3.9 Hz, 1H). **^{13}C NMR** (150 MHz, $CDCl_3$) δ = 170.38, 170.32, 170.20, 169.37, 109.22, 100.20, 80.79, 79.92, 71.00, 70.46, 69.09, 67.01, 66.82, 62.17, 61.26, 56.24, 54.30, 44.68, 41.58, 40.54, 40.00, 36.88, 35.65, 35.05, 34.63, 32.20, 31.73, 31.34, 30.27, 29.30, 28.77, 28.66, 21.02, 21.00, 20.81, 20.67, 20.59, 17.10, 16.45, 14.46, 12.27.

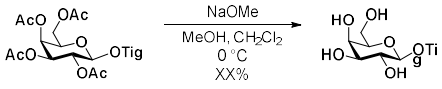

2.15 2.10

(2*R*,3*R*,4*S*,5*R*,6*R*)-2-(hydroxymethyl)-6-(((2a*S*,4*S*,5'*R*,6a*S*,6b*S*,8a*S*,8b*R*,9*S*,10*R*,11a*S*,12a*S*,12b*R*)-5',6a,8a,9-tetramethyldocosahydrospiro[naphtho[2',1':4,5]indeno[2,1-*b*]furan-10,2'-pyran]-4-yl)oxy)tetrahydro-2*H*-pyran-3,4,5-triol, 2.10. To a flame dried round bottom flask equipped with a magnetic stir bar and purged with argon, **2.15** (1.0 eq., 83.3 mg, 0.11 mmol) was added

along with anhydrous methanol ([0.01 M], 11.15 mL). After cooling the flask to 0 °C, a concentrated sodium methoxide solution was added. The reaction was stirred for 7 h, then neutralized with saturated aqueous sodium bicarbonate solution. The resulting mixture was concentrated *in vacuo*. Purification by flash column chromatography gave **2.10** as a white foam (34.1 mg, 53%). **^{1}H NMR** (600 MHz, d-pyridine) δ = 6.90 (s, 1H), 6.73 (s, 1H), 6.61 (t, *J* = 6.0 Hz, 1H), 6.33 (s, 1H), 4.96 (d, *J* = 7.6 Hz, 1H), 4.62 – 4.58 (m, 1H), 4.54 (td, *J* = 8.0, 6.3 Hz, 1H), 4.48 (ddt, *J* = 15.7, 9.9, 5.7 Hz, 3H), 4.23 (dd, *J* = 9.5, 3.4 Hz, 1H), 4.15 (t, *J* = 6.0 Hz, 1H), 3.97 (td, *J* = 11.1, 5.3 Hz, 1H), 3.58 (dd, *J* = 10.0, 4.0 Hz, 1H), 3.50 (dd, *J* = 12.8, 8.3 Hz, 1H), 2.08 – 1.99 (m, 2H), 1.94 (p, *J* = 6.9 Hz, 1H), 1.86 – 1.77 (m, 2H), 1.72 – 1.61 (m, 3H), 1.61 – 1.50 (m, 4H), 1.45 – 1.15 (m, 8H), 1.13 (d, *J* = 7.0 Hz, 3H), 1.05 (dddd, *J* = 24.5, 13.7, 11.7, 4.9 Hz, 2H), 0.87 (tt, *J* = 12.1, 3.2 Hz, 2H), 0.81 (s, 3H), 0.80 – 0.74 (m, 2H), 0.68 (d, *J* = 5.7 Hz, 3H), 0.65 (s, 3H), 0.49 (ddd, *J* = 12.3, 10.4, 4.1 Hz, 1H). **^{13}C NMR** (150 MHz, d-pyridine) δ = 109.21, 102.70, 81.11, 77.00, 76.98, 75.45, 72.71, 70.38, 66.83, 62.99, 62.62, 56.43, 54.38, 44.55, 41.96, 40.75, 40.12, 37.17, 35.79, 35.23, 34.83, 32.37, 32.10, 31.78, 30.57, 30.01, 29.96, 29.23, 28.91, 21.25, 17.30, 16.59, 15.01, 12.27.

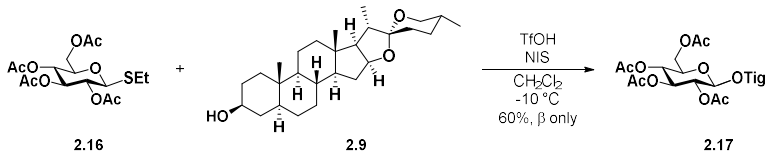

(2*R*,3*R*,4*S*,5*R*,6*R*)-2-(acetoxymethyl)-6-(((2a*S*,4*S*,5'*R*,6a*S*,6b*S*,8a*S*,8b*R*,9*S*,10*R*,11a*S*,12a*S*,12b*R*)-5',6a,8a,9-tetramethyldocosahydrospiro[naphtho[2',1':4,5]indeno[2,1-*b*]furan-10,2'-pyran]-4-yl)oxy)tetrahydro-2*H*-pyran-3,4,5-triyl triacetate, 2.17. Acceptor **2.9** (1.0 eq., 100 mg, 0.24 mmol) and donor **2.16** (3.0 eq., 282.6 mg, 0.72 mmol) were coevaporated with dichloromethane

(3 x 5 mL) followed by coevaporation with hexanes (3 x 5 mL) and placed on the high vac overnight. The donor/acceptor mixture was added 4Å powdered molecular sieves and then purged with argon. The reaction flask was then rinsed down with anhydrous dichloromethane ([0.1 M], 2.4 mL). The reaction mixture was stirred for an hour at ambient temperature before cooling to -10 °C with an ice and brine bath. *N*-iodosuccinimide (3.3 eq., 0.1782 g, 0.79 mmol) was added in one portion. After stirring for 30 min, 0.1 mL of a solution of triflic acid in anhydrous dichloromethane (1 drop of triflic acid in 0.3 mL of anhydrous dichloromethane) was added dropwise to the reaction. The reaction was quenched with triethylamine after 40 min and then diluted with dichloromethane, filtered through celite, dried (sodium sulfate), and concentrated *in vacuo.* The crude residue was purified via flash column chromatography to yield saponin **2.17** as a white foam (100.6 mg, 56%). **^{1}H NMR** (600 MHz, $CDCl_3$) δ = 5.68 (d, *J* = 5.2 Hz, 1H), 5.18 (t, *J* = 2.7 Hz, 1H), 4.92 – 4.87 (m, 1H), 4.38 (q, *J* = 7.5 Hz, 1H), 4.33 (ddd, *J* = 5.4, 2.9, 1.0 Hz, 1H), 4.21 – 4.17 (m, 2H), 3.93 (dt, *J* = 9.3, 4.0 Hz, 1H), 3.54 (tt, *J* = 10.9, 4.8 Hz, 1H), 3.47 (dt, *J* = 10.7, 3.6 Hz, 1H), 3.37 (t, *J* = 11.0 Hz, 1H), 2.11 (s, 3H), 2.09 (s, 3H), 2.09 (s, 3H), 1.97 (ddd, *J* = 12.4, 7.5, 5.4 Hz, 1H), 1.85 (p, *J* = 7.1 Hz, 1H), 1.75 (dd, *J* = 8.7, 6.8 Hz, 1H), 1.70 – 1.58 (m, 4H), 1.53 – 1.42 (m, 4H), 1.38 – 1.19 (m, 10H), 1.16 – 1.03 (m, 4H), 0.96 (d, *J* = 7.0 Hz, 3H), 0.93 – 0.81 (m, 2H), 0.78 (d, *J* = 5.5 Hz, 6H), 0.75 (s, 3H), 0.66 – 0.58 (m, 1H). **^{13}C NMR** (150 MHz, $CDCl_3$) δ = 170.55, 169.52, 169.02, 121.19, 109.08, 96.76, 80.70, 73.16, 72.76, 69.97, 68.17, 66.77, 66.70, 63.00, 62.10, 56.15, 54.21, 44.91, 41.48, 40.44, 39.91, 36.95, 36.12, 35.35, 34.97, 32.08, 31.63, 31.26, 30.17, 29.57, 29.49, 28.68, 28.48, 21.45, 20.89, 20.69, 20.65, 17.03, 16.37, 14.39, 12.11.

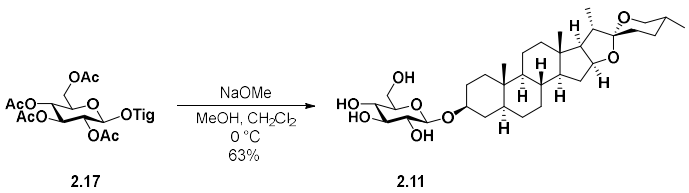

2.17 2.11

(2*R*,3*S*,4*S*,5*R*,6*R*)-2-(hydroxymethyl)-6-(((2a*S*,4*S*,5'*R*,6a*S*,6b*S*,8a*S*,8b*R*,9*S*,10*R*,11a*S*,12a*S*,12b*R*)-5',6a,8a,9-tetramethyldocosahydrospiro[naphtho[2',1':4,5]indeno[2,1-*b*]furan-10,2'-pyran]-4-yl)oxy)tetrahydro-2*H*-pyran-3,4,5-triol , 2.11.To a flame dried round bottom flask equipped with a magnetic stir bar and purged with argon and containing **2.17** (1.0 eq., 0.0800 g, 0.11 mmol) was added minimal amounts of anhydrous dichloromethane to dissolve the substrate, followed by addtion of anhydrous methanol ([0.2 M], 0.54 mL). After cooling the flask to 0 °C, a concentrated sodium methoxide solution was added. The reaction was stirred for 48 h, then neutralized with saturated aqueous sodium bicarbonate solution. The resulting mixture was concentrated *in vacuo*. Purification by flash column chromatography gave **2.11** as a white foam (43 mg, 69%). **^{1}H NMR** (500 MHz, $CDCl_3$/MeOD) δ = 5.58 (d, *J* = 5.1 Hz, 1H), 4.28 – 4.23 (m, 2H), 4.14 – 4.06 (m, 2H), 3.73 – 3.70 (m, 2H), 3.68 – 3.66 (m, 3H), 3.63 – 3.58 (m, 4H), 3.44 (q, *J* = 9.2, 6.9 Hz, 4H), 3.35 – 3.29 (m, 1H), 3.28 – 3.19 (m, 5H), 3.07 (t, *J* = 8.0 Hz, 1H), 1.99 (t, *J* = 4.8 Hz, 1H), 1.83 (dt, *J* = 12.7, 6.7 Hz, 1H), 1.77 – 1.68 (m, 2H), 1.64 – 1.58 (m, 1H), 1.41 – 1.33 (m, 6H), 1.30 – 1.25 (m, 1H), 1.00 – 0.91 (m, 3H), 0.81 (d, *J* = 6.9 Hz, 3H), 0.73 (t, *J* = 7.1 Hz, 1H), 0.68 – 0.61 (m, 9H), 0.50 (td, *J* = 11.4, 4.1 Hz, 1H). **^{13}C NMR** (150 MHz, $CDCl_3$/MeOD) δ = 109.51, 97.69, 81.00, 73.16, 73.05, 70.62, 68.71, 66.76, 62.07, 61.75, 56.23, 54.33, 44.79, 41.55, 40.49, 39.92, 37.52, 36.89, 35.48, 35.07, 32.16, 31.45, 31.14, 30.82, 30.08, 28.53, 21.06, 20.93, 16.71, 16.21, 14.05, 12.01.

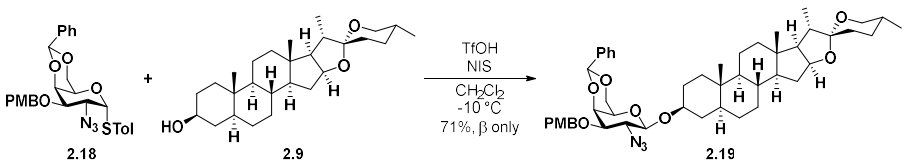

(2a*S*,4*S*,5'*R*,6a*S*,6b*S*,8a*S*,8b*R*,9*S*,10*R*,11a*S*,12a*S*,12b*R*)-4-(((2*S*,4a*R*,6*R*,7*R*,8*R*,8a*R*)-7-azido-8-((4-methoxybenzyl)oxy)-2-phenylhexahydropyrano[3,2-d][1,3]dioxin-6-yl)oxy)-5',6a,8a,9-tetramethyldocosahydrospiro[naphtho[2',1':4,5]indeno[2,1-*b*]furan-10,2'-pyran]--methane ($\mathbf{1/_1}$), 2.19. Acceptor **2.9** (1.0 equiv., 0.1000 g, 0.23 mmol) and donor **2.18** (1.0 equiv., 0.1201 g, 0.23 mmol) were coevaporated with dichloromethane (3 x 5 mL) followed by coevaporation with hexanes (3 x 5 mL) and placed on the high vac overnight. To the donor/acceptor mixture was added 4Å powdered molecular sieves and then the flask was purged with argon. The reaction flask was then rinsed down with anhydrous dichloromethane ([0.1 M], 2.31 mL). The reaction mixture was stirred for an hour at ambient temperature before cooling to -10 °C with an ice and brine bath. *N*-iodosuccinimide (2.0 equiv., 0.1040 g, 0.46 mmol) was added in one portion. After stirring for 30 min, 0.1 mL of a solution of triflic acid in anhydrous dichloromethane (1 drop of triflic acid in 0.3 mL of anhydrous dichloromethane) was added dropwise to the reaction. The reaction was quenched with triethylamine after 40 min and then diluted with dichloromethane, filtered through celite, dried (sodium sulfate), and concentrated *in vacuo.* The crude residue was purified via flash column chromatography to yield saponin **2.19** as a white foam (0.1342 g, 70%). **^{1}H NMR** (600 MHz, $CDCl_3$) δ = 7.55 – 7.50 (m, 2H), 7.37 – 7.31 (m, 6H), 6.90 – 6.84 (m, 2H), 5.46 (s, 1H), 4.66 (s, 2H), 4.38 (t, *J* = 7.9 Hz, 2H), 4.27 (d, *J* = 12.2 Hz, 1H), 4.02 (d, *J* = 3.6 Hz, 1H), 4.00 (dd, *J* = 12.3, 1.8 Hz, 1H), 3.84 – 3.78 (m, 4H), 3.66 (tt, *J* = 10.8, 4.7 Hz, 1H), 3.47 (dt, *J* = 10.3, 3.5 Hz, 1H), 3.37 (t, *J* = 10.9 Hz, 1H), 3.30 (dd, *J* = 10.3, 3.5 Hz, 1H), 3.26 (s, 1H), 1.97 (ddd, *J* = 12.5, 7.5, 5.4 Hz, 1H), 1.95 – 1.89 (m, 1H), 1.86 (p, *J* = 6.9 Hz, 1H), 1.78 – 1.72 (m, 1H), 1.73 – 1.41 (m, 12H), 1.37 (q, *J* = 12.2 Hz, 1H), 1.33 – 1.20 (m, 5H), 1.15 – 1.00 (m, 3H), 0.96 (d, *J* = 6.9 Hz,

3H), 0.89 (ddd, *J* = 20.3, 13.0, 4.7 Hz, 2H), 0.83 (s, 4H), 0.79 (d, *J* = 6.3 Hz, 4H), 0.76 (s, 3H), 0.62 (td, *J* = 11.5, 10.9, 4.0 Hz, 1H).**[13]C NMR** (150 MHz, $CDCl_3$) δ = 159.37, 137.68, 129.79, 129.44, 128.94, 128.12, 126.39, 113.82, 109.25, 101.13, 100.05, 80.84, 78.44, 72.55, 71.08, 69.26, 66.84, 66.40, 62.18, 62.00, 56.31, 55.28, 54.41, 44.77, 41.59, 40.57, 40.06, 36.99, 35.78, 35.07, 34.13, 32.30, 31.77, 31.36, 30.30, 29.24, 28.79, 28.74, 21.02, 17.13, 16.48, 14.49, 12.33.

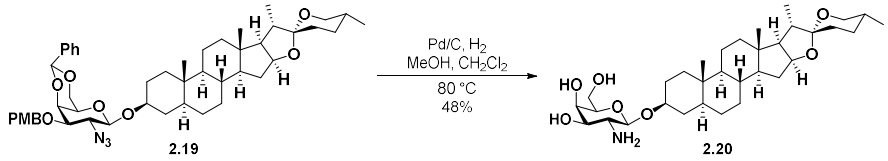

(2*R*,3*R*,4*R*,5*R*,6*R*)-5-amino-2-(hydroxymethyl)-6-(((2a*S*,4*S*,5'*R*,6a*S*,6b*S*,8a*S*,8b*R*,9*S*,10*R*,11a*S*,12a*S*,12b*R*)-5',6a,8a,9-tetramethyldocosahydrospiro[naphtho[2',1':4,5]indeno[2,1-*b*]furan-10,2'-pyran]-4-yl)oxy)tetrahydro-2*H*-pyran-3,4-diol--methane (1/1), 2.20. To a flame dried round bottom flask equipped with a magnetic stir bar and purged with argon with **2.19** (1.0 eq., 20 mg, 0.02 mmol) was added anhydrous methanol ([0.005 M], 5.0 mL) and the minimum amount of anhydrous dichloromethane needed to dissolve the starting material. Then Pd/C with 10% Pd (5.0 eq., 0.1285 g, 0.12 mmol) was added, followed by replacing the atmosphere with hydrogen gas via sparging. Then the flask was heated to 80 °C. After the reaction flask stirred at 80 °C for 2 h, the mixture was filtered through celite and the solution was concentrated *in vacuo.* Purification by flash column chromatography gave **2.20** as a white foam (6.9 mg, 48%). **[1]H NMR** (600 MHz, MeOD) δ = 4.27 (d, *J* = 8.2 Hz, 1H), 4.06 (q, *J* = 7.5 Hz, 1H), 3.56 (s, 1H), 3.44 (d, *J* = 6.0 Hz, 2H), 3.43 – 3.37 (m, 1H), 3.37 – 3.31 (m, 1H), 3.21 (t, *J* = 6.1 Hz, 1H), 3.13 (ddd, *J* = 10.8, 4.2, 2.0 Hz, 1H), 3.06 – 3.01 (m, 1H), 2.74 (t, *J* = 9.5 Hz, 1H), 1.70 – 1.62 (m, 2H), 1.59 – 1.51 (m,

2H), 1.44 – 1.33 (m, 6H), 1.33 – 1.16 (m, 5H), 1.13 – 1.05 (m, 1H), 1.05 – 0.88 (m, 10H), 0.80 (dtd, *J* = 18.7, 11.8, 10.8, 4.7 Hz, 3H), 0.66 (dd, *J* = 13.8, 4.0 Hz, 1H), 0.62 (d, *J* = 7.0 Hz, 3H), 0.61 – 0.53 (m, 1H), 0.51 (s, 3H), 0.46 (d, *J* = 6.3 Hz, 3H), 0.44 (s, 3H), 0.34 (ddd, *J* = 12.4, 10.4, 4.1 Hz, 1H). **^{13}C NMR** (150 MHz, MeOD) δ = 08.99, 80.46, 77.57, 74.58, 67.30, 66.24, 61.61, 60.39, 55.68, 53.80, 44.06, 41.06, 39.99, 39.37, 36.35, 35.07, 34.56, 33.36, 31.63, 30.93, 30.64, 29.58, 29.01, 28.57, 28.32, 28.07, 28.03, 23.61, 20.41, 16.15, 15.65, 13.49, 11.39.

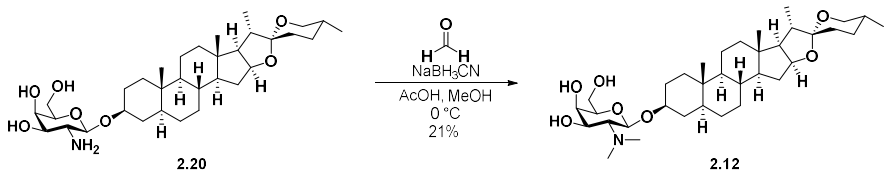

2.20 2.12

(2*R*,3*R*,4*R*,5*R*,6*R*)-5-(dimethylamino)-2-(hydroxymethyl)-6-(((2a*S*,4*S*,5'*R*,6a*S*,6b*S*,8a*S*,8b*R*,9*S*,10*R*,11a*S*,12a*S*,12b*R*)-5',6a,8a,9-tetramethyldocosahydrospiro[naphtho[2',1':4,5]indeno[2,1-*b*]furan-10,2'-pyran]-4-yl)oxy)tetrahydro-2*H*-pyran-3,4-diol, 2.12. To a flame dried round bottom flask equipped with a magnetic stir bar and purged with argon and containing **2.20** (1.0 eq., 6.5 mg, 0.01 mmol) was added anhydrous methanol ([0.17 M], 0.06 mL) at ambient temperature. Then aqueous formaldehyde (37% by weight, 100 equiv., 0.0888 g, 1.09 mmol) was added dropwise. After stirring the reaction mixture at 0 °C for 10 min, sodium cyanoborohydride (66.5 equiv., 0.0457 g, 0.73 mmol) was added portion wise. After adding a venting needle, acetic acid (82.0 equiv., 0.05 mL, 0.90 mmol) was added dropwise to the reaction mixture at 0 °C. After stirring for 16 h, the colorless reaction mixture was quenched with aqueous 1N sodium hydroxide solution, during which the reaction mixture turned white and cloudy. The resulting mixture was diluted with a mixture of dichloromethane and deionized water (5:4) before being extracted with dichloromethane (x7). The combined organic solution was dried over sodium sulfate and

concentrated *in vacuo*. Purification by flash column chromatography gave **2.12** as a white foam (1.4 mg, 21%). **^{1}H NMR** (600 MHz, MeOD) δ = 4.53 (d, *J* = 8.3 Hz, 1H), 4.20 (d, *J* = 7.6 Hz, 1H), 3.78 (d, *J* = 3.2 Hz, 1H), 3.56 (d, *J* = 6.0 Hz, 2H), 3.54 – 3.49 (m, 1H), 3.30 – 3.25 (m, 2H), 3.17 (d, *J* = 8.5 Hz, 1H), 2.73 (t, *J* = 9.6 Hz, 1H), 2.57 (s, 1H), 2.49 (s, 6H), 1.80 – 1.76 (m, 2H), 1.70 – 1.66 (m, 2H), 1.56 (dd, *J* = 8.7, 6.8 Hz, 1H), 1.53 – 1.27 (m, 8H), 1.26 – 1.17 (m, 1H), 1.16 – 1.01 (m, 11H), 0.96 – 0.88 (m, 3H), 0.75 (d, *J* = 7.0 Hz, 3H), 0.73 – 0.65 (m, 1H), 0.64 (s, 3H), 0.59 (d, *J* = 6.4 Hz, 3H), 0.56 (s, 3H), 0.45 (ddd, *J* = 12.3, 10.6, 4.0 Hz, 1H).**^{13}C NMR** (150 MHz, MeOD) δ = 109.22, 97.47, 80.66, 77.66, 74.34, 67.87, 67.60, 66.49, 64.91, 61.71, 60.70, 55.86, 53.97, 44.31, 41.25, 40.20, 39.58, 36.53, 35.31, 34.71, 34.26, 31.82, 31.17, 30.86, 29.79, 29.26, 29.18, 28.31, 28.24, 20.61, 16.51, 15.98, 13.84, 11.78.

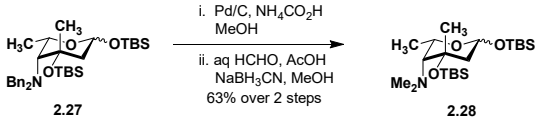

(2*S*,3*R*,4*S*)-4,6-bis((*tert*-butyldimethylsilyl)oxy)- *N,N*,2,4-tetramethyltetrahydro-2*H*-pyran-3-amine, 2.28. To a flame dried round bottom flask equipped with a magnetic stir bar with **2.27** (1.0 equiv., 0.1000 g, 0.18 mmol) was added ammonium formate (24 equiv., 0.2655 g, 4.21 mmol). The flask was then rinsed down with anhydrous methanol ([0.4 M], 4.39 mL). After purging for 5 min, Pd/C with 10% Pd (1.0 equiv., 0.1867 g, 0.18 mmol) was added and the reaction lowered to a preheated 50 °C oil bath. After stirring at 50 °C for 6 h, the reaction flask was removed from the oil bath and allowed to cool to ambient temperature. The mixture was filtered through celite and the solution was concentrated *in vacuo.*

To the crude product in a flame dried round bottom flask equipped with a magnetic stir bar was added anhydrous methanol ([0.17], 1.03 mL) at ambient temperature. Then aqueous

formaldehyde (37% by weight, 100 equiv, 1.4238 g, 17.5445 mmol) was added dropwise. After stirring at 0 °C for 10 min, the reaction mixture was added sodium cyanoborohydride (66.5 equiv., 0.7332 g, 11.67 mmol) portion wise. After adding a venting needle, acetic acid (82.0 equiv., 0.82 mL, 14.39 mmol) was added dropwise to the reaction mixture at 0 °C . After stirring for 16 h, the colorless reaction mixture was quenched with aqueous 1 N sodium hydroxide solution (18 mL), during which the reaction mixture turned white and cloudy. The resulting mixture was diluted with 20 mL dichloromethane and 8 mL deionized water before being extracted with dichloromethane (x7). The combined organic solution was dried over sodium sulfate and concentrated *in vacuo*. Purification by flash column chromatography gave **2.28** as a clear oil (46.1 mg, 63%). **^{1}H NMR** (600 MHz, $CDCl_3$) δ = 5.29 (s, 1H), 4.65 (d, *J* = 9.6 Hz, 2H), 4.19 (p, *J* = 6.0 Hz, 1H), 3.67 – 3.60 (m, 2H), 2.68 (s, 12H), 2.64 (s, 7H), 2.27 (s, 1H), 2.16 (dd, *J* = 13.5, 4.0 Hz, 1H), 2.08 (s, 2H), 2.02 (t, *J* = 11.1 Hz, 2H), 1.82 (d, *J* = 12.6 Hz, 2H), 1.70 (d, *J* = 13.4 Hz, 1H), 1.48 (s, 3H), 1.33 (s, 6H), 1.28 – 1.21 (m, 11H), 0.93 – 0.87 (m, 56H), 0.16 – 0.12 (m, 18H), 0.12 – 0.04 (m, 20H). **^{13}C NMR** (150 MHz, $CDCl_3$) δ = 95.05, 91.52, 78.07, 76.87, 72.22, 69.61, 69.20, 67.39, 46.68, 44.93, 44.70, 44.32, 32.14, 30.69, 29.70, 26.37, 26.31, 25.98, 25.68, 18.49, 18.40, 18.28, 18.26, 18.23, 17.85, -1.11, -1.16, -1.36, -1.39, -4.07, -4.46, -4.73, -5.75.

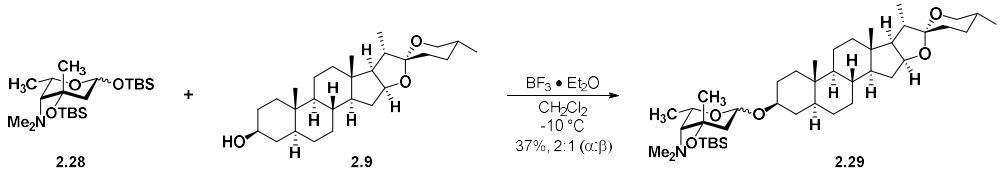

2.28 2.9 2.29

(2*S*,3*R*,4*S*)-4-((*tert*-butyldimethylsilyl)oxy)-*N*,*N*,2,4-tetramethyl-6-(((2a*S*,4*S*,5'*R*,6a*S*,6b*S*,8a*S*,8b*R*,9*S*,10*R*,11a*S*,12a*S*,12b*R*)-5',6a,8a,9-tetramethyldocosahydrospiro[naphtho[2',1':4,5]indeno[2,1-*b*]furan-10,2'-pyran]-4-

yl)oxy)tetrahydro-2*H*-pyran-3-amine, 2.29. Acceptor **2.9** (1.0 equiv., 40.0 mg, 0.10 mmol) and donor **2.28** (1.1 equiv., 44.1 mg, 0.11 mmol) were coevaporated with dichloromethane (3 x 5 mL) followed by coevaporation with hexanes (3 x 5 mL) and placed on the high vac overnight. To the donor/acceptor mixture was added 4Å powdered molecular sieves and then the mixture was purged with argon. The reaction flask was then rinsed down with anhydrous dichloromethane ([0.13 M], 1.0 mL). The reaction mixture was stirred for an hour at ambient temperature. Then $BF_3 \cdot OEt_2$ (8.0 equiv., 0.1 mL, 0.77 mmol) was added dropwise to the reaction, followed by sonication for 25 min (x3) at ambient temperature. The reaction was quenched with triethylamine, diluted with dichloromethane and filtered through celite, dried (sodium sulfate), and concentrated *in vacuo.* The crude residue was purified via flash column chromatography to yield saponin **2.29** as a white foam (24.7 mg, 37%). **^{1}H NMR** (600 MHz, $CDCl_3$) δ = 5.16 (t, *J* = 3.6 Hz, 1H), 5.08 – 5.04 (m, 2H), 4.47 (dd, *J* = 10.1, 2.6 Hz, 1H), 4.38 (q, *J* = 7.4 Hz, 3H), 4.14 – 4.02 (m, 3H), 3.68 – 3.56 (m, 1H), 3.51 – 3.42 (m, 5H), 3.37 (t, *J* = 11.0 Hz, 3H), 2.70 – 2.59 (m, 24H), 2.28 (dd, *J* = 20.7, 3.5 Hz, 3H), 2.19 (dd, *J* = 13.7, 4.4 Hz, 1H), 2.15 (dd, *J* = 13.6, 4.5 Hz, 2H), 1.97 (ddd, *J* = 12.4, 7.4, 5.4 Hz, 3H), 1.85 (p, *J* = 6.9 Hz, 3H), 1.78 – 1.56 (m, 21H), 1.55 – 1.36 (m, 18H), 1.33 – 1.13 (m, 51H), 0.96 (d, *J* = 6.9 Hz, 8H), 0.93 – 0.83 (m, 41H), 0.81 (s, 7H), 0.79 (d, *J* = 6.3 Hz, 7H), 0.75 (s, 8H), 0.68 – 0.60 (m, 3H), 0.17 – 0.12 (m, 24H). **^{13}C NMR** (150 MHz, $CDCl_3$) δ = 109.20, 80.81, 66.81, 62.15, 56.23, 54.29, 44.63, 41.57, 40.53, 40.36, 35.75, 35.06, 34.16, 32.21, 31.73, 31.55, 31.34, 30.27, 29.67, 29.33, 28.77, 26.26, 25.74, 22.62, 20.98, 18.27, 17.10, 16.45, 14.46, 14.09, 12.30, 0.98, -1.19, -1.42.

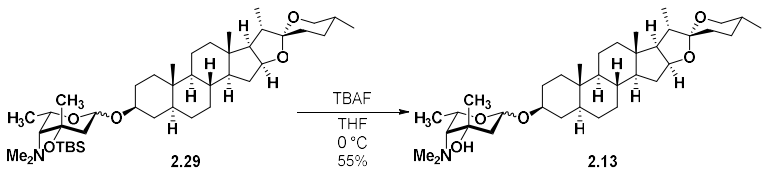

(2*S*,3*R*,4*S*)-3-(dimethylamino)-2,4-dimethyl-6-(((2a*S*,4*S*,5'*R*,6a*S*,6b*S*,8a*S*,8b*R*,9*S*,10*R*,11a*S*,12a*S*,12b*R*)-5',6a,8a,9-tetramethyldocosahydrospiro[naphtho[2',1':4,5]indeno[2,1-*b*]furan-10,2'-pyran]-4-yl)oxy)tetrahydro-2*H*-pyran-4-ol, 2.13. To a flame dried round bottom flask equipped with a magnetic stir bar and purged with argon containing **2.29** (1.0 eq., 15.6 mg, 0.02 mmol) was added anhydrous tetrahydrofuran ([0.022 M], 1.0 mL). After dropwise addition of a 1 M solution of tetrabutylammonium fluoride (TBAF) in tetrahydrofuran (20.0 eq., 0.44 mL, 0.44 mmol), the reaction was heated to 50 °C. The reaction stirred for 24 h before adding more of the 1M solution of tetrabutylammonium fluoride (TBAF) in tetrahydrofuran (20.0 eq., 0.44 mL, 0.44 mmol). At 48 h, the reaction was diluted with ethyl acetate and then washed with 1N hydrochloric acid (x3), saturated aqueous sodium carbonate solution (x1), and brine (x1). The organic solution was dried over sodium sulfate and concentrated *in vacuo*. Purification by flash column chromatography gave **2.13** as a white foam (7.2 mg, 55%). **^{1}H NMR** (600 MHz, $CDCl_3$/MeOD) δ =. 5.35 (t, *J* = 4.7 Hz, 1H), 4.39 (q, *J* = 7.5 Hz, 1H), 4.15 – 4.06 (m, 1H), 3.67 – 3.63 (m, 3H), 3.49 – 3.45 (m, 1H), 3.40 (d, *J* = 8.5 Hz, 0H), 3.38 – 3.33 (m, 8H), 2.72 (s, 4H), 2.25 – 2.20 (m, 1H), 1.99 (ddd, *J* = 25.2, 12.5, 6.1 Hz, 3H), 1.86 (t, *J* = 6.9 Hz, 1H), 1.81 – 1.37 (m, 18H), 1.20 – 0.99 (m, 3H), 0.96 (d, *J* = 7.0 Hz, 3H), 0.88 (t, *J* = 7.0 Hz, 5H), 0.82 (d, *J* = 1.5 Hz, 2H), 0.79 (d, *J* = 6.4 Hz, 3H), 0.76 (s, 3H), 0.64 (t, *J* = 11.5 Hz, 1H). **HRMS** (ESI) $C_{36}H_{61}NO_5$, Calculated: $[M+H]^+$, 588.4623; Found: $[M+H]^+$, 588.4586.

2.7.4. Compounds for Anticancer Assay: *In vitro* cytotoxicity evaluation in H69AR and HCT116 Cell lines

Staurosporine purchased from Sigma-Aldrich was solubilized in DMSO at 1mM and evaluated in the cytotoxicity assays using a high test concentration of 1 μM. Test materials were soubilized in DMSO at 10 mM immediately prior to assay set up and evaluated using a high test concentration of 40 μM and five serial half-logarithmic dilutions.

2.7.5. *In Vitro* Anti-Cancer Evaluations

Cells were counted by the Trypan Blue Dye exclusion method and seeded in 96 well flat bottom microtiter plates at 1 x 10^4 cells per well in 100 μL/well. Cells were incubated overnight at 37 °C/ 5 % CO_2 to allow the cells to adhere to the plates. The medium was removed and replaced with 100 μL/well of fresh medium. Then 100 μL of each compound at six concentrations was transferred to the 96-well plate containing the cells, in triplicate. Following 3 days inbubation at 37 °C/ 5 % CO_2, cell viability was measured using XTT tetrazolium dye as described below. Table 4 lists the tumor cell line, vendor catalog number and culture medium.

Table 4 Cancer Cell Line Information

Cell line	Cell Type	Vendor	Culture Medium
HCT116	Human colorectal carcinoma	ATCC CCL247	McCoy's 5A, 10% FBS, 2 mM L-glutamine
H69AR	Human lung carcinoma	ATCC CRL11351	RPMI1640, 20% FBS, 2 mM L-glutamine

2.7.6. XTT Staining for Compound Cytotoxicity

Following incubation at 37 °C in a 5 % CO_2 incubator for three days, the test plates were stained with the tetrazolium dye XTT (2,3-bis(2-methoxy-4-nitro-5-sulfophenyl)-5-[(phenylamino)carbonyl] -2H-tetrazolium hydroxide). XTT-tetrazolium was metabolized by the mitochondrial enzymes of metabolically active cells to a soluble formazan product, allowing rapid quantitative analysis of the inhibition of cell killing by test substances. XTT solution was prepared daily as a stock of 1 mg/mL in RPMI1640. Phenazine methosulfate (PMS) solution was prepared at 0.15 mg/mL in PBS and stored in the dark at -20 °C. XTT/PMS stock was prepared immediately before use by adding 40 µL of PMS per mL of XTT solution. Then, 50 µL of XTT/PMS was added to each well of the plate and the plate was reincubated for 4 hours at 37 °C. Plates were sealed with adhesive plate sealers and shaken gently or inverted several times to mix the soluble formazan product and the plate was read spectrophotometrically at 450/650 nm with a Molecular Devices Vmax plate reader.

2.7.7. Data Analysis and Evaluation

Microsoft Excel 2010 was used to analyze and graph the raw data. TC_{50} (50% reduction in cell viability) values are tabulated.

2.8. Relevant Spectra

^{1}H NMR (600 MHz, $CDCl_3$) spectra of 2.15

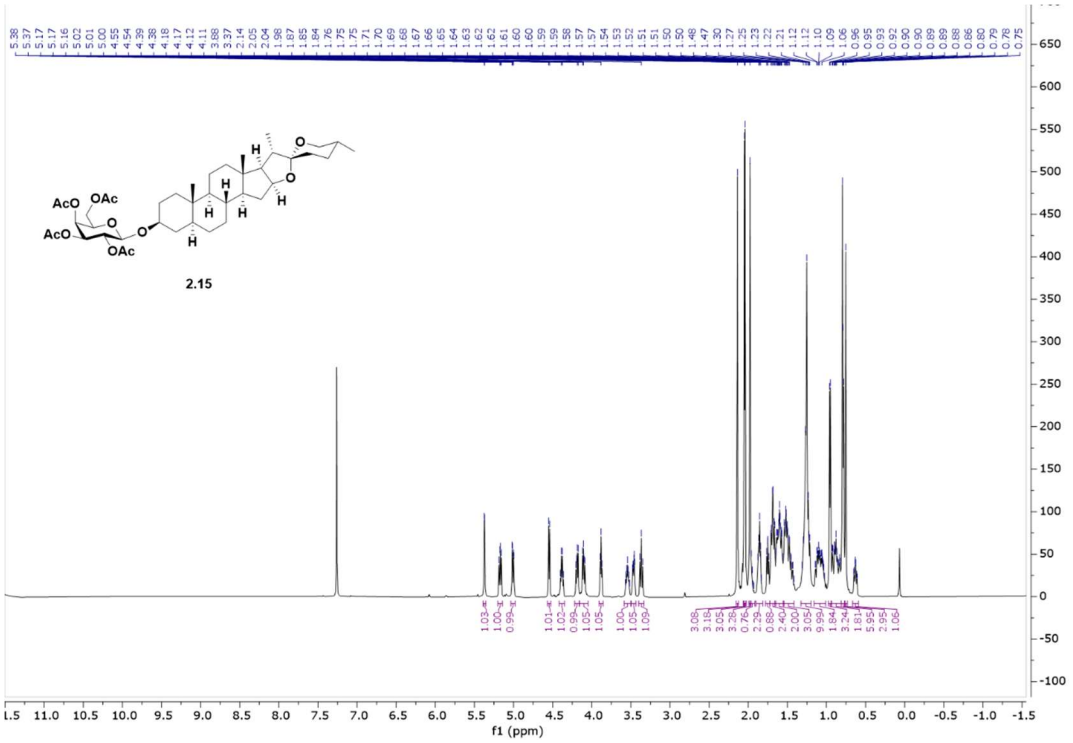

^{13}C NMR (150 MHz, $CDCl_3$) spectra of **2.15**

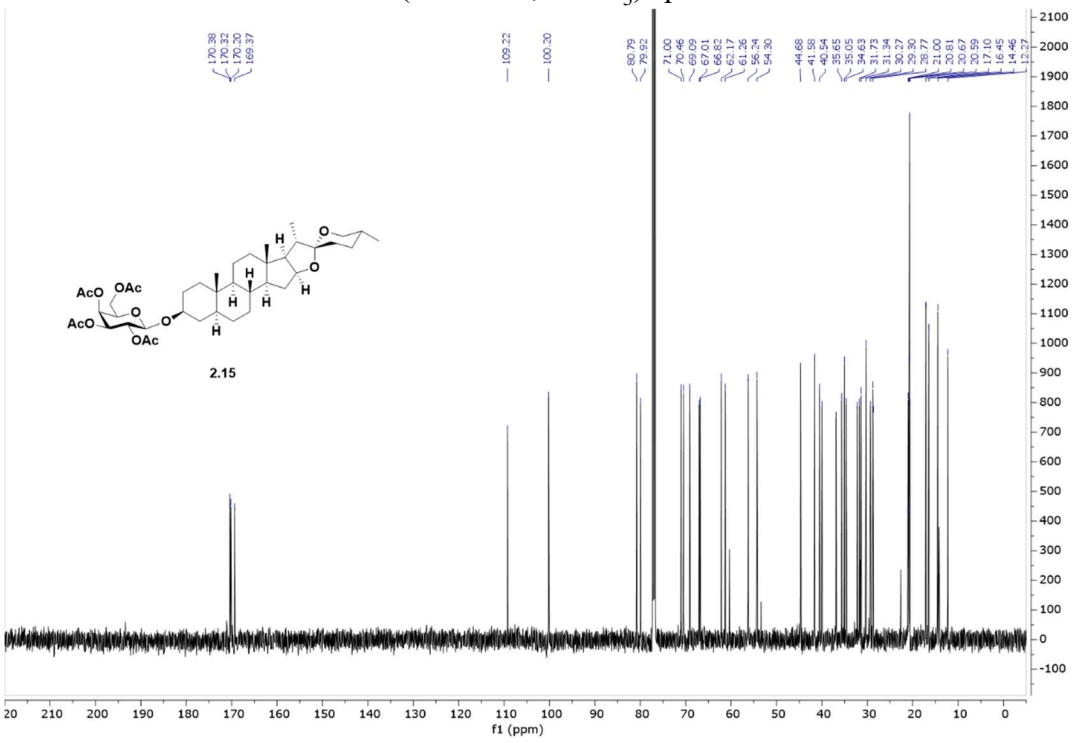

^{1}H ^{13}C HSQC NMR (600 MHz, $CDCl_3$) spectra of **2.15**

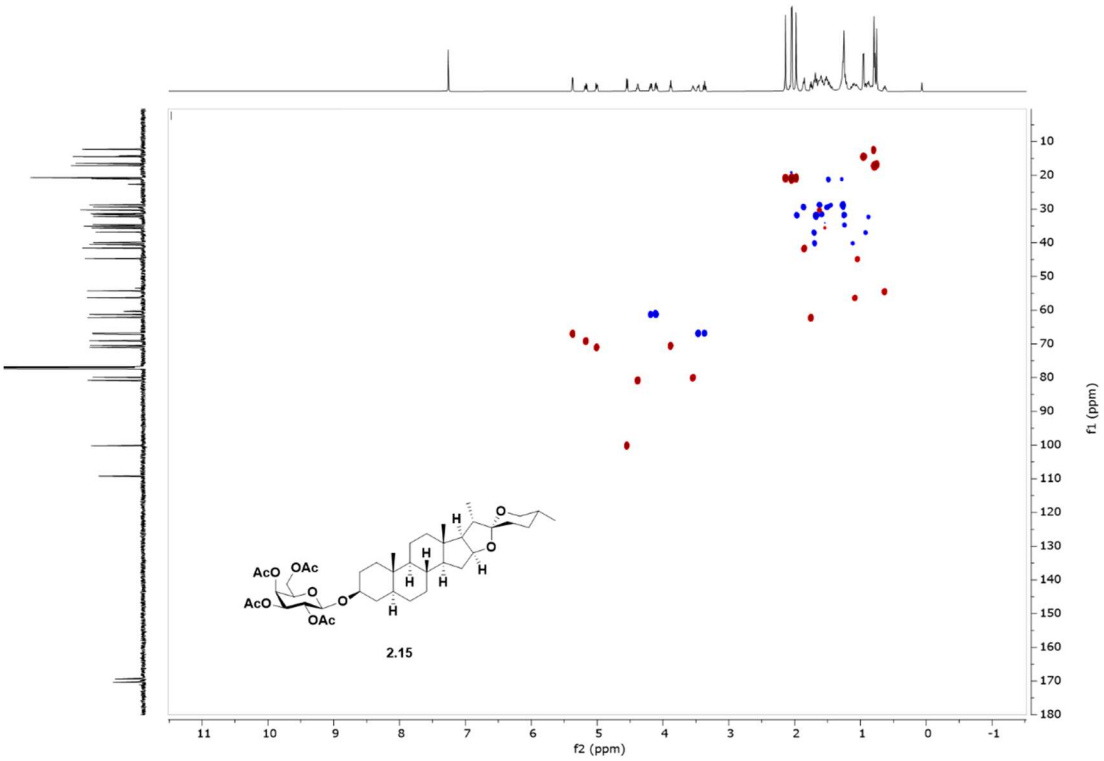

^{1}H ^{13}C HSQC NMR (600 MHz, $CDCl_3$) spectra zoomed in region of **2.15**

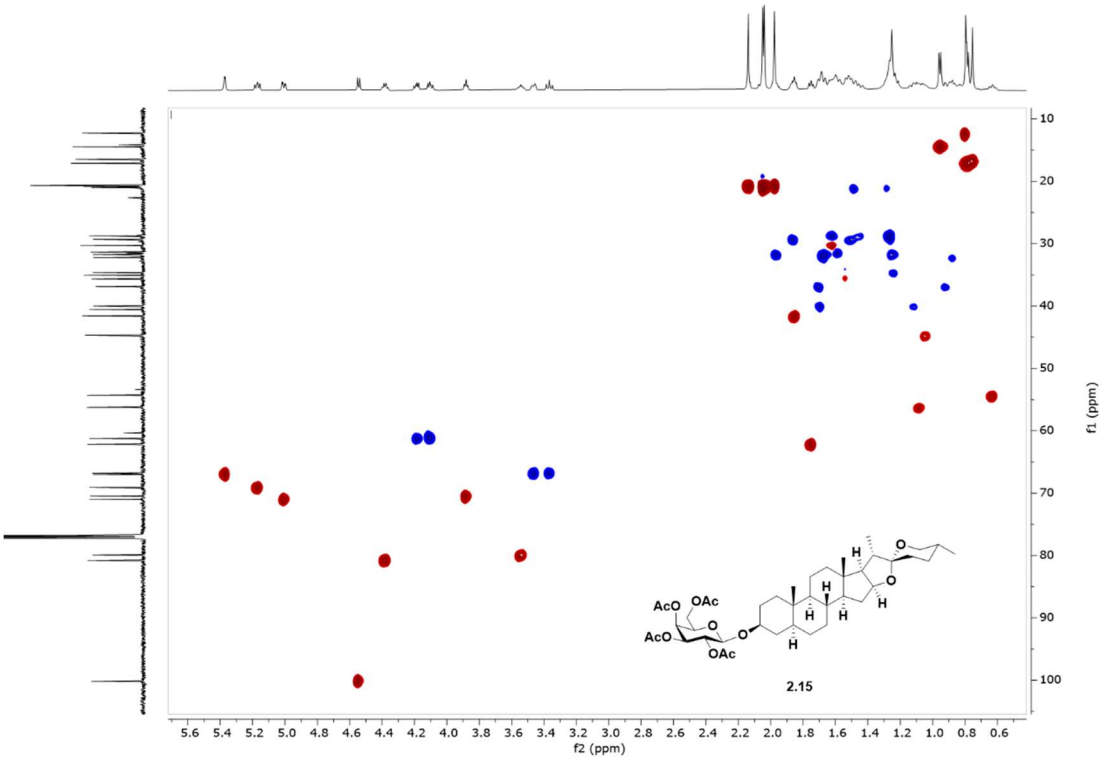

^{1}H ^{1}H COSY NMR (600 MHz, $CDCl_3$) spectra of **2.15**

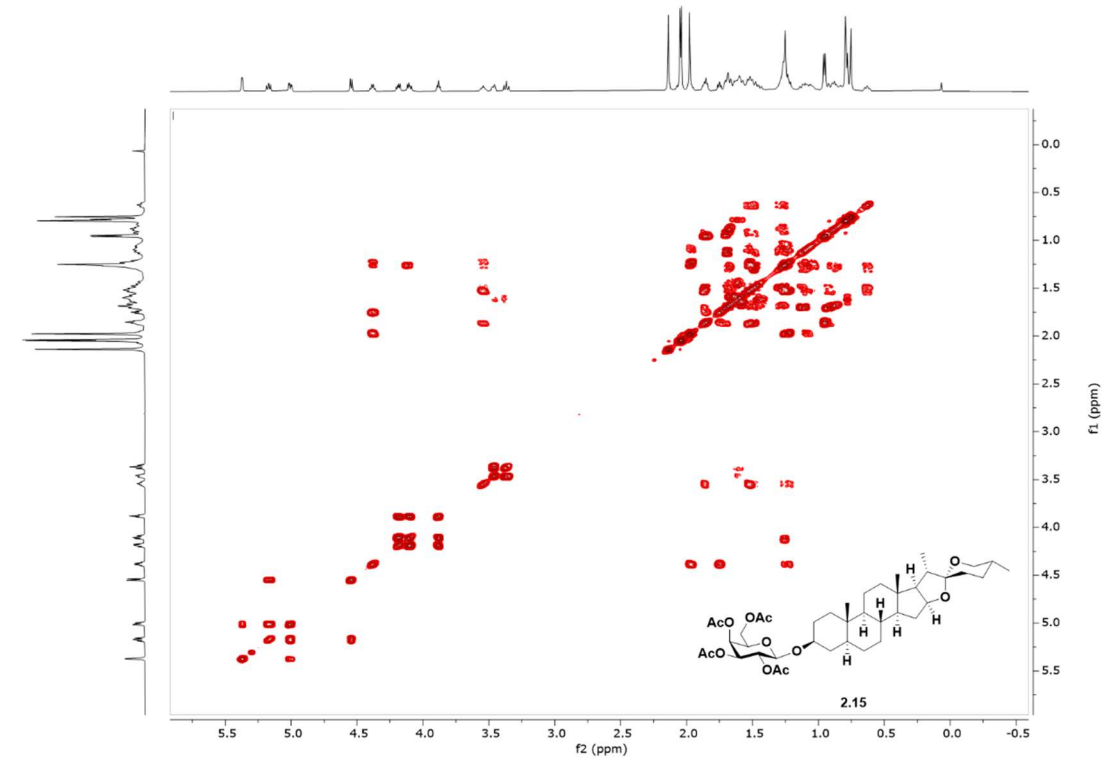

^{1}H ^{13}C HMBC NMR (600 MHz, $CDCl_3$) spectra zoomed in region of **2.15**

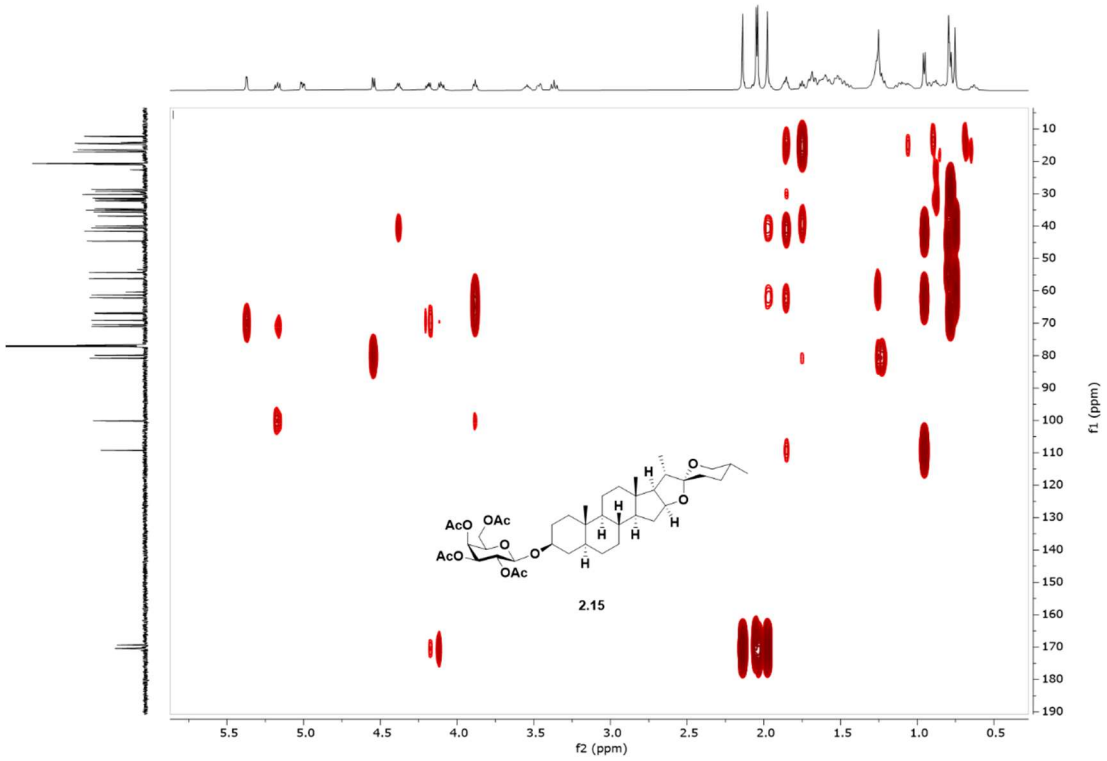

^{1}H NMR (600 MHz, d-pyridine) spectra of **2.10**

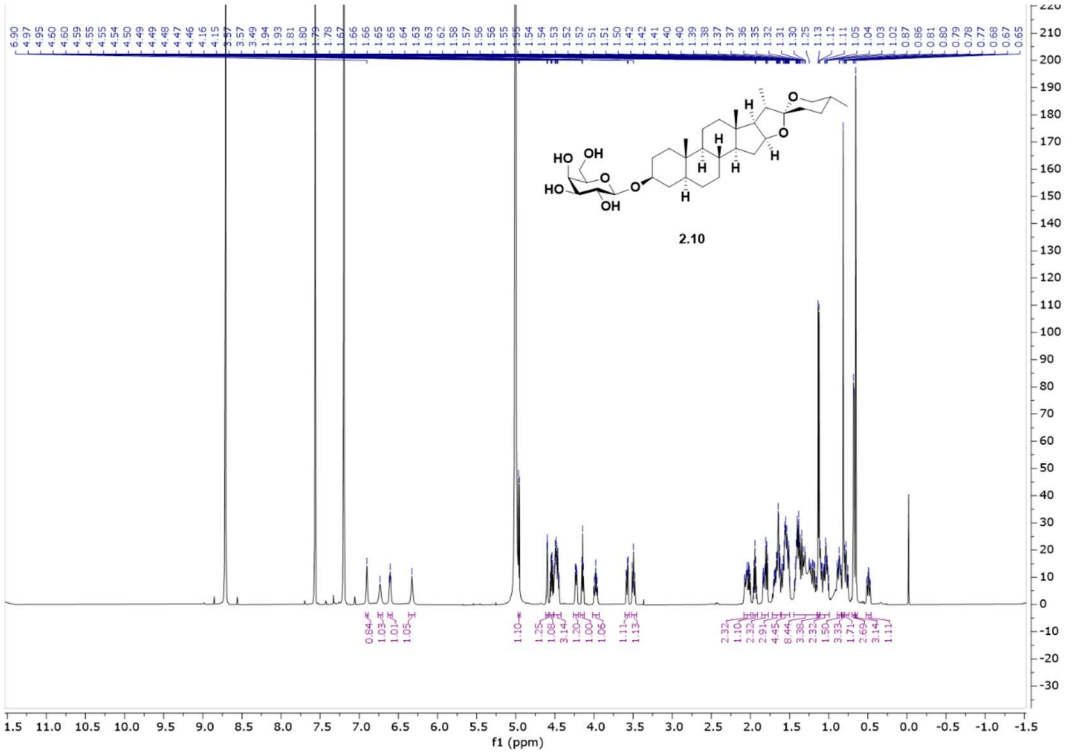

^{13}C NMR (150 MHz, d-pyridine) spectra of **2.10**

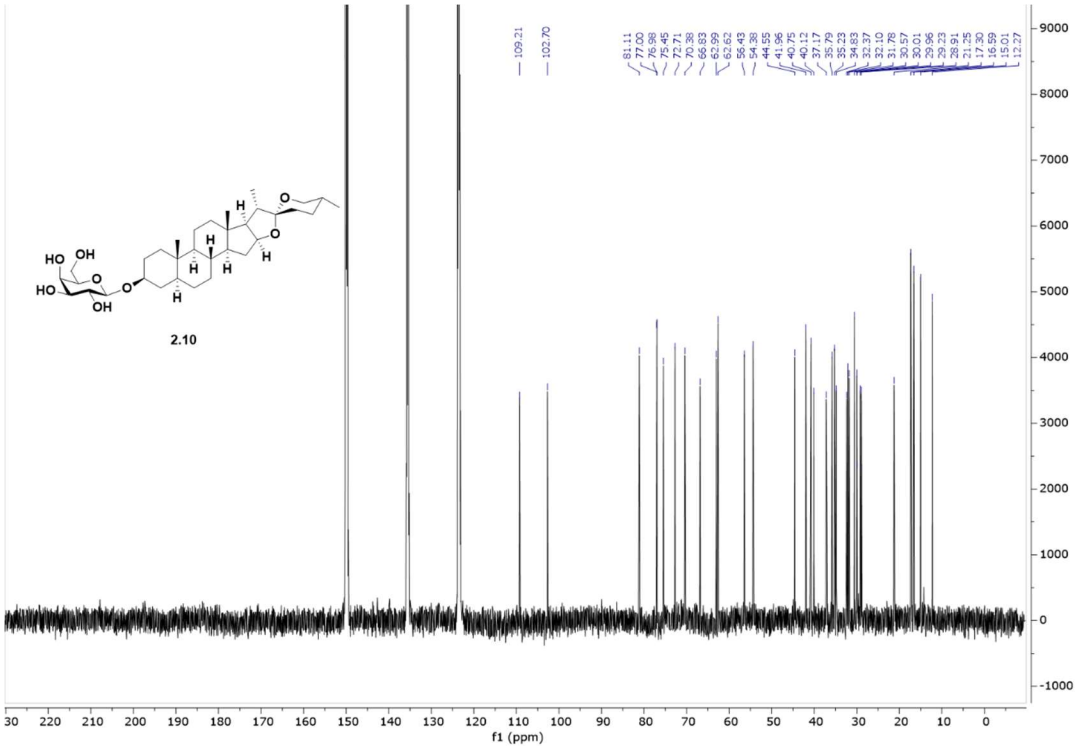

^{1}H ^{13}C HSQC NMR (600 MHz, d-pyridine) spectra of **2.10**

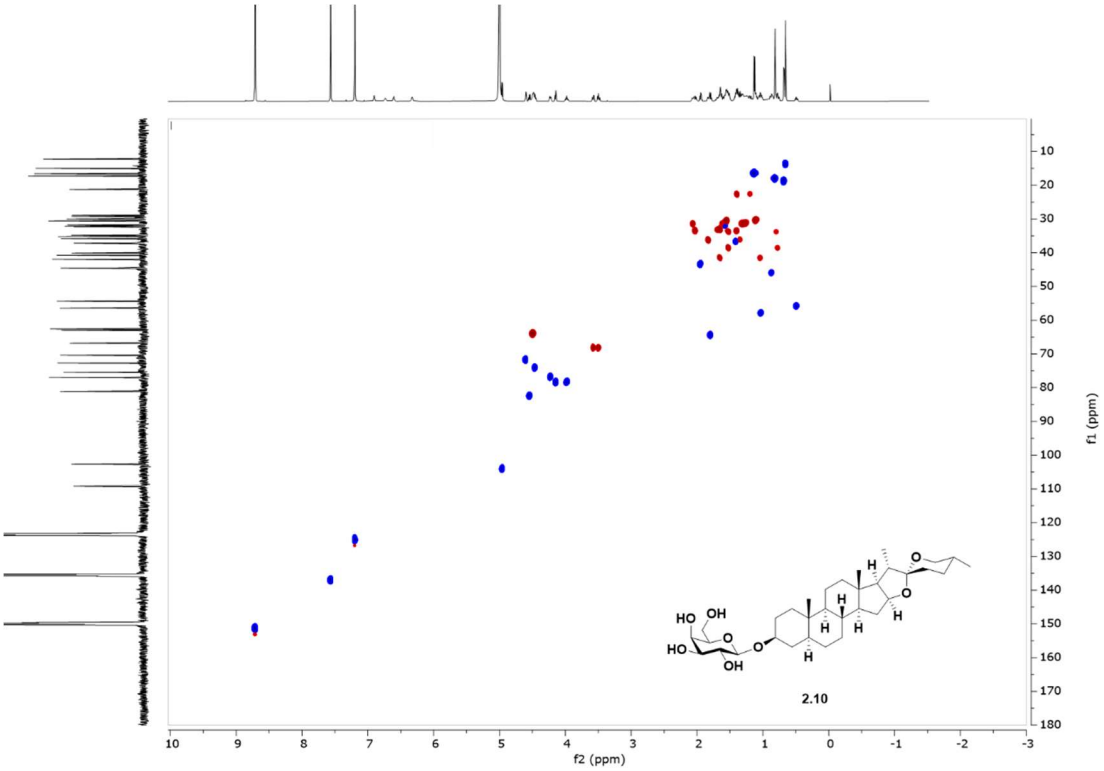

^{1}H ^{13}C HSQC NMR (600 MHz, d-pyridine) spectra zoomed in region of **2.10**

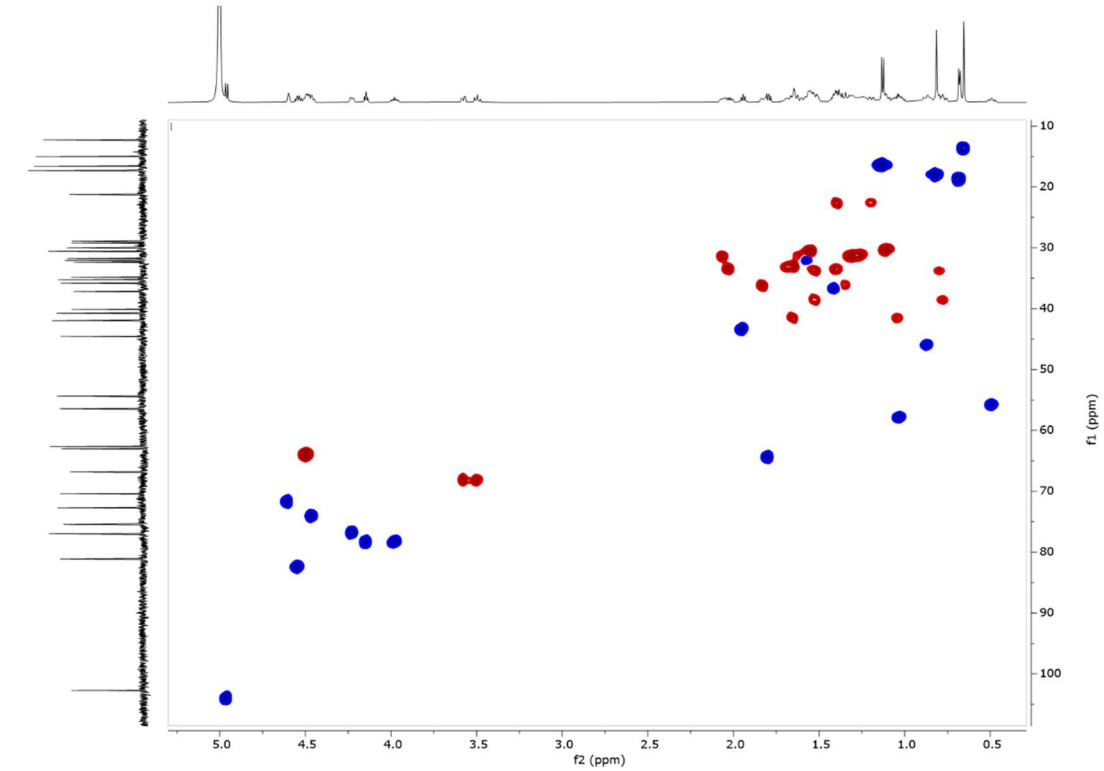

^{1}H ^{1}H COSY NMR (600 MHz, d-pyridine) spectra of **2. 10**

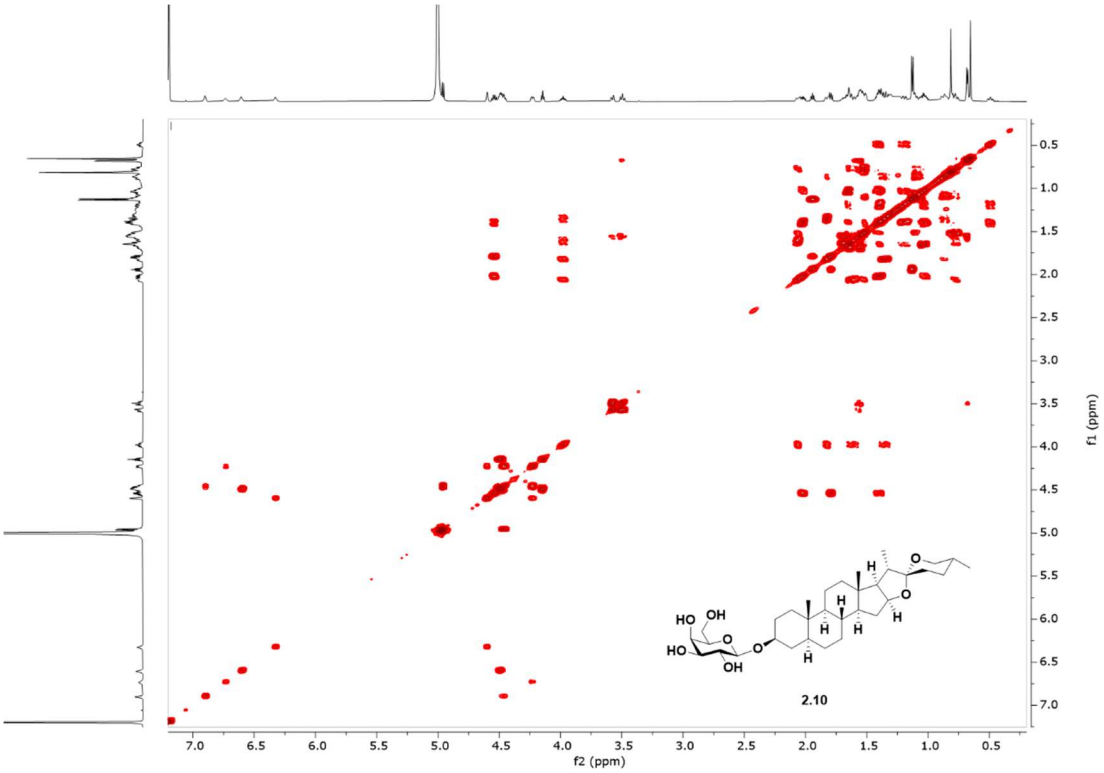

^{1}H ^{13}C HMBC NMR (600 MHz, d-pyridine) spectra zoomed in region of **2. 10**

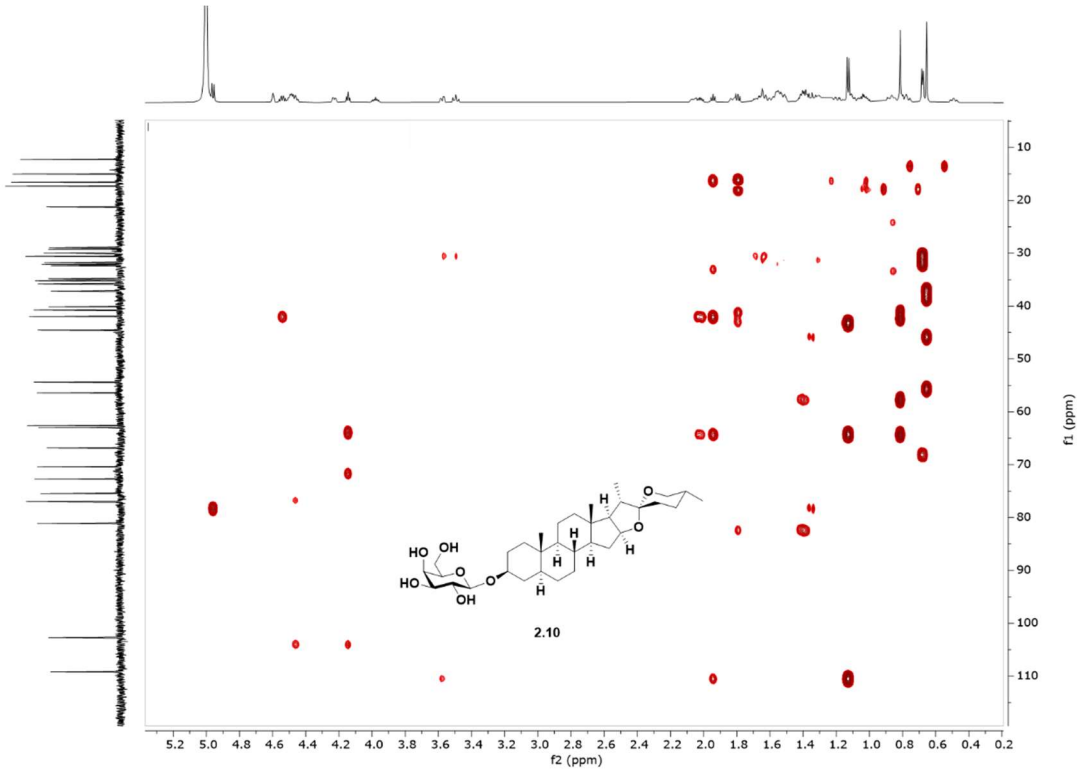

^{1}H NMR (600 MHz, $CDCl_3$) spectra of **2.17**

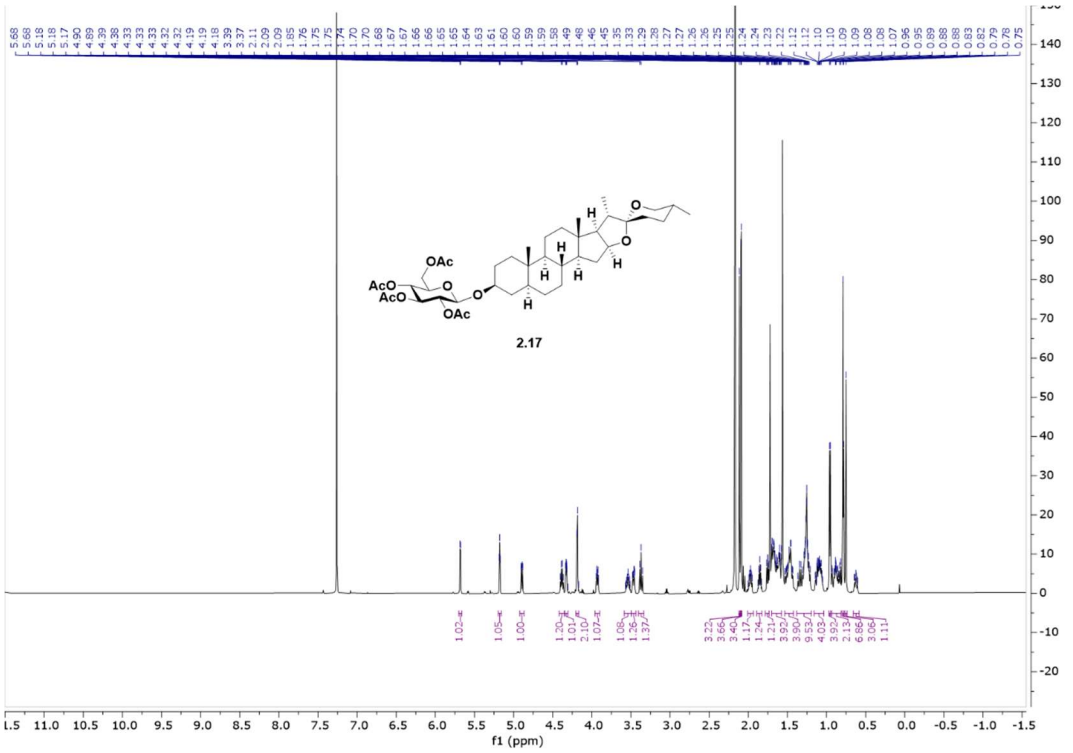

^{13}C NMR (150 MHz, $CDCl_3$) spectra of **2.17**

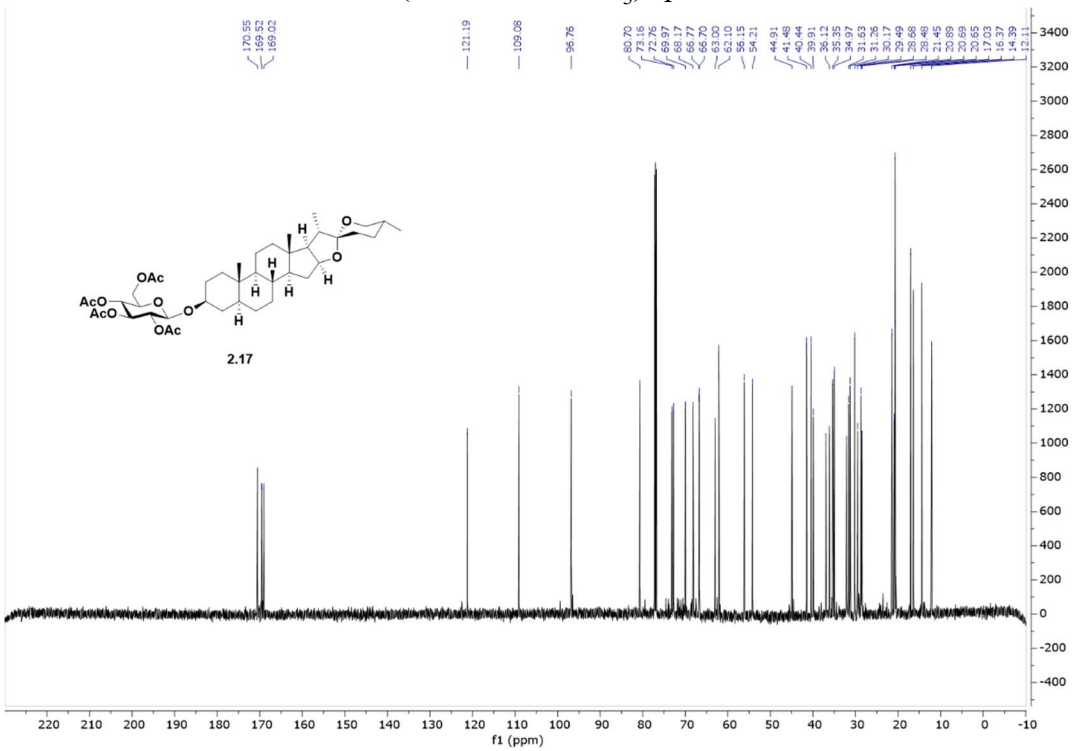

^{1}H ^{13}C HSQC NMR (600 MHz, $CDCl_3$) spectra of **2.17**

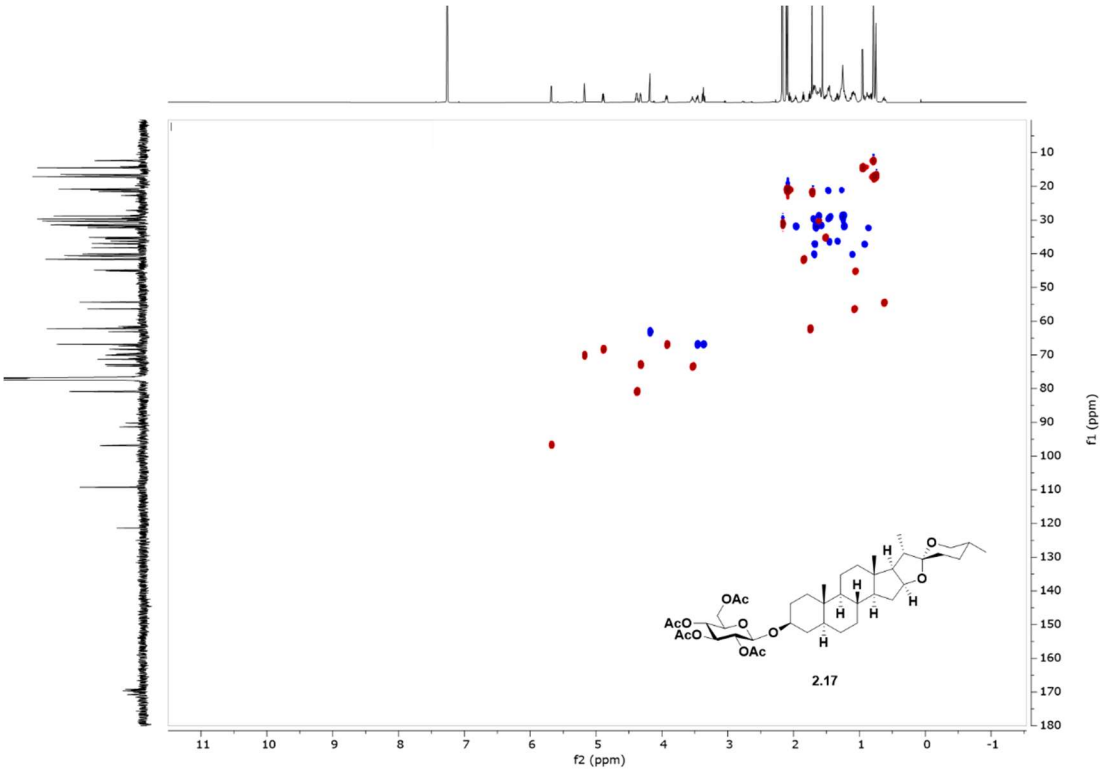

^{1}H ^{13}C HSQC NMR (600 MHz, $CDCl_3$) spectra zoomed in region of **2. 17**

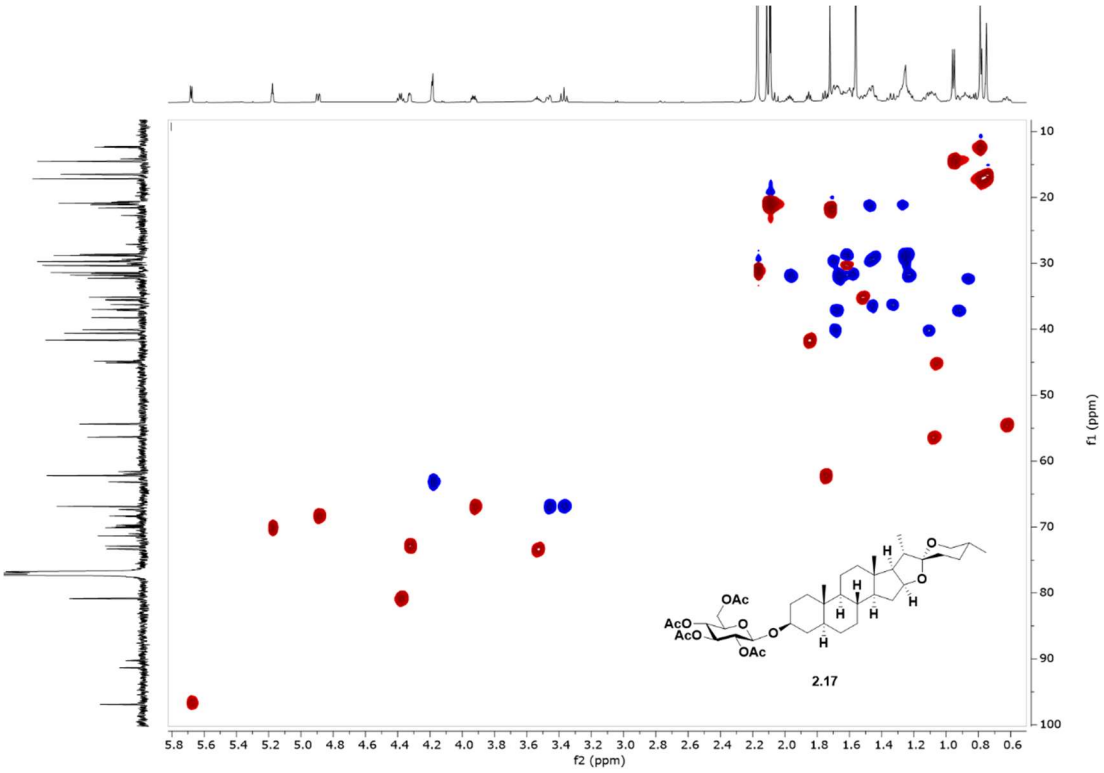

^{1}H NMR (600 MHz, $CDCl_3$/MeOD) spectra of **2.11**

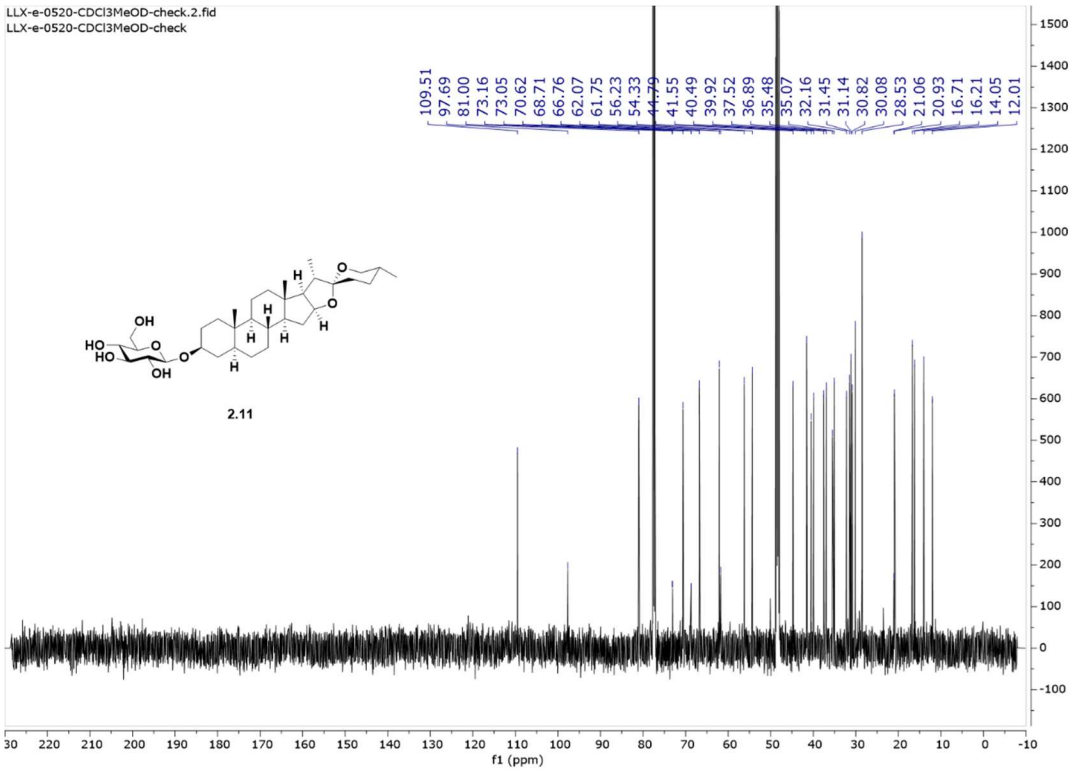

^{13}C NMR (150 MHz, $CDCl_3$/MeOD) spectra of **2.11**

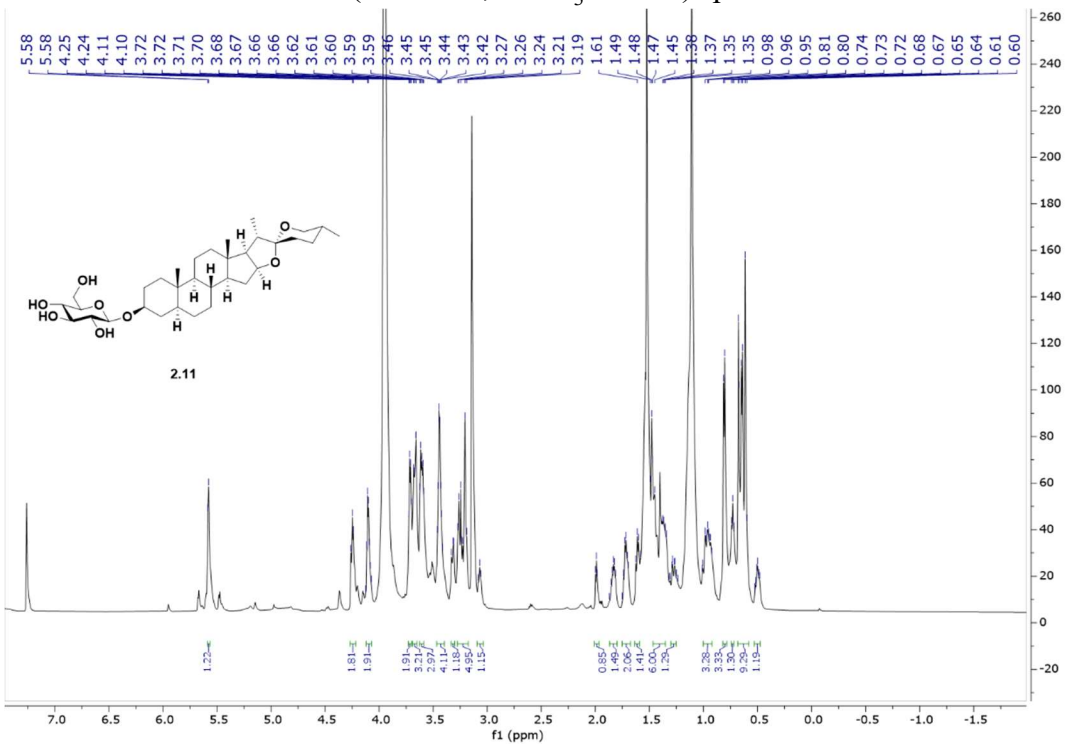

^{1}H ^{13}C HSQC NMR (600 MHz, $CDCl_3$/MeOD) spectra of **2. 11**

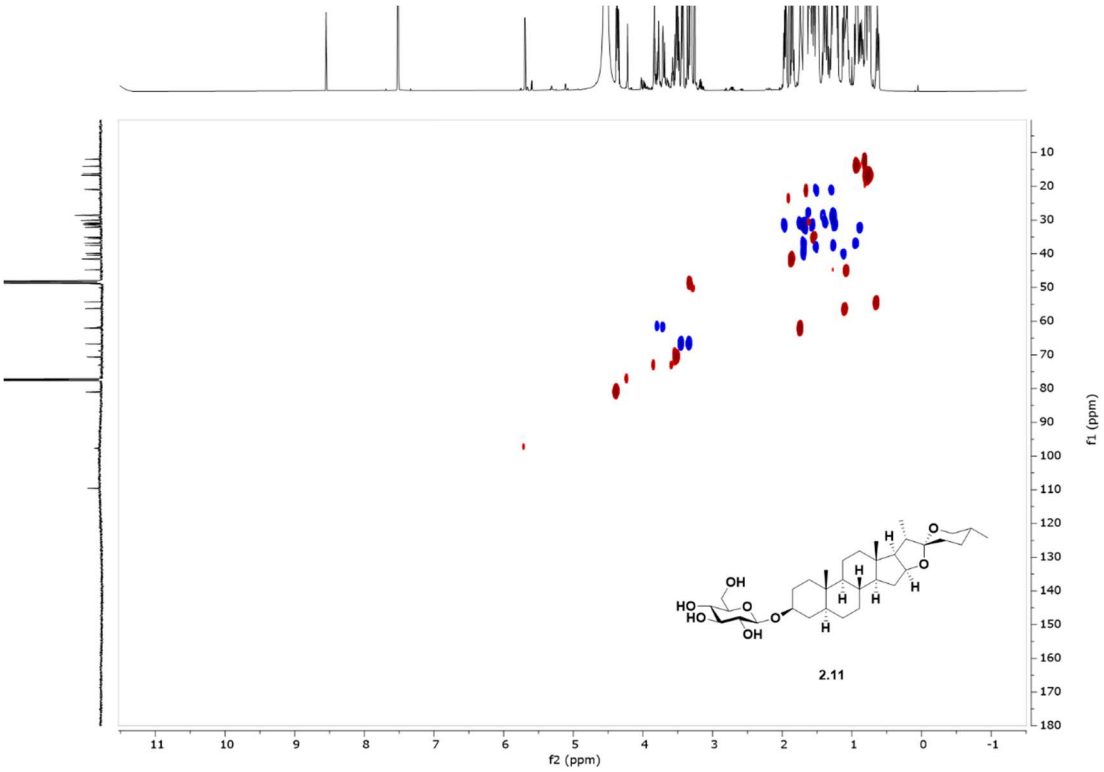

^{1}H ^{13}C HSQC NMR (600 MHz, $CDCl_3$/MeOD) spectra zoomed in region of **2. 11**

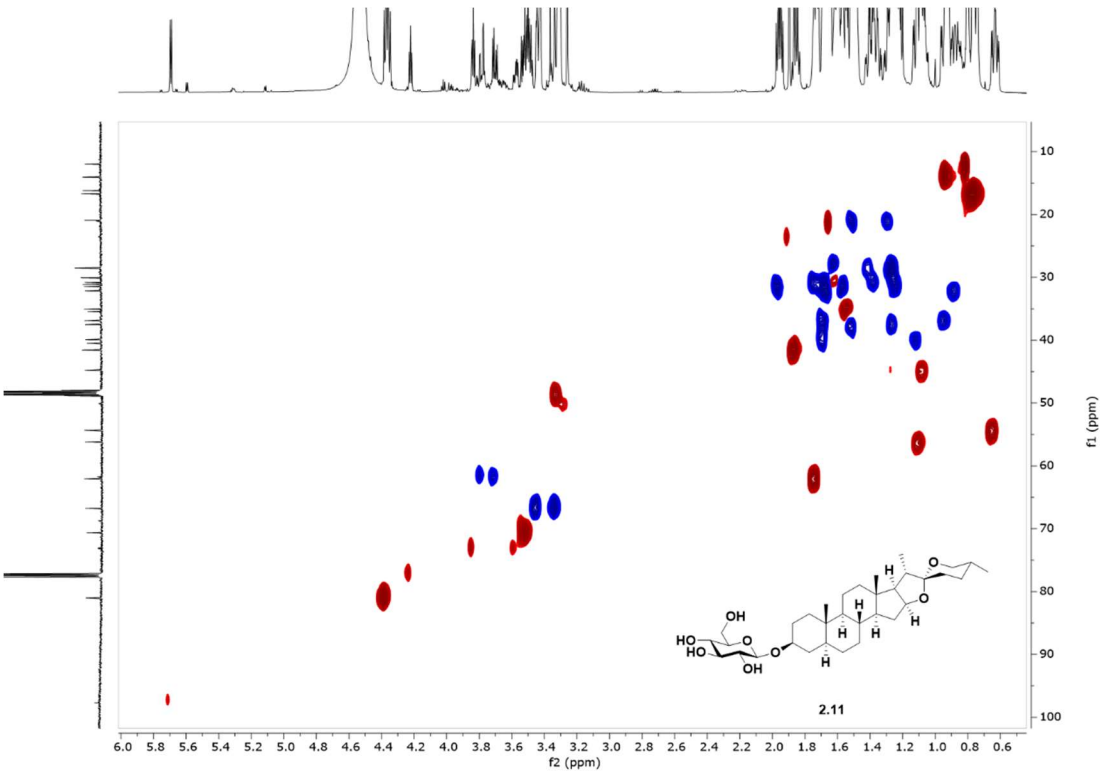

^{1}H NMR (600 MHz, $CDCl_3$) spectra of **2.19**

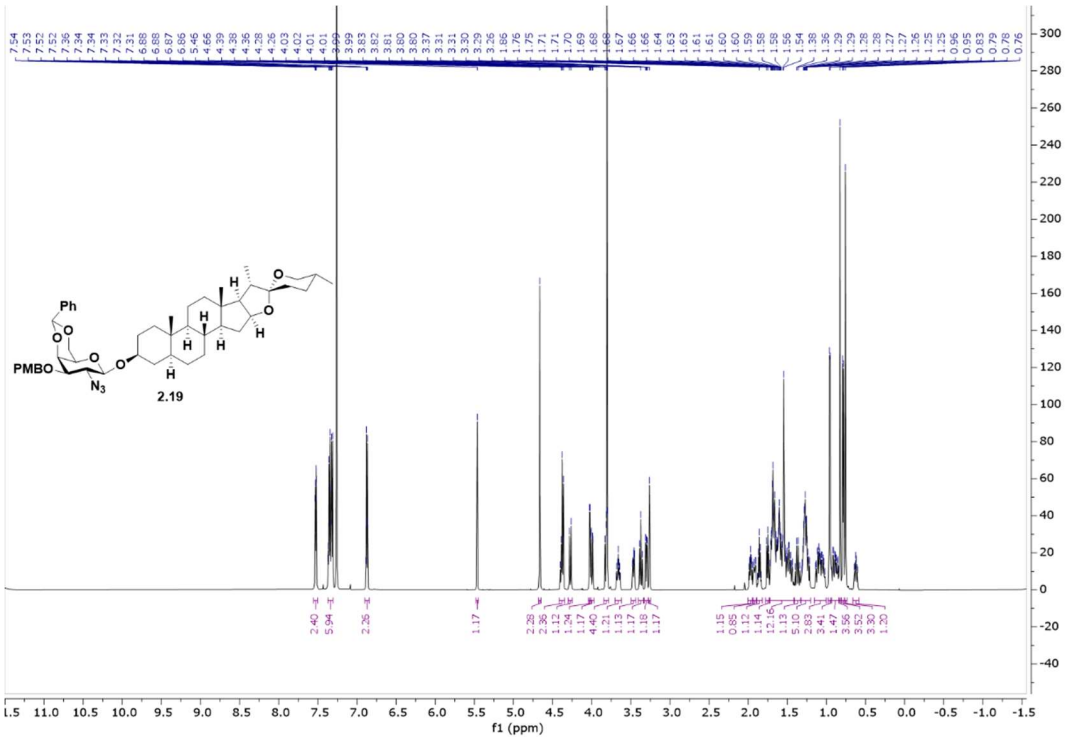

^{13}C NMR (150 MHz, $CDCl_3$) spectra of **2.19**

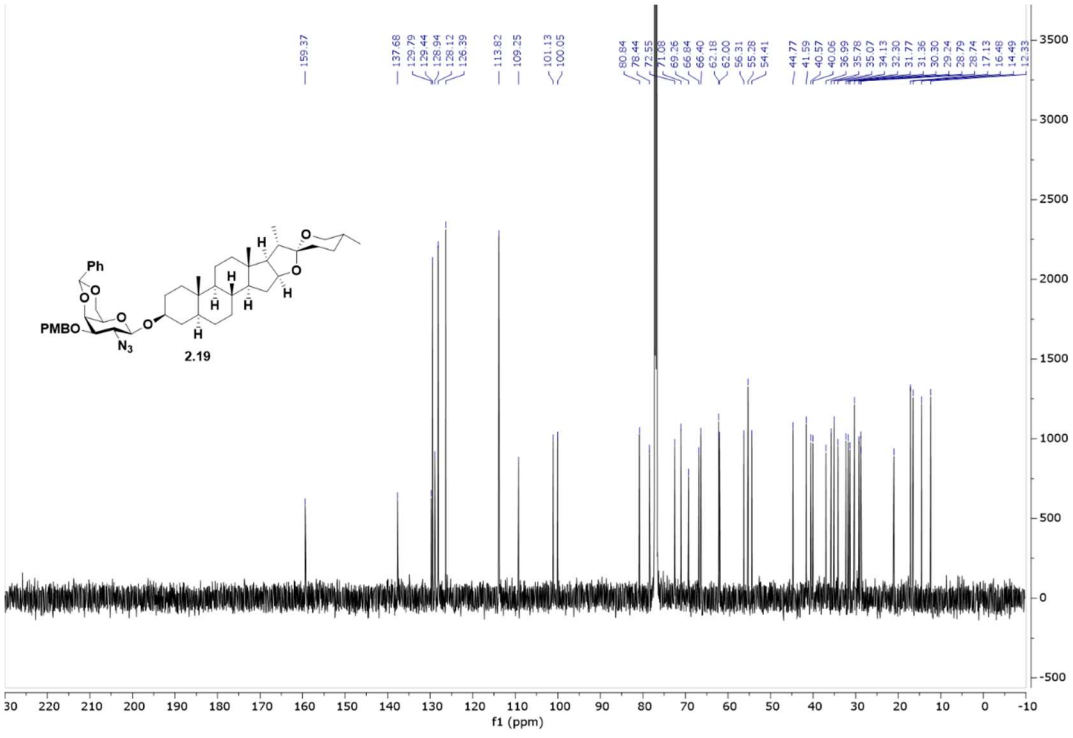

^{1}H ^{13}C HSQC NMR (600 MHz, $CDCl_3$) spectra of **2. 19**

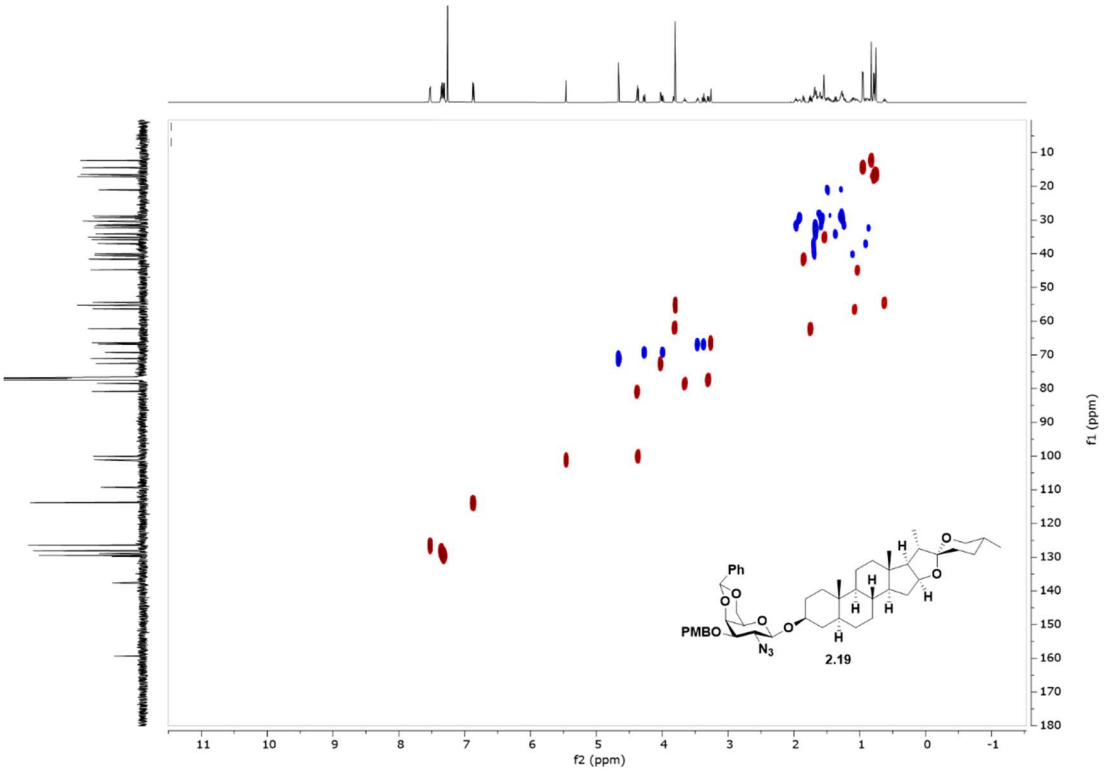

^{1}H ^{13}C HSQC NMR (600 MHz, $CDCl_3$) spectra zoomed in region of **2. 19**

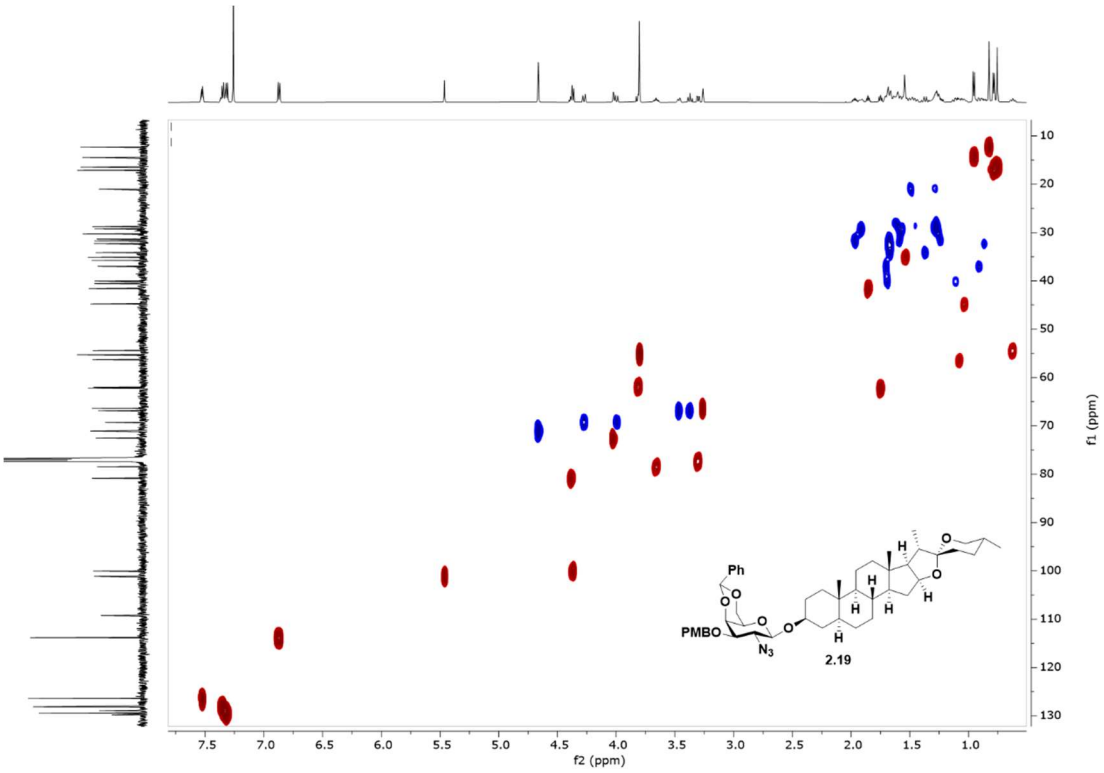

^{1}H ^{1}H COSY NMR (600 MHz, $CDCl_3$) spectra of **2. 19**

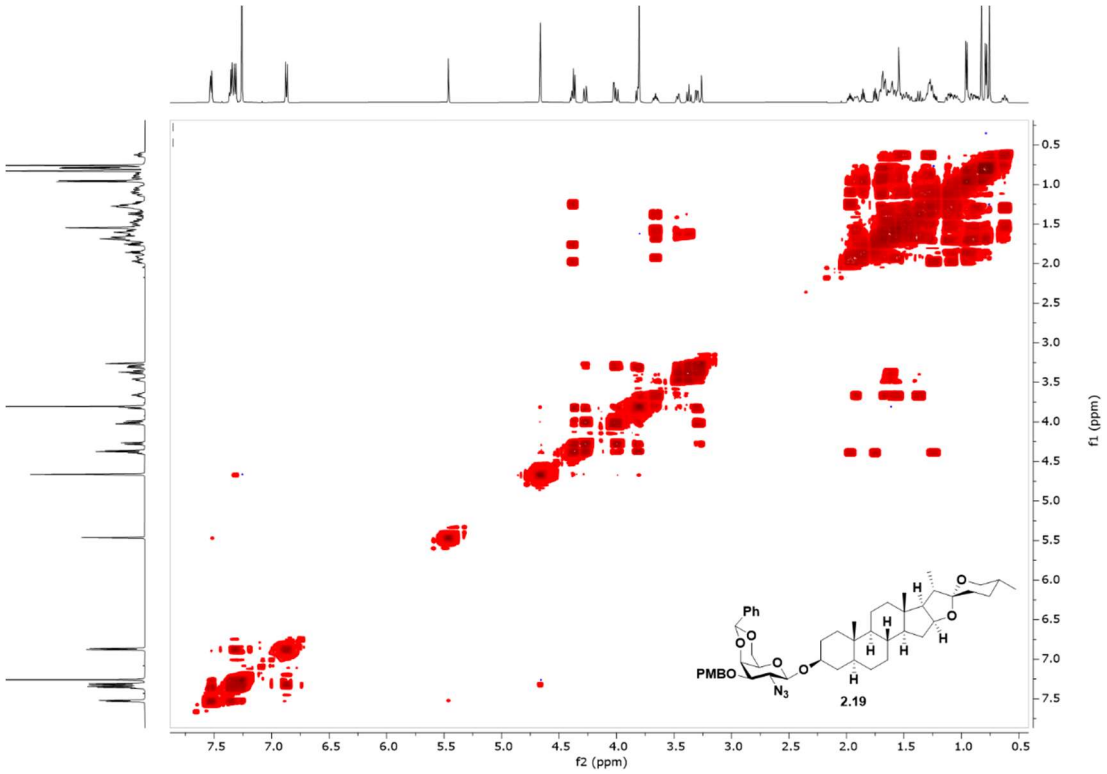

^{1}H ^{13}C HMBC NMR (600 MHz, $CDCl_3$) spectra zoomed in region of **2. 19**

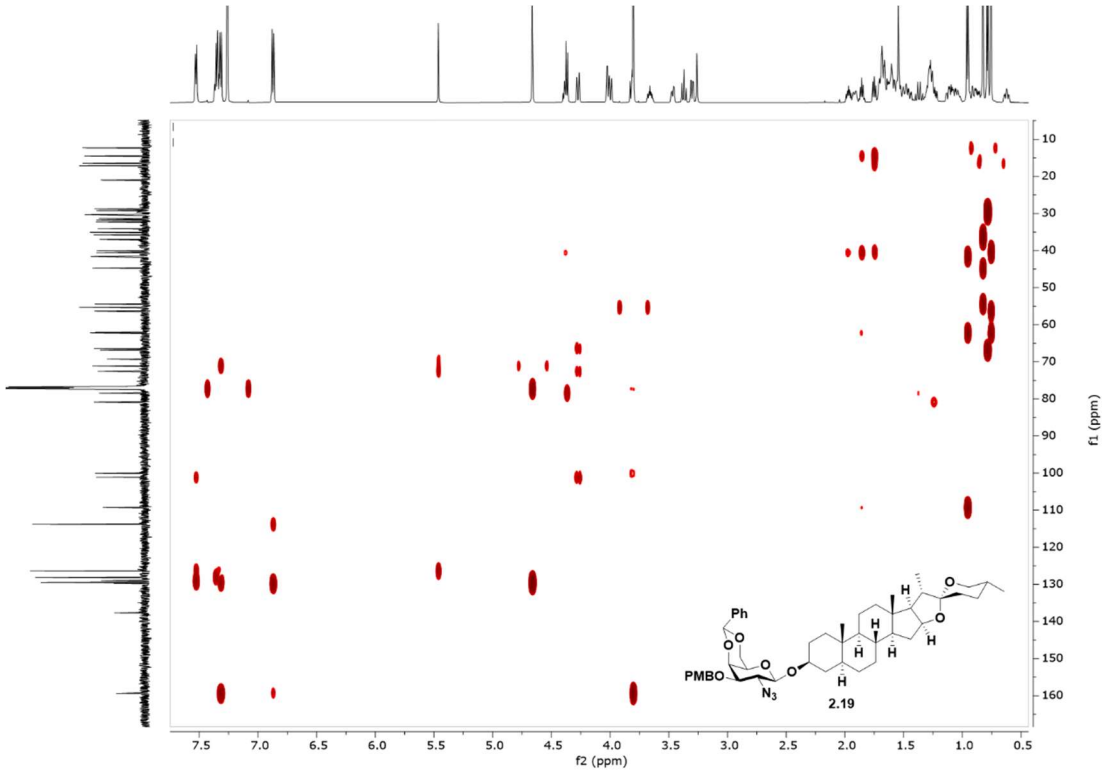

^{1}H NMR (600 MHz, MeOD) spectra of **2.20**

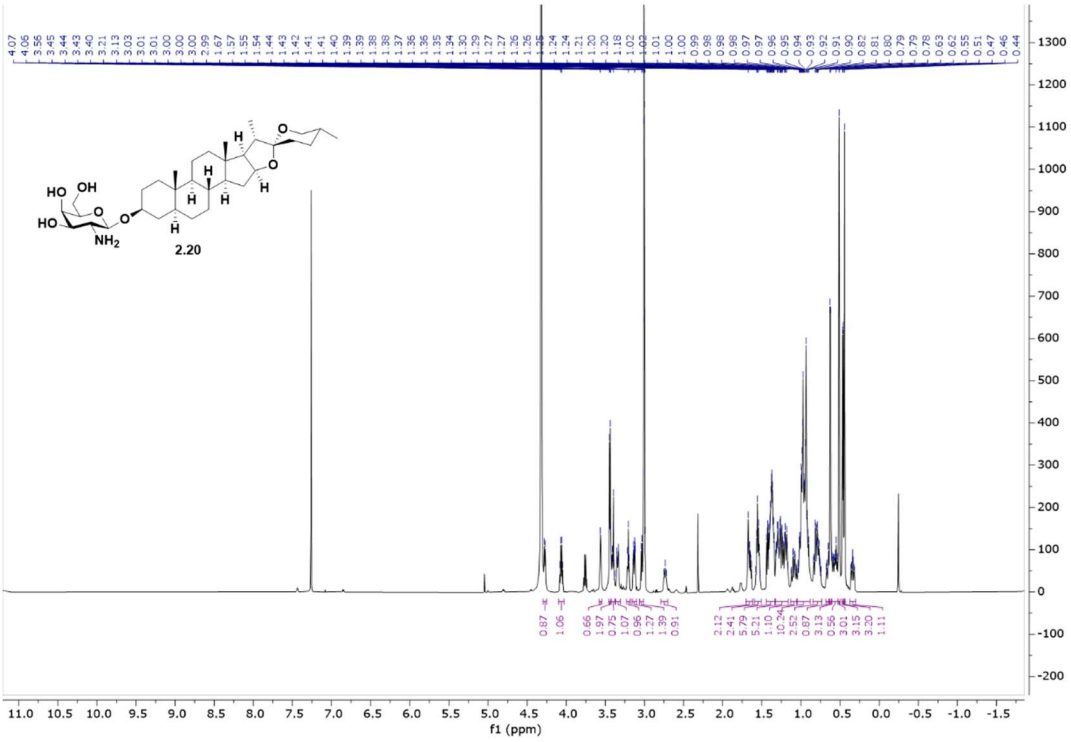

^{13}C NMR (150 MHz, MeOD) spectra of **2.20**

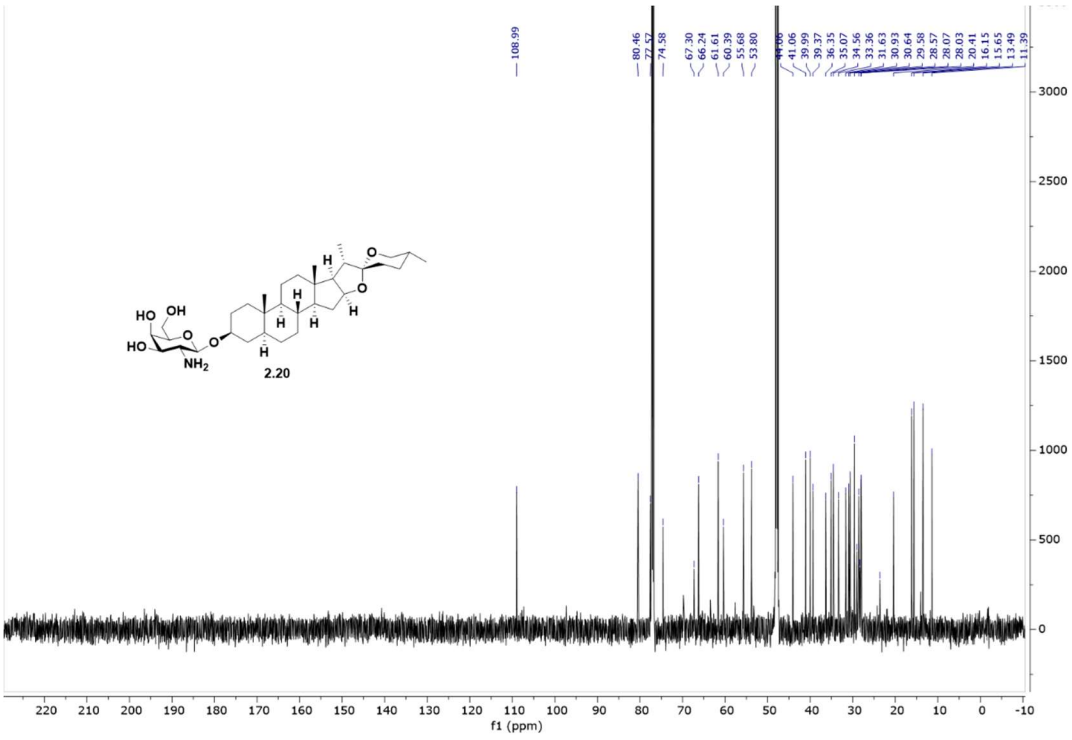

^{1}H ^{13}C HSQC NMR (600 MHz, MeOD) spectra of **2.20**

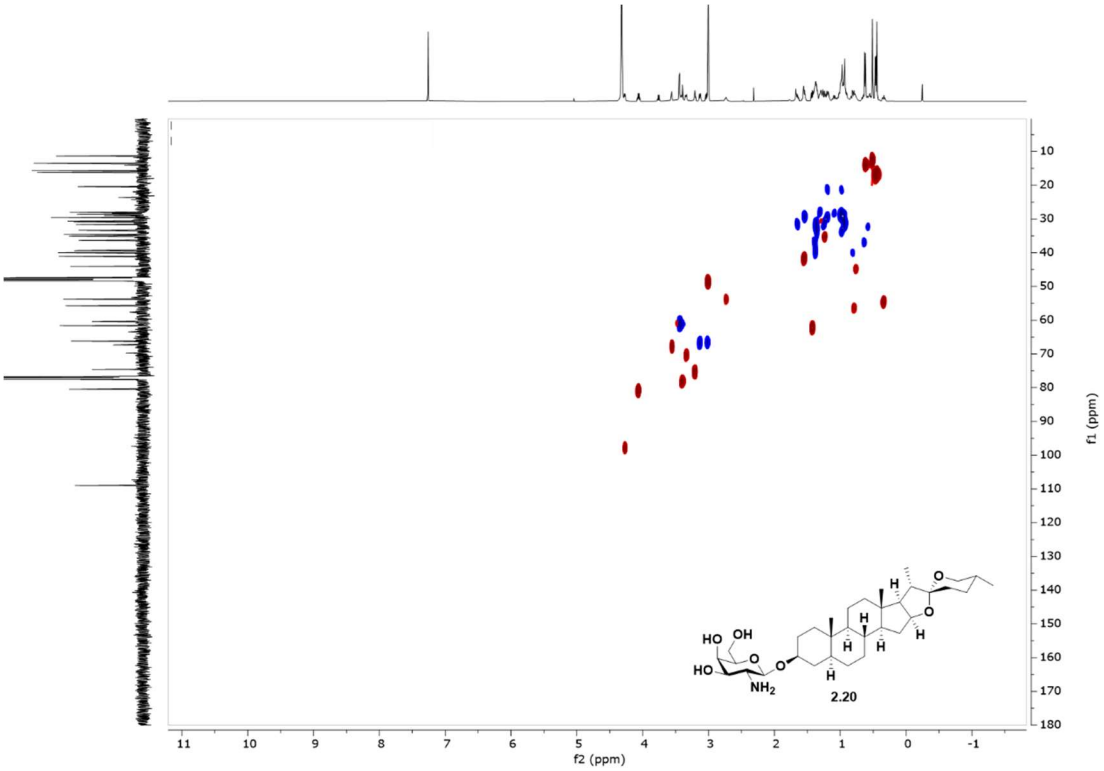

^{1}H ^{13}C HSQC NMR (600 MHz, MeOD) spectra zoomed in region of **2. 20**

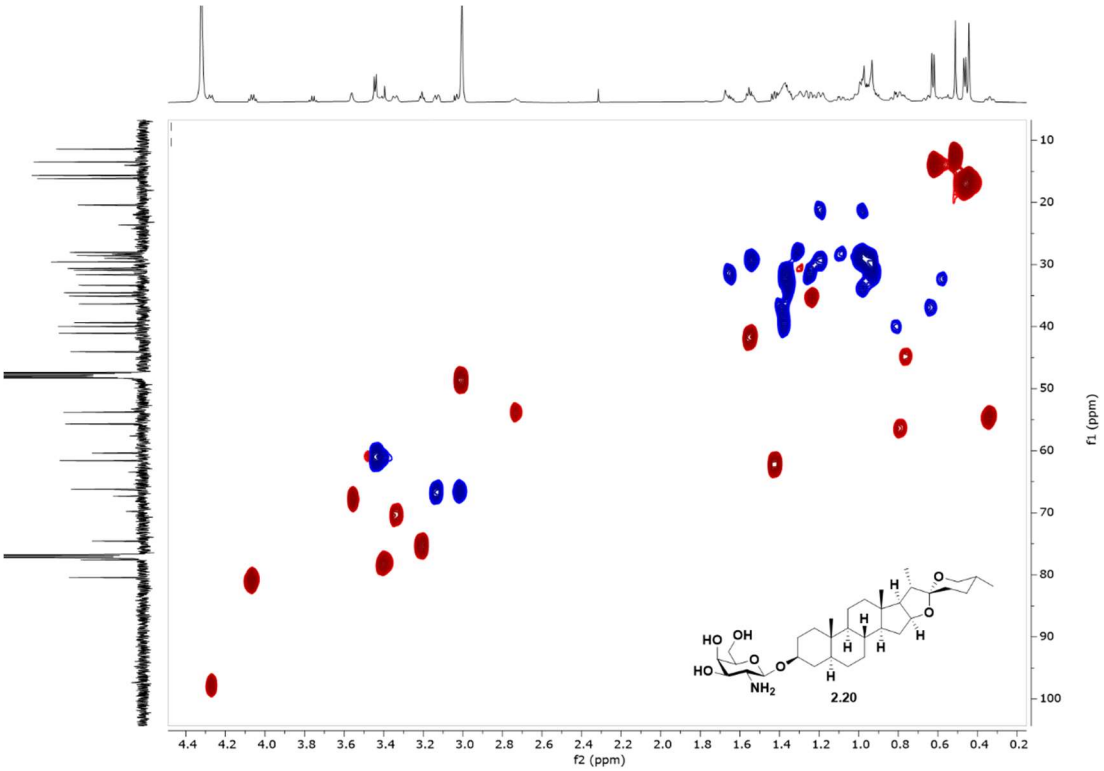

^{1}H NMR (600 MHz, MeOD) spectra of **2.12**

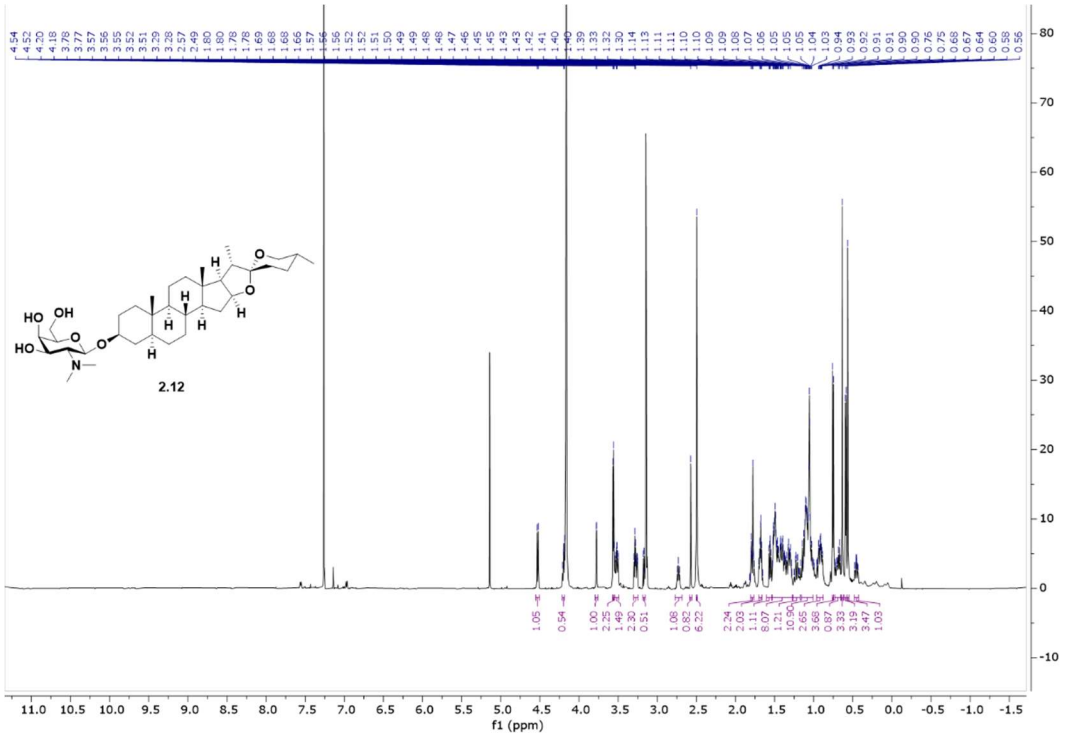

^{13}C NMR (150 MHz, MeOD) spectra of **2.12**

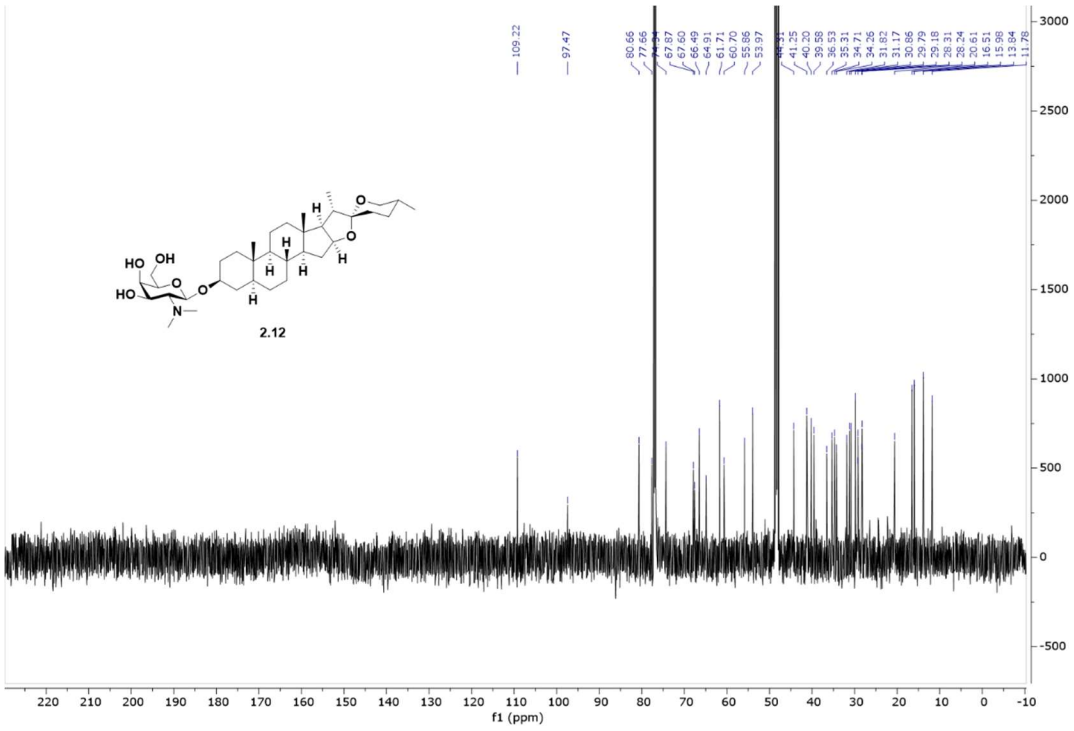

^{1}H ^{13}C HSQC NMR (600 MHz, MeOD) spectra of **2.12**

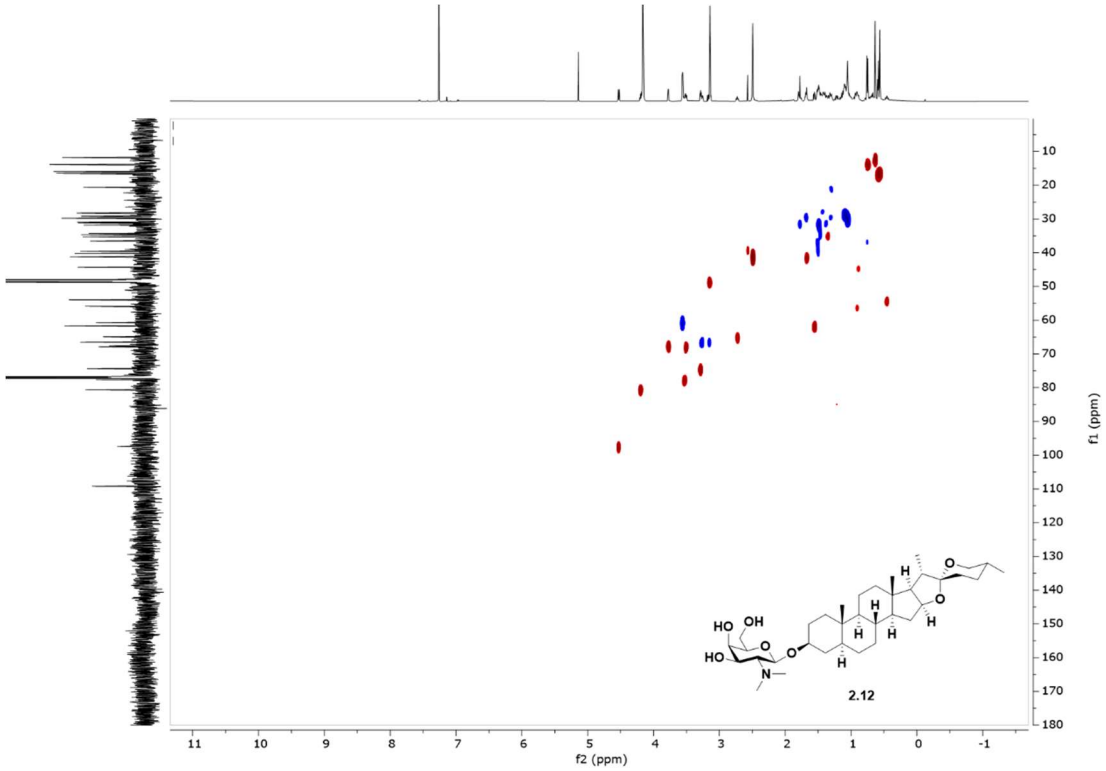

^{1}H ^{13}C HSQC NMR (600 MHz, MeOD) spectra zoomed in region of **2. 12**

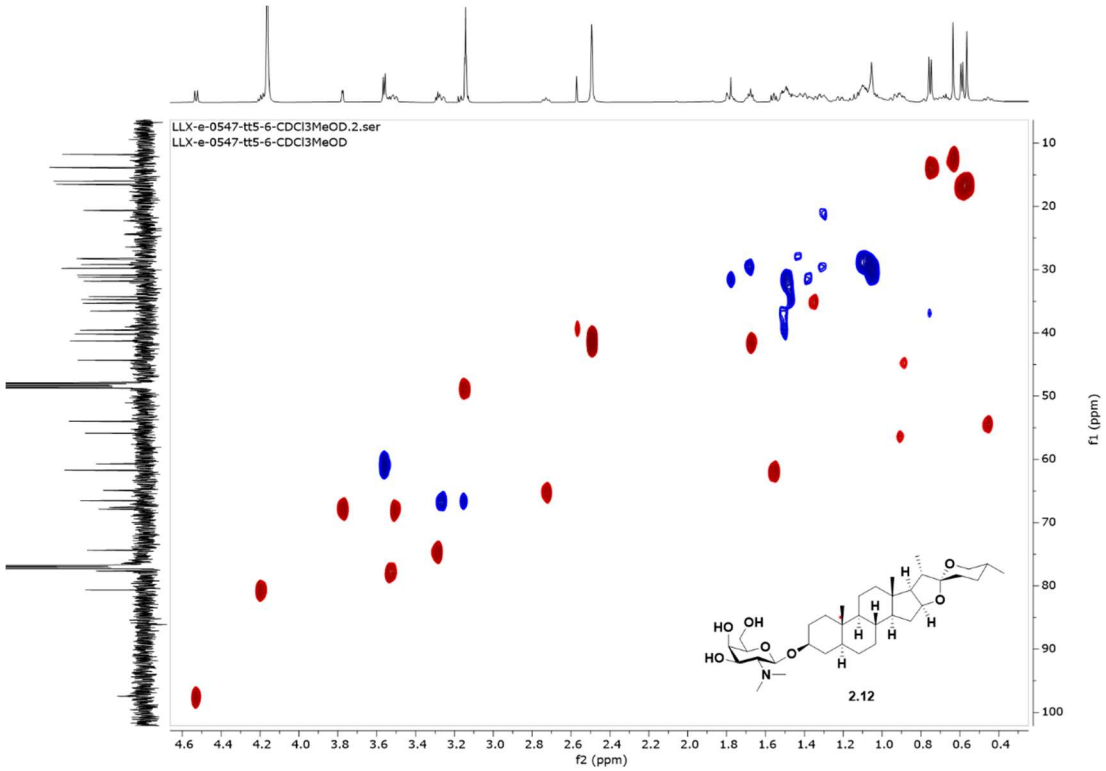

^{1}H ^{1}H COSY NMR (600 MHz, MeOD) spectra of **2. 12**

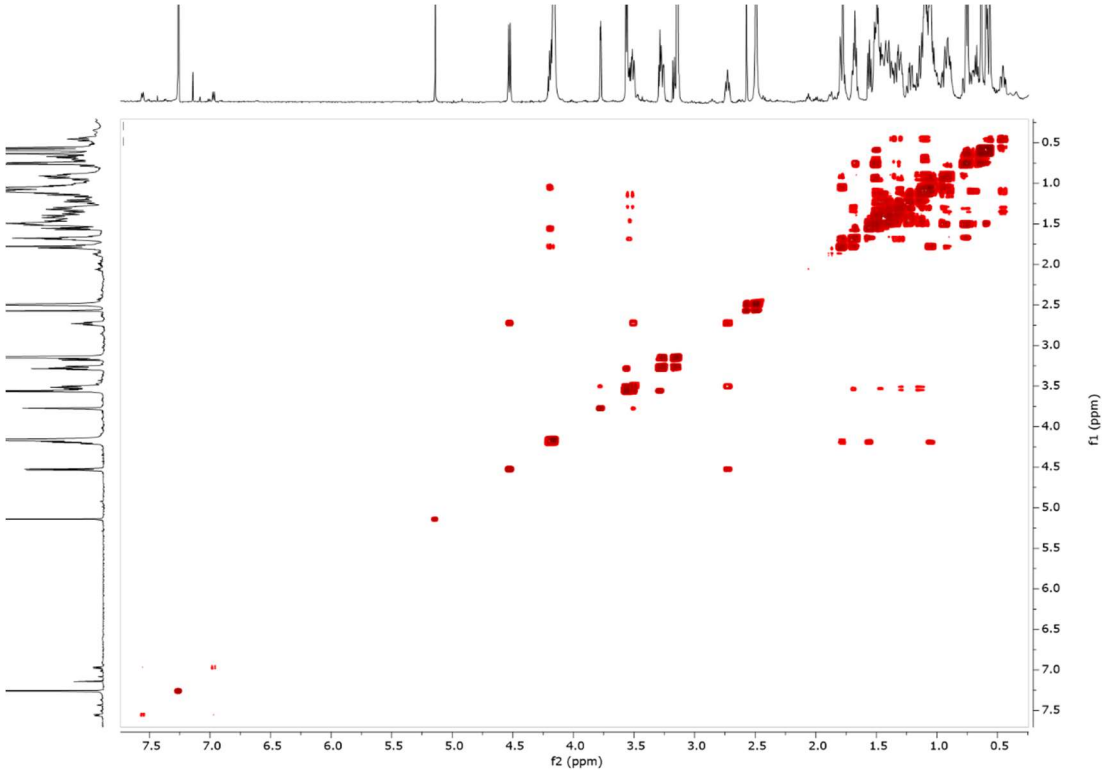

^{1}H NMR (600 MHz, $CDCl_3$) spectra of **2.28**

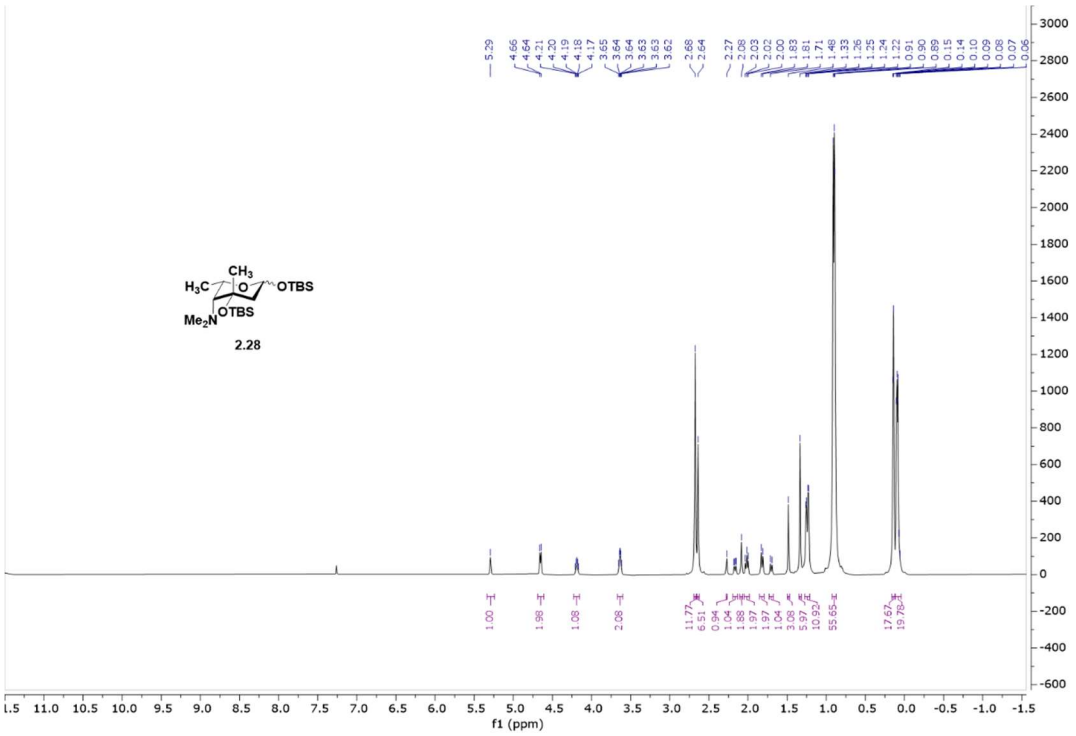

^{13}C NMR (150 MHz, $CDCl_3$) spectra of **2.28**

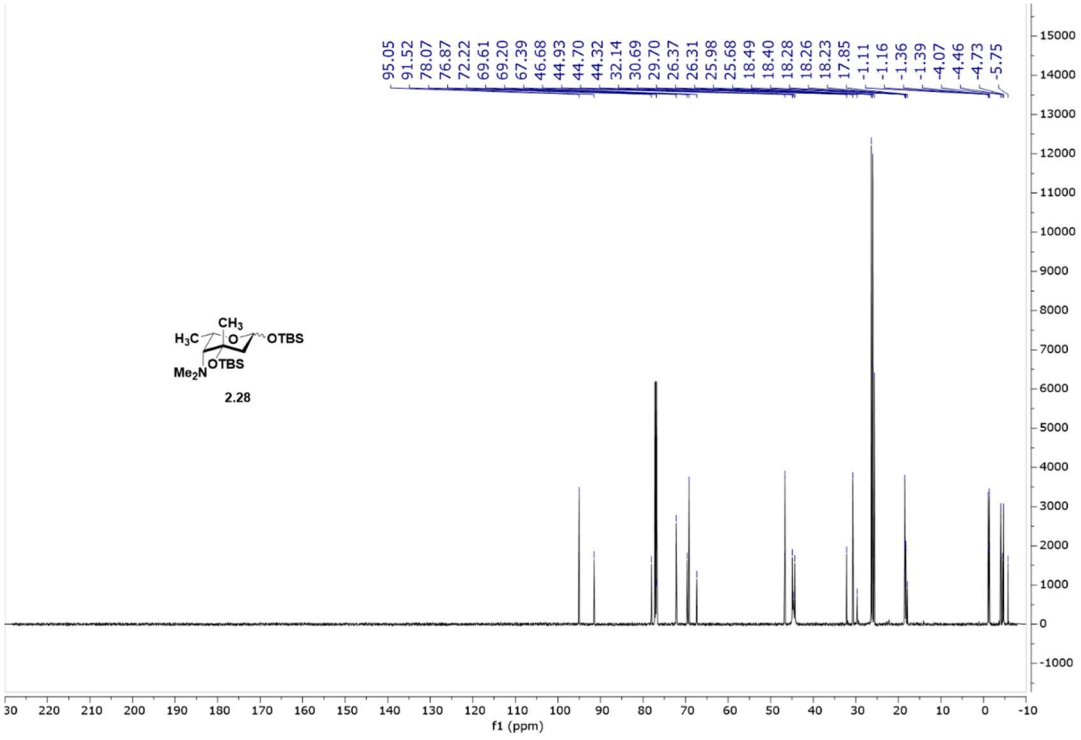

^{1}H ^{13}C HSQC NMR (600 MHz, $CDCl_3$) spectra of **2.28**

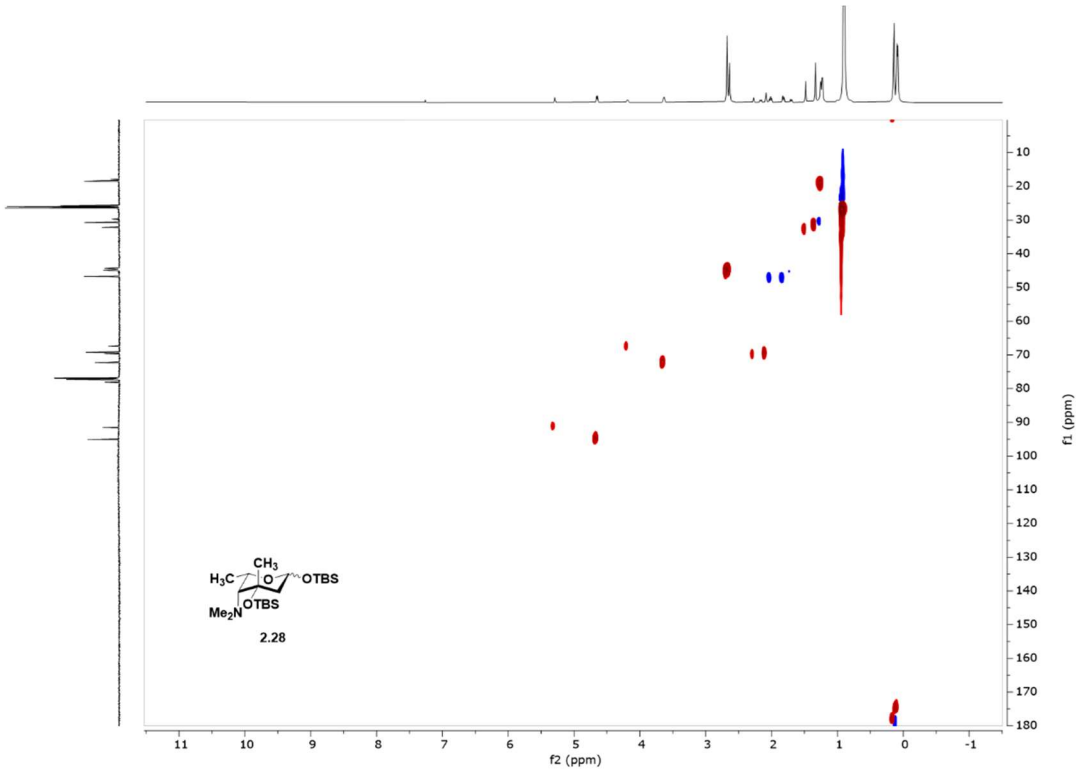

^{1}H ^{13}C HSQC NMR (600 MHz, $CDCl_3$) spectra zoomed in region of **2. 28**

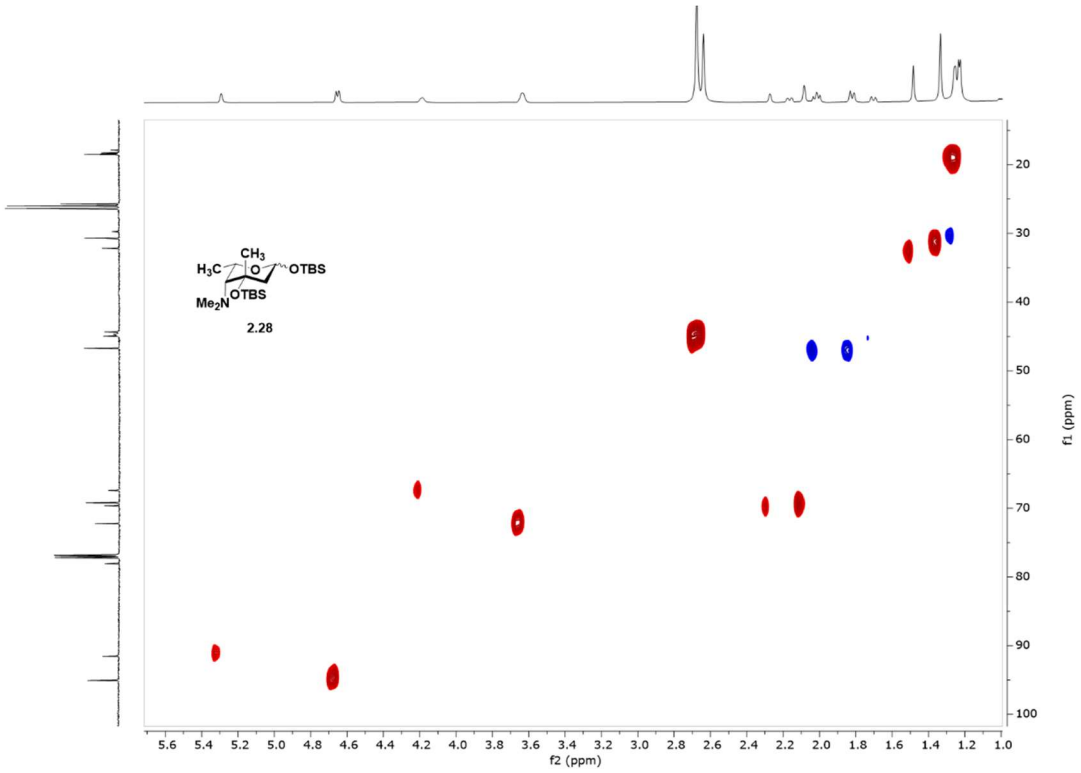

^{1}H ^{1}H COSY NMR (600 MHz, $CDCl_3$) spectra of **2. 28**

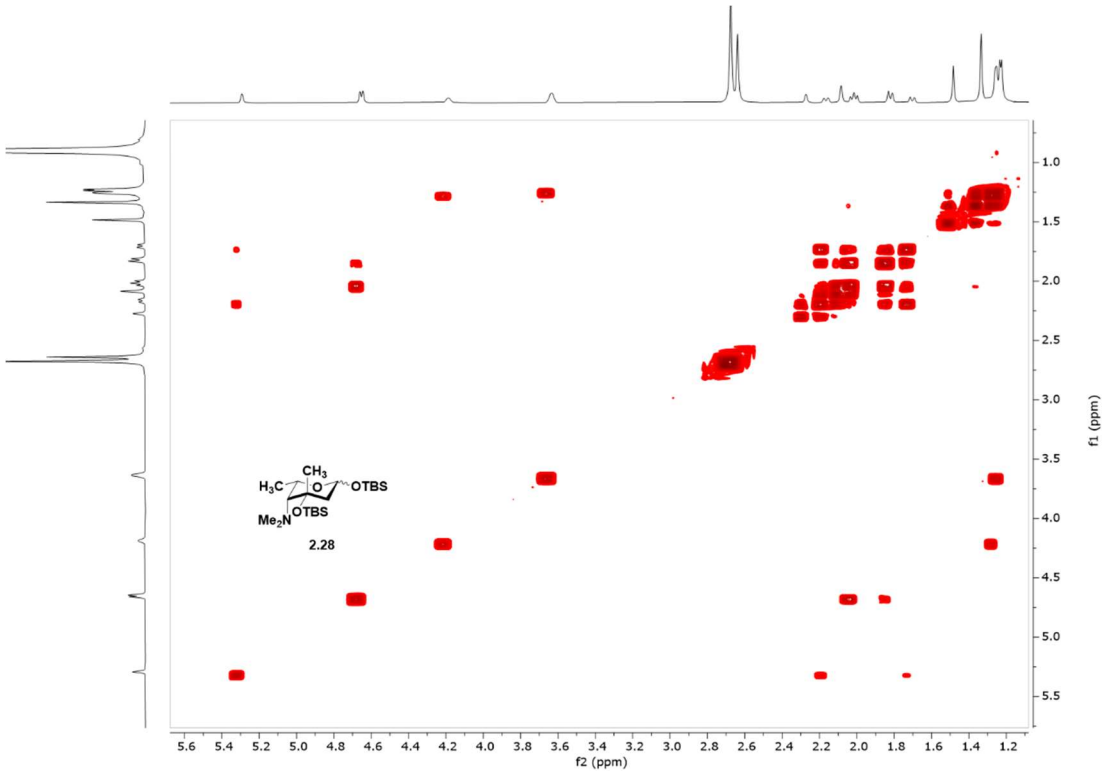

^{1}H ^{13}C HMBC NMR (600 MHz, $CDCl_3$) spectra zoomed in region of **2. 28**

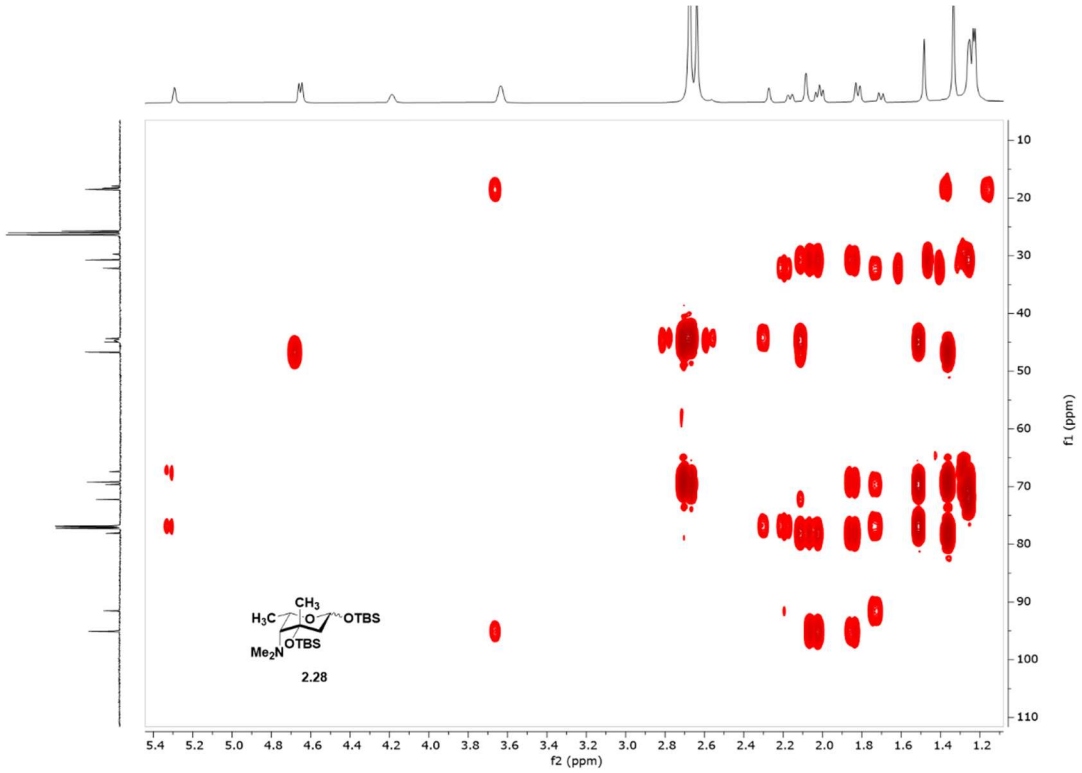

^{1}H NMR (600 MHz, $CDCl_3$) spectra of **2.29**

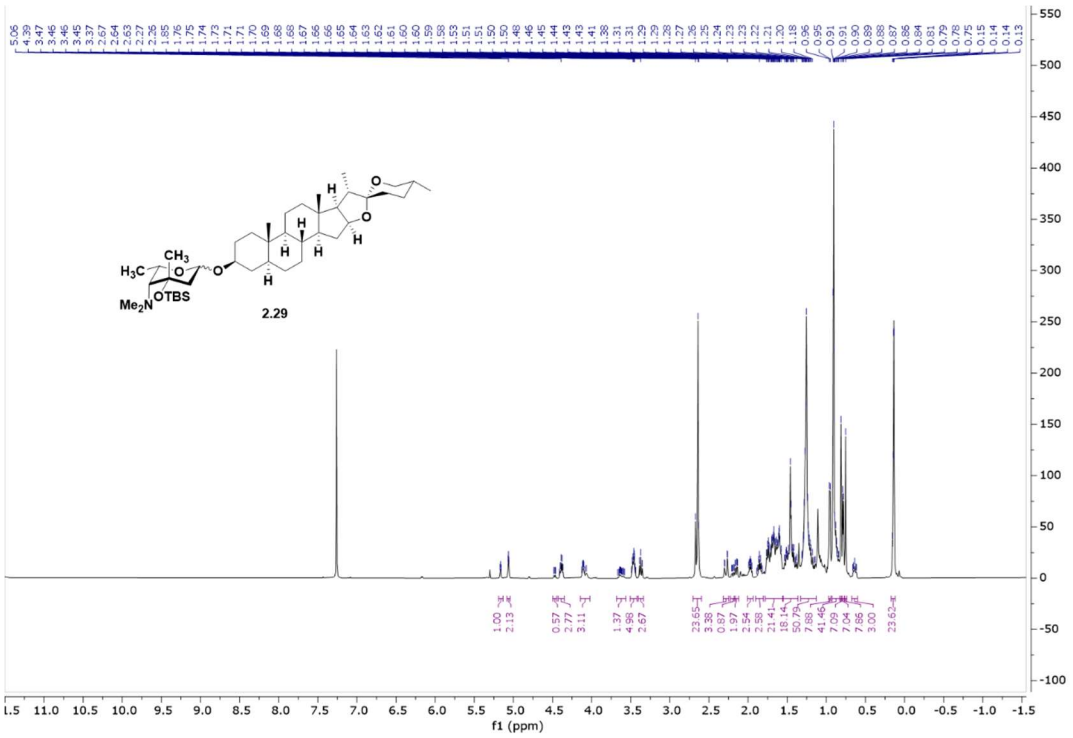

^{13}C NMR (150 MHz, $CDCl_3$) spectra of **2.29**

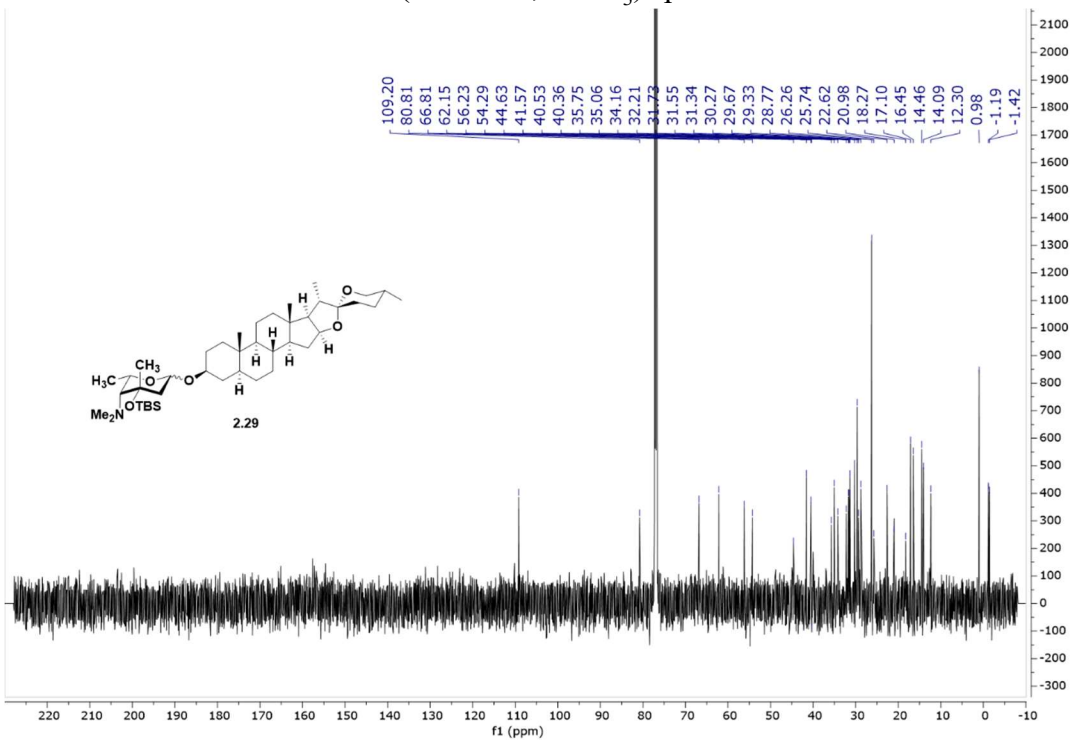

^{1}H ^{13}C HSQC NMR (600 MHz, $CDCl_3$) spectra of **2.29**

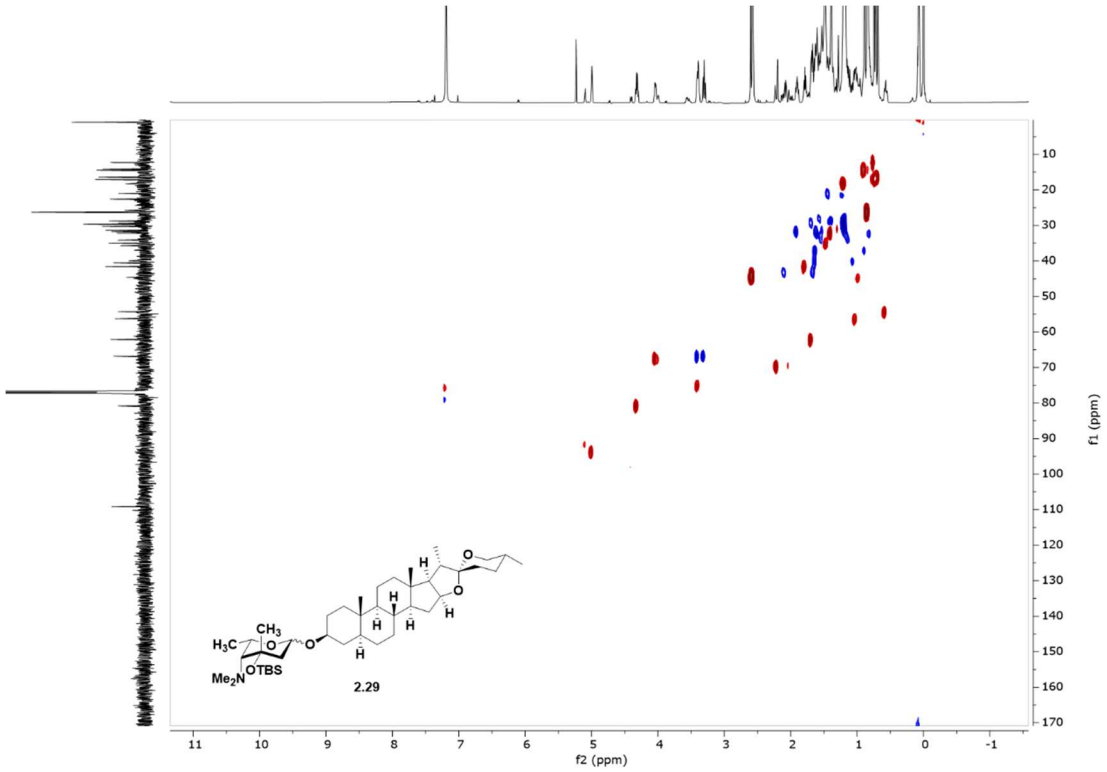

^{1}H ^{13}C HSQC NMR (600 MHz, $CDCl_3$) spectra zoomed in region of **2. 29**

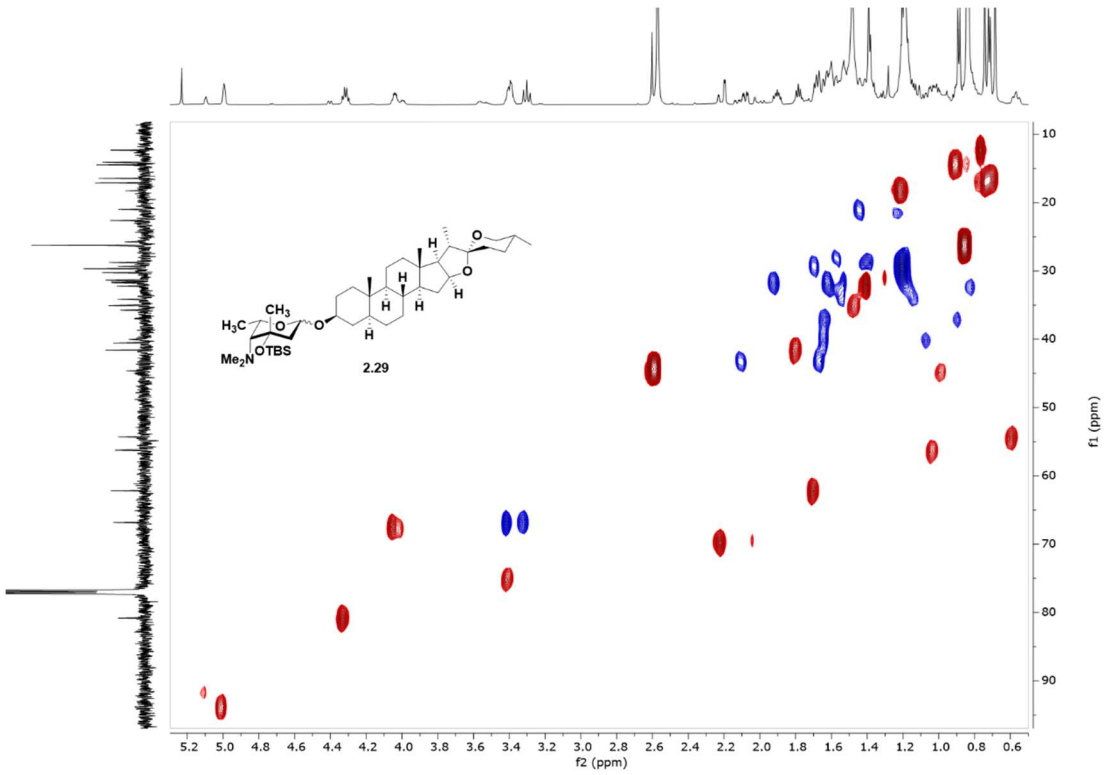

^{1}H ^{1}H COSY NMR (600 MHz, $CDCl_3$) spectra of **2. 29**

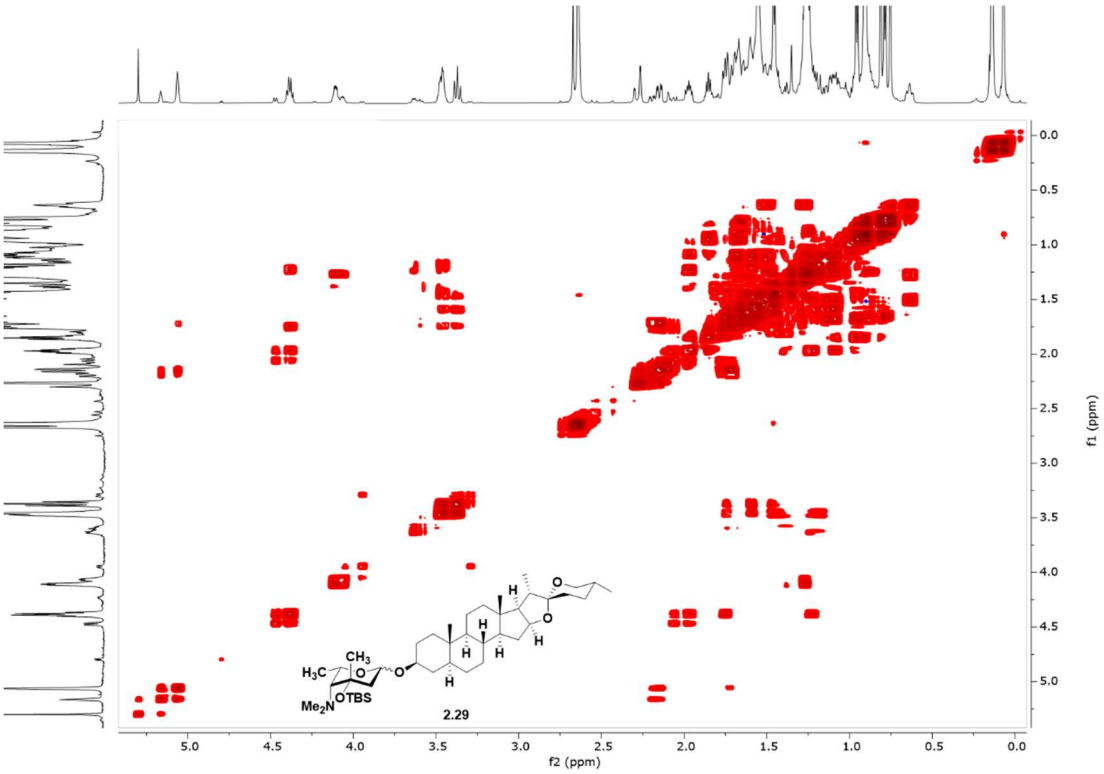

^{1}H ^{13}C HMBC NMR (600 MHz, $CDCl_3$) spectra zoomed in region of **2. 29**

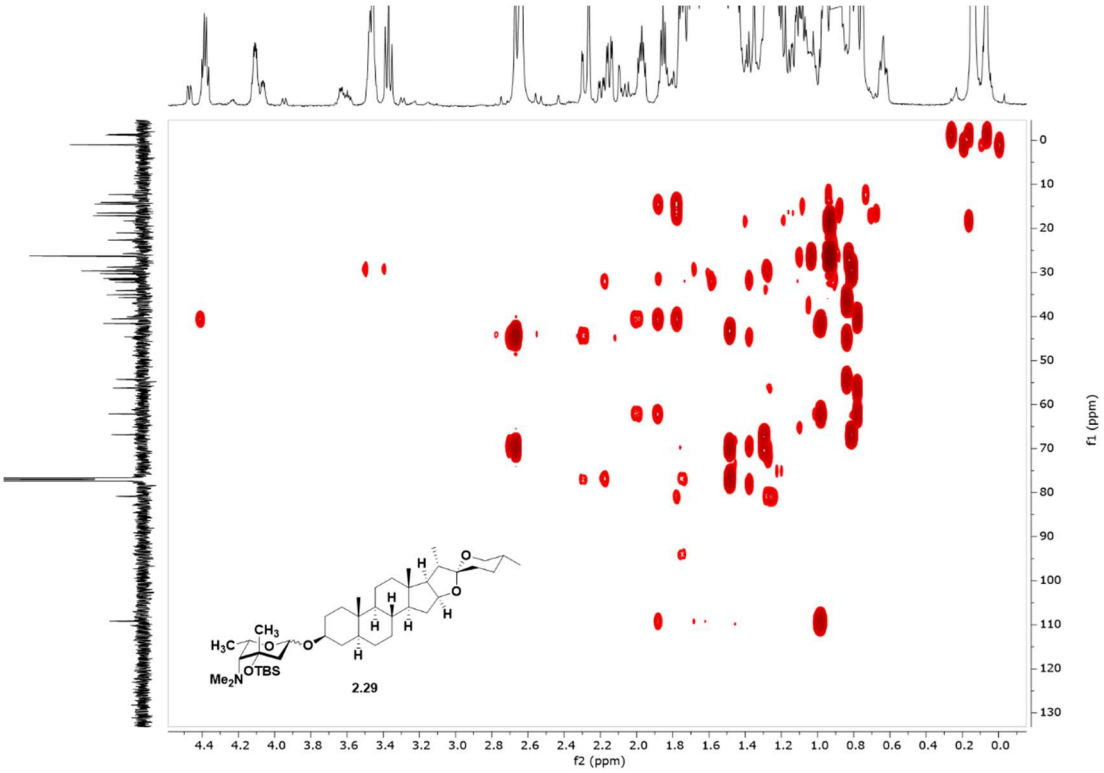

^{1}H NMR (600 MHz, $CDCl_3$) spectra of **2.13**

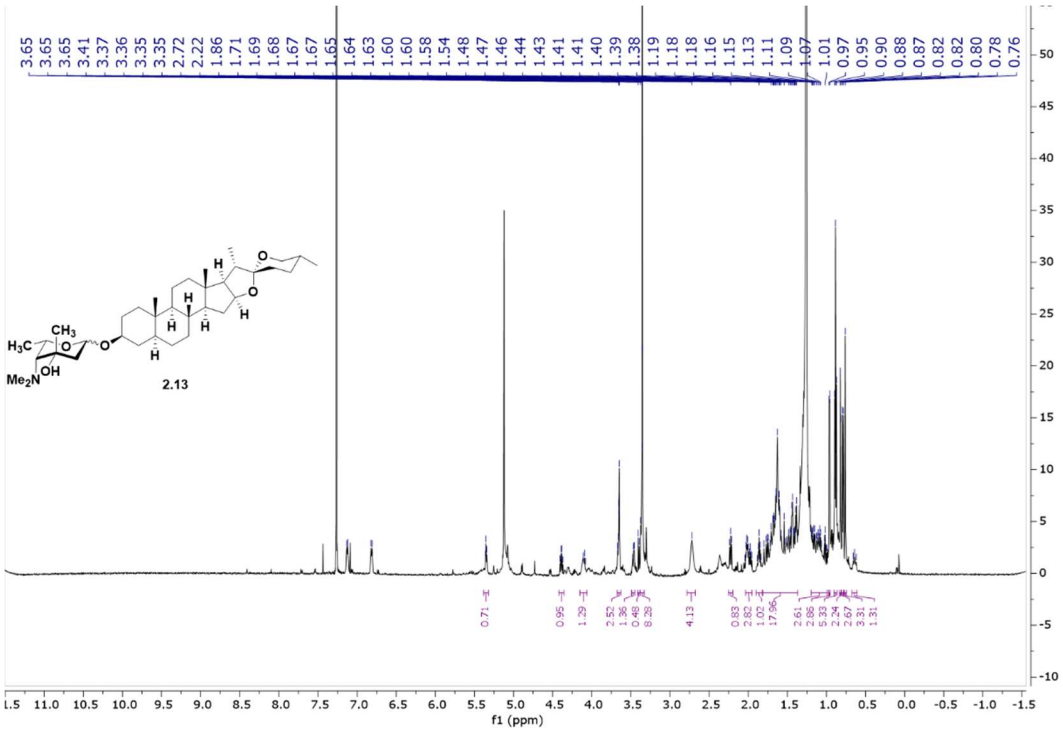

^{1}H ^{13}C HSQC NMR (600 MHz, $CDCl_3$) spectra of **2. 13**

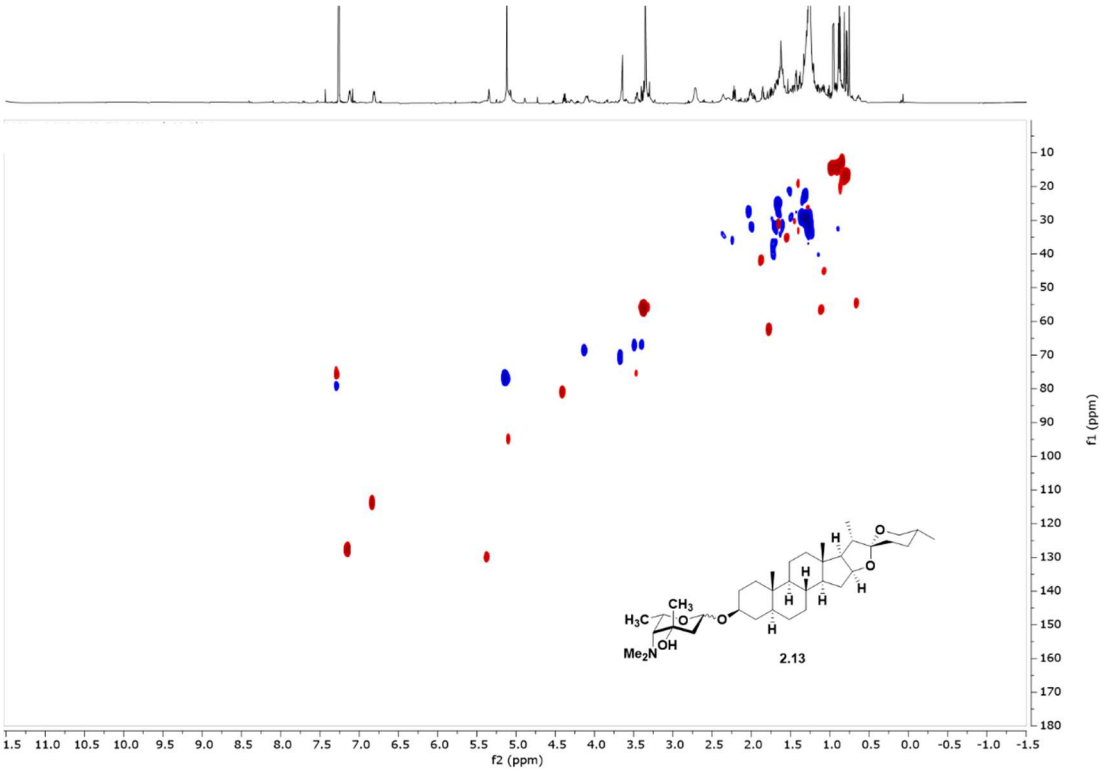

^{1}H ^{13}C HSQC NMR (600 MHz, $CDCl_3$) spectra zoomed in region of **2. 13**

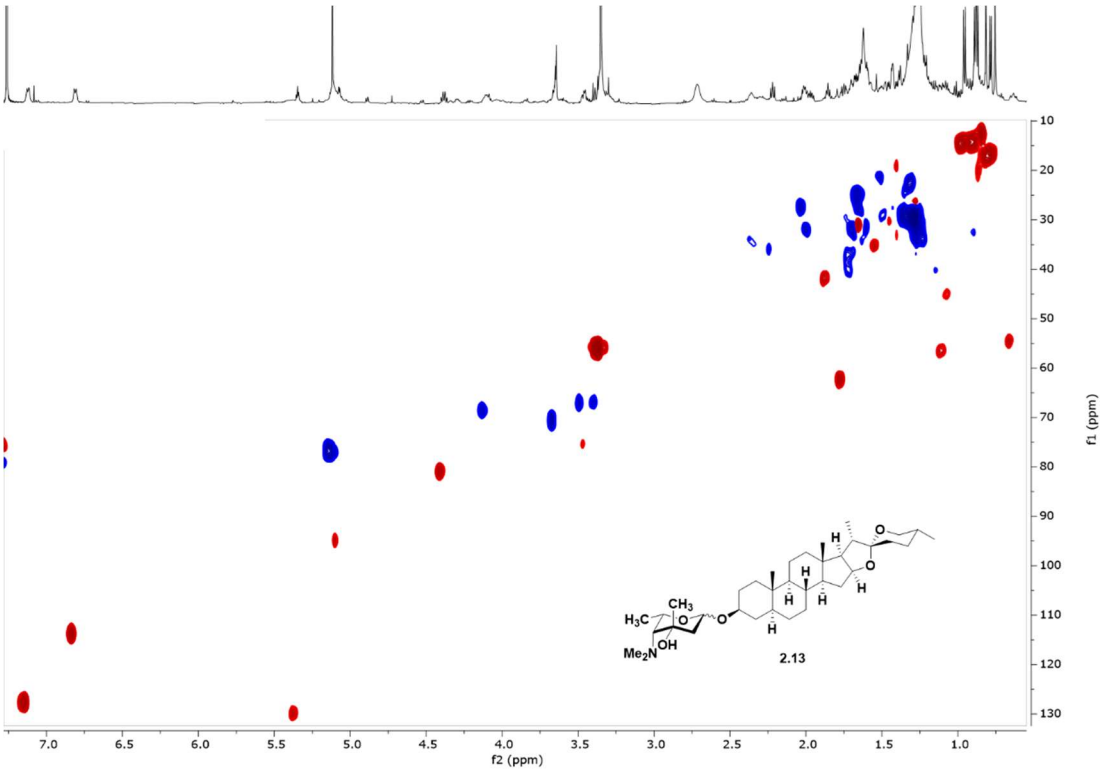

^{1}H ^{1}H COSY NMR (600 MHz, $CDCl_3$) spectra of **2. 13**

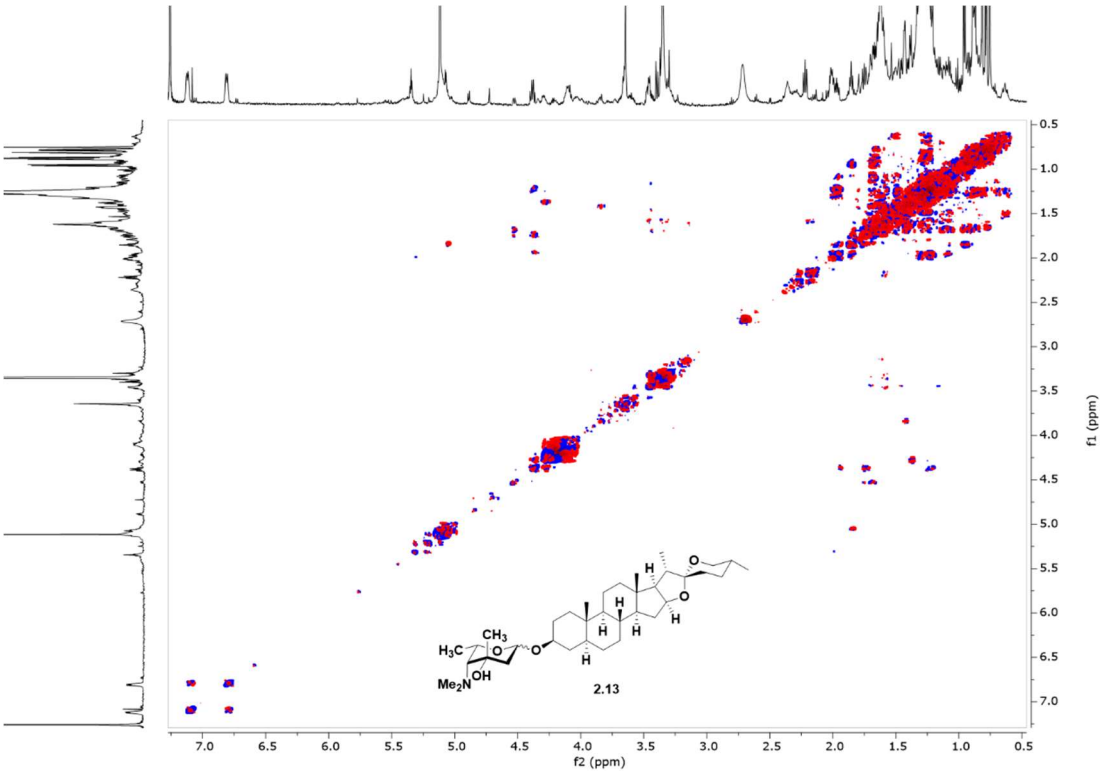

^{1}H ^{13}C HMBC NMR (600 MHz, $CDCl_3$) spectra zoomed in region of **2. 13**

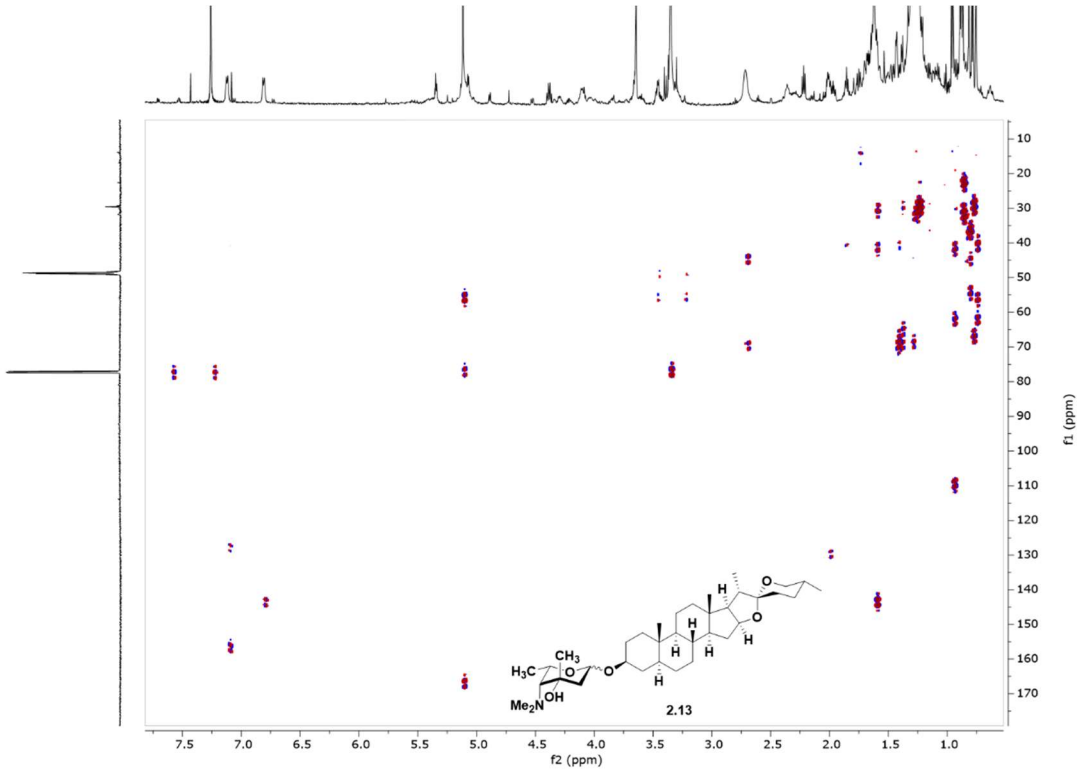

3. References

1. Wright, G. D., Solving the Antibiotic Crisis. *ACS Infect Dis.* **2015,** *1*, 80-84.
2. Kadri, S. S., Key Takeaways From the U.S. CDC's 2019 Antibiotic Resistance Threats Report for Frontline Providers. *Crit Care Med.* **2020,** *48*, 939-945.
3. Melander, R. J.; Melander, C., The Challenge of Overcoming Antibiotic Resistance: An Adjuvant Approach? *ACS Infect Dis.* **2017,** *3*, 559-563.
4. Algburi, A.; Comito, N.; Kashtanov, D.; Dicks, L. M. T.; Chikindas, M. L., Control of Biofilm Formation: Antibiotics and Beyond. *Appl Environ Microbiol.* **2017,** *83*, e02508-16.
5. Worthington, R. J.; Richards, J. J.; Melander, C., Small molecule control of bacterial biofilms. *Org Biomol Chem.* **2012,** *10*, 7457-7474.
6. Hall-Stoodley, L.; Stoodley, P., Evolving concepts in biofilm infections. *Cell Microbiol.* **2009,** *11*, 1034-1043.
7. Blackledge, M. S.; Worthington, R. J.; Melander, C., Biologically inspired strategies for combating bacterial biofilms. *Curr Opin Pharmacol.* **2013,** *13*, 699-706.
8. Craft, K. M.; Townsend, S. D., Mother Knows Best: Deciphering the Antibacterial Properties of Human Milk Oligosaccharides. *Acc. Chem. Res.* **2019,** *52* (3), 760-768.
9. Townsend, S. D., Human Milk Oligosaccharides: Defense Against Pathogens. *Breastfeeding Medicine* **2019,** *14* (S1), S-5-S-6.
10. Eickhoff, T. C.; Klein, J. O.; Daly, A. K.; Ingall, D.; Finland, M., Neonatal Sepsis and Other Infections Due to Group B Beta-Hemolytic *Streptococci*. *N. Engl. J. Med.* **1964,** *271* (24), 1221-1228.
11. Franciosi, R. A.; Knostman, J. D.; Zimmerman, R. A., Group B *streptococcal* neonatal and infant infections. *J. Pediatr.* **1973,** *82* (4), 707-718.
12. Horvath, B.; Lakatos, F.; Tóth, C.; Bödecs, T.; Bódis, J., Silent chorioamnionitis and associated pregnancy outcomes: a review of clinical data gathered over a 16-year period. *J. Perinat. Med.* **2014,** *42* (4), 441-447.
13. Morrow, A. L.; Ruiz-Palacios, G. M.; Jiang, X.; Newburg, D. S., Human-Milk Glycans That Inhibit Pathogen Binding Protect Breast-feeding Infants against Infectious Diarrhea. *J. Nutr.* **2005,** *135* (5), 1304-1307.
14. Moore, R. E.; Xu, L. L.; Townsend, S. D., Prospecting Human Milk Oligosaccharides as a Defense Against Viral Infections. *ACS Infect Dis.* **2021,** *7* (2), 254-263.
15. Ackerman, D. L.; Craft, K. M.; Townsend, S. D., Infant food applications of complex carbohydrates: Structure, synthesis, and function. *Carbohydrate Res.* **2017,** *437*, 16-27.
16. Craft, K. M.; Townsend, S. D., The Human Milk Glycome as a Defense Against Infectious Diseases: Rationale, Challenges, and Opportunities. *ACS Infect Dis.* **2018,** *4* (2), 77-83.
17. Craft, K. M.; Townsend, S. D., Mother Knows Best: Deciphering the Antibacterial Properties of Human Milk Oligosaccharides. *Acc Chem Res.* **2019,** *52*, 760-768.
18. Bode, L., Human milk oligosaccharides: Every baby needs a sugar mama. *Glycobiology* **2012,** *22* (9), 1147-1162.
19. Ackerman, D. L.; Craft, K. M.; Doster, R. S.; Weitkamp, J. H.; Aronoff, D. M.; Gaddy, J. A.; Townsend, S. D., Antimicrobial and Antibiofilm Activity of Human Milk Oligosaccharides against *Streptococcus agalactiae, Staphylococcus aureus*, and *Acinetobacter baumannii*. *ACS Infect Dis.* **2018,** *4*, 315-324.

20. Craft, K. M.; Gaddy, J. A.; Townsend, S. D., Human Milk Oligosaccharides (HMOs) Sensitize Group B *Streptococcus* to Clindamycin, Erythromycin, Gentamicin, and Minocycline on a Strain Specific Basis. *ACS Chem Biol.* **2018,** *13*, 2020-2026.
21. Chambers, S. A.; Moore, R. E.; Craft, K. M.; Thomas, H. C.; Das, R.; Manning, S. D.; Codreanu, S. G.; Sherrod, S. D.; Aronoff, D. M.; McLean, J. A.; Gaddy, J. A.; Townsend, S. D., A Solution to Antifolate Resistance in Group B *Streptococcus*: Untargeted Metabolomics Identifies Human Milk Oligosaccharide-Induced Perturbations That Result in Potentiation of Trimethoprim. *mBio.* **2020,** *11*, e00076-20.
22. Craft, K. M.; Thomas, H. C.; Townsend, S. D., Interrogation of Human Milk Oligosaccharide Fucosylation Patterns for Antimicrobial and Antibiofilm Trends in Group B *Streptococcus*. *ACS Infect Dis.* **2018,** *1755-1765*, 1755-1765.
23. Craft, K. M.; Thomas, H. C.; Townsend, S. D., Sialylated variants of lacto-N-tetraose exhibit antimicrobial activity against Group B Streptococcus. *Org Biomol Chem.* **2018,** *17*, 1893-1900.
24. Roy, R.; Tiwari, M.; Donelli, G.; Tiwari, V., Strategies for combating bacterial biofilms: A focus on anti-biofilm agents and their mechanisms of action. *Virulence.* **2018,** *9*, 522-554.
25. Foster, L. L.; Yusa, S. I.; Kuroda, K., Solution-Mediated Modulation of *Pseudomonas aeruginosa* Biofilm Formation by a Cationic Synthetic Polymer. *Antibiotics (Basel).* **2019,** *8*, 61-77.
26. Aiassa, V.; Barnes, A. I.; Albesa, I., In vitro oxidant effects of D-glucosamine reduce adhesion and biofilm formation of *Staphylococcus epidermidis*. *Rev Argent Microbiol.* **2012,** *44*, 16-20.
27. Lopez, D.; Vlamakis, H.; Kolter, R., Biofilms. *Cold Spring Harb Perspect Biol.* **2010,** *2*, a000398.
28. Wang, P.; Aussedat, B.; Vohra, Y.; Danishefsky, S. J., An Advance in the Chemical Synthesis of Homogeneous N-Linked Glycopolypeptides by Convergent Aspartylation. *Angew. Chem. Int. Ed.* **2012,** *51* (46), 11571-11575.
29. Wang, P.; Dong, S.; Brailsford, J. A.; Iyer, K.; Townsend, S. D.; Zhang, Q.; Hendrickson, R. C.; Shieh, J.; Moore, M. A. S.; Danishefsky, S. J., At Last: Erythropoietin as a Single Glycoform. *Angew. Chem. Int. Ed.* **2012,** *51* (46), 11576-11584.
30. Wang, P.; Dong, S.; Shieh, J.-H.; Peguero, E.; Hendrickson, R.; Moore Malcolm, A. S.; Danishefsky Samuel, J., Erythropoietin Derived by Chemical Synthesis. *Science* **2013,** *342* (6164), 1357-1360.
31. Wilson, R. M.; Dong, S.; Wang, P.; Danishefsky, S. J., The Winding Pathway to Erythropoietin Along the Chemistry–Biology Frontier: A Success At Last. *Angew. Chem. Int. Ed.* **2013,** *52* (30), 7646-7665.
32. Brun, M. A.; Disney, M. D.; Seeberger, P. H., Miniaturization of Microwave-Assisted Carbohydrate Functionalization to Create Oligosaccharide Microarrays. *ChemBioChem* **2006,** *7* (3), 421-424.
33. Chambers, S. A.; Townsend, S. D., Bioorthogonal human milk oligosaccharide probes for antimicrobial target identification within *Streptococcus agalactiae*. *Carbohydrate Research* **2020,** *488*, 107895.
34. Chan, K. K.; Lei, Q.; Tang, J.; Sun, X.-L., Synthesis of aryl azide chain-end functionalized N-linked glycan polymers and their photo-labelling of specific protein. *RSC Advances* **2020,** *10* (63), 38561-38565.

35. K.Kochetkov, L. M. L. S. N. A. D., A new simple synthesis of amino sugar β-d-glycosylamines. *Carbohydr Res.* **1986,** *146*, C1-C5.
36. Edward, J. T., Stability of Glycosides to Acid Hydrolysis. *Chem. Ind.* **1955,** *3*, 1102-1104.
37. Lemieux, R. U., Effects of unshared pairs of electrons and their solvation on conformational equilibria. *Pure Appl. Chem.* **1971,** *25* (3), 527-548.
38. Lemieux, R. U.; Kullnig, R. K.; Bernstein, H. J.; Schneider, W. G., Configurational Effects on the Proton Magnetic Resonance Spectra of Six-membered Ring Compounds1. *JACS* **1958,** *80* (22), 6098-6105.
39. Lemieux, R. U.; Koto, S.; Voisin, D., The Exo-Anomeric Effect. In *Anomeric Effect*, AMERICAN CHEMICAL SOCIETY: 1979; Vol. 87, pp 17-29.
40. Wang, C.; Chen, Z.; Wu, W.; Mo, Y., How the Generalized Anomeric Effect Influences the Conformational Preference. *Chemistry – A European Journal* **2013,** *19* (4), 1436-1444.
41. Perrin, C. L.; Armstrong, K. B.; Fabian, M. A., The origin of the anomeric effect: conformational analysis of 2-methoxy-1,3-dimethylhexahydropyrimidine. *JACS* **1994,** *116* (2), 715-722.
42. Wang, C.; Ying, F.; Wu, W.; Mo, Y., How Solvent Influences the Anomeric Effect: Roles of Hyperconjugative versus Steric Interactions on the Conformational Preference. *The Journal of Organic Chemistry* **2014,** *79* (4), 1571-1581.
43. Romers, C.; Altona, C.; Buys, H. R.; Havinga, E., Geometry and Conformational Properties of Some Five- and Six-Membered Heterocyclic Compounds Containing Oxygen or Sulfur. In *Topics in Stereochemistry*, 1969; pp 39-97.
44. Pinto, B. M.; Schlegel, H. B.; Wolfe, S., Bond angle variations in XCY fragments and their relationship to the anomeric effect. *Can. J. Chem.* **1987,** *65* (7), 1658-1662.
45. Fuchs, B.; Schleifer, L.; Tartakowsky, E., Probing the anomeric effect: the structural criterion. *Nouveau journal de chimie (1977)* **1984,** *8* (5), 275-278.
46. Box, V. G. S., Explorations of the origins of the reverse anomeric effect of the monosaccharides using the QVBMM (molecular mechanics) force field. *J. Mol. Struct.* **2000,** *522* (1), 145-164.
47. Lemieux, R. U.; Morgan, A. R., THE ABNORMAL CONFORMATIONS OF PYRIDINIUM α-GLYCOPYRANOSIDES. *Can. J. Chem.* **1965,** *43* (8), 2205-2213.
48. Perrin, C. L., Reverse anomeric effect: fact or fiction? *Tetrahedron* **1995,** *51* (44), 11901-11935.
49. Perrin, C. L., Reverse anomeric effect and steric hindrance to solvation of ionic groups. *Pure Appl. Chem.* **1995,** *67* (5), 719-728.
50. Randell, K. D.; Johnston, B. D.; Green, D. F.; Pinto, B. M., Is There a Generalized Reverse Anomeric Effect? Substituent and Solvent Effects on the Configurational Equilibria of Neutral and Protonated N-Arylglucopyranosylamines and N-Aryl-5-thioglucopyranosylamines. *J. Org. Chem.* **2000,** *65* (1), 220-226.
51. Mo, Y., Computational evidence that hyperconjugative interactions are not responsible for the anomeric effect. *Nature Chemistry* **2010,** *2* (8), 666-671.
52. Wang, C.; Ying, F.; Wu, W.; Mo, Y., How solvent influences the anomeric effect: roles of hyperconjugative versus steric interactions on the conformational preference. *J. Org. Chem.* **2014,** *79*, 1571-1581.
53. Mo, Y., Computational evidence that hyperconjugative interactions are not responsible for the anomeric effect. *Nat Chem.* **2010,** *2*, 666-671.

54. Smith, I. C.; Jarrell, H. C., Carbohydrates of the cellular surface: organization and dynamics as seen by 2H n.m.r. *Biochem Soc Trans.* **1990,** *18*, 825-827.
55. Gaweda, K.; Plazinski, W., The endo- and exo-Anomeric Effects in Furanosides. A Computational Study. *Eur. J. Org. Chem.* **2020,** *2020* (6), 674-679.
56. DeMatteo, M. P.; Snyder, N. L.; Morton, M.; Baldisseri, D. M.; Hadad, C. M.; Peczuh, M. W., Septanose Carbohydrates: Synthesis and Conformational Studies of Methyl α-d-glycero-d-Idoseptanoside and Methyl β-d-glycero-d-Guloseptanoside. *J. Org. Chem.* **2005,** *70* (1), 24-38.
57. Randell, K. D.; Johnston, B. D.; Green, D. F.; Pinto, B. M., Is there a generalized reverse anomeric Effect? substituent and solvent effects on the configurational equilibria of neutral and protonated N-arylglucopyranosylamines and N-aryl-5-thioglucopyranosylamines. *J. Org. Chem.* **2000,** *65*, 220-226.
58. Moore, R. E.; Craft, K. M.; Xu, L. L.; Chambers, S. A.; Nguyen, J. M.; Marion, K. C.; Gaddy, J. A.; Townsend, S. D., Leveraging Stereoelectronic Effects in Biofilm Eradication: Synthetic β-Amino Human Milk Oligosaccharides Impede Microbial Adhesion As Observed by Scanning Electron Microscopy. *J Org Chem* **2020,** *85* (24), 16128-16135.
59. Anisfeld, S. T.; Lansbury, P. T., A Convergent Approach to the Chemical Synthesis of Asparagine-Linked Glycopeptides. *J Org Chem.* **1990,** *55*, 5560-5562.
60. Cohenanisfeld, S. T.; Lansbury, P. T., A Practical, Convergent Method for Glycopeptide Synthesis. *JACS* **1993,** *115*, 10531-10537.
61. Nagorny, P.; Sane, N.; Fasching, B.; Aussedat, B.; Danishefsky, S. J., Probing the Frontiers of Glycoprotein Synthesis: The Fully Elaborated beta-Subunit of the Human Follicle-Stimulating Hormone. *Angew Chem Int.* **2012,** *51*, 975-979.
62. Wang, P.; Dong, S. W.; Shieh, J. H.; Peguero, E.; Hendrickson, R.; Moore, M. A. S.; Danishefsky, S. J., Erythropoietin Derived by Chemical Synthesis. *Science.* **2013,** *342*, 1357-1360.
63. Wilson, R. M.; Dong, S. W.; Wang, P.; Danishefsky, S. J., The Winding Pathway to Erythropoietin Along the Chemistry-Biology Frontier: A Success At Last. *Angew. Chem. Int. Ed.* **2013,** *52*, 7646-7665.
64. Wang, P.; Dong, S. W.; Brailsford, J. A.; Iyer, K.; Townsend, S. D.; Zhang, Q.; Hendrickson, R. C.; Shieh, J.; Moore, M. A. S.; Danishefsky, S. J., At Last: Erythropoietin as a Single Glycoform. *Angew. Chem. Int. Ed.* **2012,** *51*, 11576-11584.
65. Ackerman, D. L.; Craft, K. M.; Doster, R. S.; Weitkamp, J.-H.; Aronoff, D. M.; Gaddy, J. A.; Townsend, S. D., Antimicrobial and Antibiofilm Activity of Human Milk Oligosaccharides against *Streptococcus agalactiae, Staphylococcus aureus,* and *Acinetobacter baumannii. ACS Infect Dis.* **2018,** *4* (3), 315-324.
66. Craft, K. M.; Gaddy, J. A.; Townsend, S. D., Human Milk Oligosaccharides (HMOs) Sensitize Group B Streptococcus to Clindamycin, Erythromycin, Gentamicin, and Minocycline on a Strain Specific Basis. *ACS Chem Bio* **2018,** *13* (8), 2020-2026.
67. Coppa, G. V.; Pierani, P.; Zampini, L.; Carloni, I.; Carlucci, A.; Gabrielli, O., Oligosaccharides in human milk during different phases of lactation. *Acta Paediatrica* **1999,** *88* (s430), 89-94.
68. Tang, J.; Ozhegov, E.; Liu, Y.; Wang, D.; Yao, X.; Sun, X.-L., Straightforward Synthesis of N-Glycan Polymers from Free Glycans via Cyanoxyl Free Radical-Mediated Polymerization. *ACS Macro Letters* **2017,** *6* (2), 107-111.
69. Liu, X.; Zhang, G. S.; Chan, K.; Li, J. J., Microwave-assisted Kochetkov amination followed by permanent charge derivatization: a facile strategy for glycomics. *ChemComm.* **2010,** *46*, 7424-7426.

70. Bejugam, M.; Flitsch, S. L., An efficient synthetic route to glycoamino acid building blocks for glycopeptide synthesis. *Org Lett.* **2004,** *6*, 4001-4004.
71. Liu, X.; Zhang, G.; Chan, K.; Li, J., Microwave-assisted Kochetkov amination followed by permanent charge derivatization: a facile strategy for glycomics. *ChemComm.* **2010,** *46* (39), 7424-7426.
72. Bejugam, M.; Flitsch, S. L., An Efficient Synthetic Route to Glycoamino Acid Building Blocks for Glycopeptide Synthesis. *Org Lett* **2004,** *6* (22), 4001-4004.
73. Vetter, D.; Gallop, M. A., Strategies for the Synthesis and Screening of Glycoconjugates. 1. A Library of Glycosylamines. *Bioconjug. Chem.* **1995,** *6* (3), 316-318.
74. Ackerman, D. L.; Doster, R. S.; Weitkamp, J. H.; Aronoff, D. M.; Gaddy, J. A.; Townsend, S. D., Human Milk Oligosaccharides Exhibit Antimicrobial and Antibiofilm Properties against Group B *Streptococcus*. *ACS Infect Dis.* **2017,** *3*, 595-605.
75. Chambers, S. A.; Gaddy, J. A.; Townsend, S. D., Synthetic Ellagic Acid Glycosides Inhibit Early Stage Adhesion of *Streptococcus agalactiae* Biofilms as Observed by Scanning Electron Microscopy. *Chemistry.* **2020,** *26*, 9923-9928.
76. Gaddy, J. A.; Tomaras, A. P.; Actis, L. A., The *Acinetobacter baumannii* 19606 OmpA protein plays a role in biofilm formation on abiotic surfaces and in the interaction of this pathogen with eukaryotic cells. *Infect Immun.* **2009,** *77*, 3150-3160.
77. Gaddy, J. A.; Radin, J. N.; Cullen, T. W.; Chazin, W. J.; Skaar, E. P.; Trent, M. S.; Algood, H. M., *Helicobacter pylori* Resists the Antimicrobial Activity of Calprotectin via Lipid A Modification and Associated Biofilm Formation. *mBio.* **2015,** *6*, e01349-e15.
78. Craft, K. M.; Townsend, S. D., Synthesis of lacto-N-tetraose. *Carbohydr Res.* **2017,** *440-441*, 43-50.
79. Leitao Jr, M. M., Global disparities in oncology: pinpointing and addressing the causes. *Int J Gynaecol Obstet* . **2021,** *153,* 2, 188-189.
80. McGowan, J. V.; Chung, R.; Maulik, A.; Piotrowska, I.; Walker, J. M.; Yellon, D. M., Anthracycline Chemotherapy and Cardiotoxicity. *Cardiovasc.Drugs Ther.* **2017,** *31* (1), 63-75.
81. Hevener, K.; Verstak, T. A.; Lutat, K. E.; Riggsbee, D. L.; Mooney, J. W., Recent developments in topoisomerase-targeted cancer chemotherapy. *Acta Pharmaceutica Sinica B* **2018,** *8* (6), 844-861.
82. Lefrak, E. A.; Piťha, J.; Rosenheim, S.; Gottlieb, J. A., A clinicopathologic analysis of adriamycin cardiotoxicity. *Cancer* **1973,** *32* (2), 302-314.
83. Alvarez-Cardona, J.; Lenihan, D. J., Anthracycline Cardiotoxicity: It Is Possible to Teach an Old Dog Some New Tricks. *Cardiol. Clin. s* **2019,** *37* (4), 355-363.
84. Nitiss, J. L., Targeting DNA topoisomerase II in cancer chemotherapy. *Nat. Rev. Cancer* **2009,** *9* (5), 338-350.
85. Coley, H. M., Mechanisms and strategies to overcome chemotherapy resistance in metastatic breast cancer. *Cancer Treat. Rev.* **2008,** *34* (4), 378-390.
86. Leonard, R. C. F.; Williams, S.; Tulpule, A.; Levine, A. M.; Oliveros, S., Improving the therapeutic index of anthracycline chemotherapy: Focus on liposomal doxorubicin (Myocet™). *The Breast* **2009,** *18* (4), 218-224.
87. Oviatt, A. A.; Kuriappan, J. A.; Minniti, E.; Vann, K. R.; Onuorah, P.; Minarini, A.; De Vivo, M.; Osheroff, N., Polyamine-containing etoposide derivatives as poisons of human type II topoisomerases: Differential effects on topoisomerase IIα and IIβ. *Bioorganic Med. Chem. Lett.* **2018,** *28* (17), 2961-2968.

88. Huseman, E. D.; Byl, J. A. W.; Chapp, S. M.; Schley, N. D.; Osheroff, N.; Townsend, S. D., Synthesis and Cytotoxic Evaluation of Arimetamycin A and Its Daunorubicin and Doxorubicin Hybrids. *ACS Cent. Sci.* **2021,** *7* (8), 1327-1337.
89. Wander, D. P. A.; van der Zanden, S. Y.; van der Marel, G. A.; Overkleeft, H. S.; Neefjes, J.; Codée, J. D. C., Doxorubicin and Aclarubicin: Shuffling Anthracycline Glycans for Improved Anticancer Agents. *J. Med. Chem* **2020,** *63* (21), 12814-12829.
90. Takechi, M.; Tanaka, Y., Haemolytic Time Course Differences between Steroid and Triterpenoid Saponins. *Planta Med* **1995,** *61* (01), 76-77.
91. Li, Y.; Fan, L.; Sun, Y.; Miao, X.; Zhang, F.; Meng, J.; Han, J.; Zhang, D.; Zhang, R.; Yue, Z.; Mei, Q., Paris saponin VII from *trillium tschonoskii* reverses multidrug resistance of adriamycin-resistant MCF-7/ADR cells via P-glycoprotein inhibition and apoptosis augmentation. *J. Ethnopharmacol.* **2014,** *154* (3), 728-734.
92. Ikeda, T.; Tsumagari, H.; Honbu, T.; Nohara, T., Cytotoxic Activity of Steroidal Glycosides from Solanum Plants. *Biol Pharm Bull.* **2003,** *26* (8), 1198-1201.
93. Ikeda, T.; Yamauchi, K.; Nakano, D.; Nakanishi, K.; Miyashita, H.; Ito, S.-i.; Nohara, T., Chemical trans-glycosylation of bioactive glycolinkage: synthesis of an α-lycotetraosyl cholesterol. *Tetrahedron Lett.* **2006,** *47* (26), 4355-4359.
94. Chakraborty, D.; Jain, C. K.; Maity, A.; Ghosh, S.; Choudhury, S. R.; Jha, T.; Majumder, H. K.; Mondal, N. B., *Chenopodium album* metabolites act as dual topoisomerase inhibitors and induce apoptosis in the MCF7 cell line. *MedChemComm* **2016,** *7* (5), 837-844.
95. Sharma, S. C.; Chand, R.; Sati, O. P.; Sharma, A. K., Oligofurostanosides from *Solanum nigrum. Phytochemistry* **1983,** *22* (5), 1241-1244.
96. 川崎, 敏.; 西岡, 五., Digitalis Saponins. II. Leaf Saponins of *Digitalis purpurea L*. *Chem. Pharm. Bull.* **1964,** *12* (11), 1311-1315.
97. Tuan Anh, H. L.; Tran, P. T.; Thao, D. T.; Trang, D. T.; Dang, N. H.; Van Cuong, P.; Kiem, P. V.; Minh, C. V.; Lee, J.-H., Degalactotigonin, a Steroidal Glycoside from<i> Solanum nigrum, Induces Apoptosis and Cell Cycle Arrest via Inhibiting the EGFR Signaling Pathways in Pancreatic Cancer Cells. *BioMed Res. Int.* **2018,** *2018*, 3120972.
98. Zhao, Z.; Jia, Q.; Wu, M.-S.; Xie, X.; Wang, Y.; Song, G.; Zou, C.-Y.; Tang, Q.; Lu, J.; Huang, G.; Wang, J.; Lin, D.-C.; Koeffler, H. P.; Yin, J.-Q.; Shen, J., Degalactotigonin, a Natural Compound from *Solanum nigrum L.*, Inhibits Growth and Metastasis of Osteosarcoma through GSK3β Inactivation–Mediated Repression of the Hedgehog/Gli1 Pathway. *Clin. Cancer Res.* **2018,** *24* (1), 130-144.

About the Author

I was born in March of 1994 to loving parents, and later gained a younger brother who I am close with. Growing up, I have always been drawn to the arts and sciences. Since I grew up near NYC, I had ample opportunity to visit the Metropolitan Museum of Art, one of my favorite places to spend the day.

As a child, we often hear how pursuing a career in the arts would not lead to a stable future, so I was thankful that I enjoyed both the sciences as well as the arts. The most enjoyable class still remained art; constantly being in awe of new creations, colors, and techniques to create hyper reality or even an alternate reality. It was not till high school, where my chemistry teacher's experiments and clear passion for the field made me change my mind. In that class, the logical reasoning behind the experimental teachings and beautiful colorful reactions captured my interest. At the time, I was more interested in chemical engineering, however, soon discovered engineering was not something I wanted to explore. I still enjoyed painting and drawing, taking classes with two different art teachers once a week. I learned various techniques and still entertained the notion of pursuing art as I steadily participated and won awards in nation-wide contests throughout the years. Although I was one out of four seniors who earned a five for AP Art, I was the only one who chose to pursue a STEM path, instead of attending an art institution.

Beginning college at Vanderbilt was extremely hard, adjusting to a new lifestyle, learning more about myself with the infinite possibilities to explore. Biology and chemistry were my main interests, though it soon became clear that I enjoyed and was better at chemistry, which was fine since I wanted to go to medical school. Dr. Michelle Sulikowski's organic chemistry course was one I immensely enjoyed, seeing how drawing mechanisms and pushing arrows to the products

could actually be what happens inside a reaction flask. She not only became my major advisor, but someone who supported me while I searched for labs to work in.

It was mainly serendipity that I was able to work in Dr. Townsend's lab. One of my close friends found that he had posted that he was searching for an undergraduate to clean glassware after setting up his lab space over the summer. Upon submitting my application in hopes of first working for a semester before being able to do research, I soon received a response to meet. Our meeting was simple and short. After expressing interest in conducting research, Dr. Townsend wholeheartedly began to teach. I am grateful for his laidback approach and emphasis on safety. It is learning directly from him that I was able to develop the foundations for reaction condition selection, reaction setup up and monitoring, as well as compound purification and analysis. I was given the opportunity to mentor another undergraduate with what I learned. The environment he cultivated in the group led me to comfortably learn from anyone in the group, him or the graduate students. The graduate students were all willing to share their knowledge, allow me to shadow them, and teach me novel things. Exposure to graduate coursework and graduate students who clearly were interested and hungry for progress and growth contributed to my understanding of how to approach and think about research.

While I had initially been interested in medical school, my time in the Townsend lab made me realize I still enjoyed chemistry, so the summer before senior year, I began to express interest in applying to chemistry jobs that only required a BA. I have to say, it is the continued support of the friends I had in high school, new ones fostered at Vanderbilt, and my family that had enabled me to come to this conclusion to pursue chemistry. I am fortunate to have a mentor like Dr. Townsend, who consulted other professors, like Dr. Schley about my prospects as a graduate student in chemistry. After a hectic exploration of chiropractic school, traditional Chinese

medicine institutions and even acceptance into a pharmacognosy program, I did end up at UIC for their chemistry program.

I finally began my commitment to learning organic chemistry in Dr. Leslie Aldrich's research group, one that had only been established the previous year. I was fortunate enough to publish two articles during my time there, including the first one out of her lab, where I contributed by synthesizing medicinal compound analogs. In addition to wonderful lab mates and classmates who are continually my support, I had the opportunity to mentor not one, but rather five different individuals. I ended up learning so much about myself while teaching them and picking up on how to cater to each of their learning styles.

I did eventually make my way back to Vanderbilt where I began anew in my graduate career, hopefully a bit wiser, or at least with a better understanding of my abilities. Dr. Townsend welcomed me back and I felt privileged to learn under the tutelage of not only Dr. Townsend, but also many others who have since graduated. I have really learned by standing on these giants' shoulders through lessons, lectures, shadowing opportunities and more. They embody who I want to be as a mentor, to pass along the knowledge that I have gained, not just in chemical reactions, but how to go about through life, and graduate school. I choose to work with Dr. Townsend once again because of his passion for chemistry, advancing the field, and mentoring students. Also, for the open communication style where I felt comfortable voicing my shortcomings and failure, to seek out help when I am unsure what to do next, knowing that as long as I expressed how much I care and want to overcome the challenge, he will match the enthusiasm and energy. As I worked with fellow graduate students of the same cohort or younger, I saw how change was constant as new students joined the group and department and hopefully passed along what I have learned to them and the undergraduates I have mentored as well.

After these four years, I have defended my Ph.D. and will head off to the Massachusetts Institute of Technology to begin the next phase of my career as a postdoctoral fellow. I had entered graduate school with the intention of pursuing a career in industry. I have however observed how things have changed from my undergraduate days till now, there are an abundance of professors at Vanderbilt who I think highly of. Over the years I have grown to feel that conducting organic chemistry research is not just a science, but also an art form that I aim to continue to developing and learning.